THE ELECTRONIC SPECTRA

OF

THE SO_3F RADICAL

THE ELECTRONIC SPECTRA

OF

THE FLUOROSULFATE RADICAL

BY

CHARLES HERBERT WARREN, B.Sc.

A Thesis

Submitted to the Faculty of Graduate Studies

in Partial Fulfillment of the Requirements

for the Degree

Doctor of Philosophy

McMaster University

October, 1968

DOCTOR OF PHILOSOPHY (1968)
(Chemistry)

MCMASTER UNIVERSITY
Hamilton, Ontario

TITLE: The Electronic Spectra of the Fluorosulfate Radical

AUTHOR: Charles Herbert Warren, B.Sc. (University of Western Ontario)

SUPERVISOR: Professor G. W. King

NUMBER OF PAGES: xi, 189, a.15

SCOPE AND CONTENTS:

Three electronic absorption systems of the fluorosulfate radical in the gas phase have been observed in the near infrared and visible regions of the spectra and have been assigned to the electronic transitions $^2E(2) - {}^2A_2$, $^2E(1) - {}^2A_2$ and $^2A_1 - {}^2A_2$. Molecular orbital calculations on the fluorosulfate radical have been done in order to aid the interpretation of the electronic spectra of the radical. Vibrational and rotational analyses of the visible absorption system ($^2E(2) - {}^2A_2$) have been carried out. The geometry of the radical in the upper $^2E(2)$ state has been found to be similar to that of the $^2A_2$ ground state. The ground state fundamental frequencies of the radical have been determined. The presence of a Jahn-Teller-spin-orbit interaction has been proposed for the $^2E(2)$ state.

DEDICATION

TO MY WIFE MARY

ACKNOWLEDGEMENTS

I wish to express my sincere thanks to Dr. G. W. King for his continued advice and encouragement throughout the course of this research and thesis preparation. I am also very grateful for the invaluable assistance and computer programs provided by Dr. D. P. Santry for the molecular orbital calculations of the fluorosulfate radical. My thanks are extended also to Dr. A. E. Douglas for the use of his Ebert spectrograph and research facilities located at the National Research Council in Ottawa. I would also like to thank Dr. J. Milne and Dr. F. Aubke for their assistance in the preparation of peroxydisulfuryl difluoride. I also wish to acknowledge the stimulus provided by my research colleagues.

Finally, this research was made possible through generous financial assistance from the National Research Council of Canada (1964-68).

TABLE OF CONTENTS

LIST OF TABLES

LIST OF FIGURES

Page

CHAPTER 1

INTRODUCTION

1.1 Separation of the Wave Equation

The time independent Schrödinger equation for a molecule can be written as

$$H \psi_T = E_T \psi_T \tag{1.1}$$

where H is the Hamiltonian operator, E_T are the energy eigenvalues, and ψ_T are the corresponding energy eigenfunctions which form the stationary states of systems in which the energy is conserved. If one neglects translation of the molecule as a whole, and also nuclear and electronic spin, the quantum mechanical Hamiltonian operator for a polyatomic molecule can be written as

$$H = -\sum_i \frac{\hbar^2}{2m_i} \nabla_i^2 - \sum_A \frac{\hbar^2}{2M_A} \nabla_A^2 - \sum_{A,i} \frac{Z_A e^2}{r_{Ai}} + \sum_{A>B} \frac{Z_A Z_B e^2}{r_{AB}} + \sum_{i>j} \frac{e^2}{r_{ij}} \tag{1.2}$$

where $\hbar$ is Planck's constant divided by 2π

m_i and M_A are the masses of the i^{th} electron and the A^{th} nucleus respectively

∇^2 is the Laplacian operator

Z_A is the atomic number of nucleus A

e is the absolute value of the electronic charge

r_{pq} is the distance between particles p and q.

Born and Oppenheimer[1] were the first to show that it is a good approximation to assume that the electrons adapt themselves instantaneously to the nuclear configuration. This approximation allows one to separate the nuclear and electronic motions and to write the molecular wavefunction ψ_T as the product

$$\psi_T = \psi_e \cdot \psi_N \tag{1.3}$$

where ψ_e are eigenfunctions of the electronic Hamiltonian H_e

$$H_e \psi_e = E_e \psi_e \tag{1.4}$$

For a fixed nuclear configuration

$$H_e = -\sum \frac{\hbar^2}{2m_i} \nabla_i^2 - \sum_{A,i} \frac{Z_A e^2}{r_{Ai}} + \sum_{i>j} \frac{e^2}{r_{ij}} \tag{1.5}$$

Each electronic eigenfunction ψ_e for an electronic state of the molecule and its corresponding eigenvalue E_e vary as the internuclear separations are changed. The variation in E_e as a function of these coordinates simply provides part of the potential function in which the nuclei move. The Hamiltonian describing the nuclear motion will therefore be

$$H_N = -\sum_A \frac{\hbar^2}{2M_A} \nabla_A^2 + \sum_{A>B} \frac{Z_A Z_B e^2}{r_{AB}} + E_e \tag{1.6}$$

This operator has eigenfunctions ψ_N and eigenvalues E_N;

$$H_N \psi_N = E_N \psi_N \tag{1.7}$$

The kinetic energy term, $-\sum_A (\hbar^2/2M_A) \nabla_A^2$ contains both vibrational and rotational contributions. Since, in general, the rotational motion is slow compared to the vibrational motion of the nuclei and the motion of the electrons in the molecule, one can to a first (rigid rotor)^2 approximation assume that the vibration and rotation of a molecule are independent of one another.

Use of the above approximation makes it possible to express the total wavefunction as the product, and the total energy as the sum of, electronic, vibrational, and rotational contributions.

$$\psi_T = \psi_e (r,R_o) \psi_{VIB}(R) \psi_{ROT} (\Theta,\phi,\chi) \tag{1.8}$$

$$E_T = E_e + E_{VIB} + E_{ROT} \tag{1.9}$$

where r represents the coordinates of the electrons, R_o stands for the equilibrium position of the nuclei, R denotes the displacement of the nuclei from their equilibrium position in terms of 3N-6 internal coordinates and (Θ,ϕ,χ) are the Euler angles which determine the orientation of the molecule relative to axes attached to the molecule with a fixed direction in space.

If small interactions occur among these three components, they are generally treated by means of perturbation theory. However, if the

interactions, especially those involved in the separation of electronic and vibrational motions, are large, as in the Renner and Jahn-Teller effects, the above approximations are no longer valid.

1.2 Spectroscopic Transitions

If the term representing the interaction of the molecule with an oscillating electromagnetic field is introduced into the Schrödinger equation for such a system, it can be shown by means of time-dependent perturbation theory[3] that a non-zero probability arises of finding the system in a state E_m if originally it was in the state E_n, and if radiation of wavenumber

$$\nu = \frac{E_m - E_n}{hc} \qquad E_m > E_n \tag{1.10}$$

was present. If, in this equation, E is measured in ergs, Planck's constant h is expressed in erg sec. and the velocity of light c is in cm sec^{-1}, then ν is given in wavenumber units (cm^{-1}).

Only electric dipole transitions will be considered since magnetic dipole and electric quadrupole transitions are weaker by factors of approximately 10^{-5} and 10^{-7} respectively.

The probability of a transition between two states described by the eigenfunctions ψ_n and ψ_m is proportional to the square of the transition moment integral M defined by

$$\bar{M} = \int \psi_m^* \, \bar{P} \, \psi_n \, d\tau$$

where the integral is taken over the whole configuration space for the molecule and $\bar{P}$ is the electric dipole moment operator. If the above integral is non-zero for the two states n and m, then the transition between them is said to be allowed; if it is zero, then the transition under consideration is forbidden as a dipole transition.

The range of wavenumbers which spectroscopy covers extends from 10^{-2} to 10^{5} cm^{-1}. Because techniques for the detection and measurement of radiation vary as one traverses the above range, and because different types of transitions occur in different regions of this range, spectroscopy is divided into several branches.

Microwave spectroscopy concerns itself with the investigation of spectra in the microwave region (10^{-2} - 10 cm^{-1}). These spectra generally result from transitions between rotational levels associated with one vibrational level.

Infrared and Raman spectroscopy (50 -10^{4} cm^{-1}) pertain to the investigation of transitions between vibrational levels associated with the ground electronic state. Changes in rotational energy can accompany each vibrational transition.

Electronic excitation causes spectra which normally fall in the visible and ultraviolet regions (10^{4} - 10^{5} cm^{-1}). Changes in vibrational and rotational energy can accompany each electronic transition.

1.3 Historical Section

Peroxydisulfuryl difluoride, $S_2O_6F_2$, was first prepared by Dudley and Cady[4] in 1957. The structure of this molecule was determined from the results of chemical reactions between it and other substances,

from the infrared spectrum, and from the nuclear magnetic resonance spectrum. They concluded that the structure of the molecule is as shown below.

*

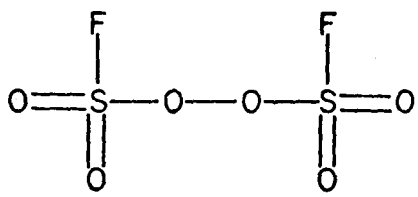

They also determined the temperature dependence of the vapour pressure of the peroxide between 9 and 68°C. This was reported as

$$\log_{10} P(\text{mm}) = 5.49916 - \frac{1.2925 \times 10^2}{T} - \frac{2.5921 \times 10^5}{T^2}$$

In 1963, Dudley and Cady[5] published a paper on the equilibrium between peroxydisulfuryl difluoride and the fluorosulfate free radical. These authors found that when gaseous samples of the former material were heated to about 100°C, a yellow colour developed. Since the peroxide is colourless, this yellow colour indicated the presence of another substance. They investigated the temperature and concentration dependence of the intensity of the visible spectrum and found that a plot of absorbance versus the square root of the peroxide concentration gave a linear relationship.

---

* The planarity or non-planarity of the peroxide was not established by these authors.

An equilibrium constant was obtained from measurement of the pressure variation of $S_2O_6F_2$ samples versus temperature. The equilibrium constant was reported as

$$\log Kp = 7.981 - 4.785 \times 10^3 T^{-1}$$

These relationships can be explained on the basis of non-identical dissociation products. However, the colour, the speed with which equilibruim was attained, and the formation of fluorosulfates by chemical reactions of peroxydisulfuryl difluoride led the authors to conclude that each of the two molecules formed by the dissociation of one molecule of peroxydisulfuryl difluoride (the "dimer") is a fluorosulfate free radical.

$$S_2O_6F_2 \rightleftharpoons 2SO_3F\cdot$$

The oxidizing capacity and structural stability of the fluorosulfate radical is shown by the ability of peroxydisulfuryl difluoride to oxidize substances such as nitric oxide[6], nitrogen dioxide[6], iodine[7], bromine[7], sulphur dioxide[8], and sulphur tetrafluoride[9], to fluorosulfate derivatives.

In 1964, Castellano, Gatti, Sicre, and Schumacher[10] published a paper on the equilibrium between peroxydisulfuryl difluoride and the fluorosulfate radical. Their results were in agreement with those of Cady[5]. The spectroscopic absorption of the radical was reported to occur from 8000 to 2000 Å. Very intense discrete absorption was observed in the visible region. A few very weak bands occurred from 5500 Å downwards. Between 5100 Å and 4500 Å very intense bands were

observed while from 4200 Å downwards little structure was detected in the absorption.

The short wavelength part of the visible spectrum was overlapped by a relatively strong continuum whose intensity rapidly decreased from 3700 Å to 2700 Å at which point it then increased in intensity down to 2000 Å.

The above results were obtained on a low resolution spectrograph. No attempt at an analysis was made by the authors.

Further evidence in favour of the existence of the SO_3F radical was obtained from electron spin resonance. In 1965, Franz Neumayr and N. Vanderkooi Jr.[11] observed that when the dimer ($S_2O_6F_2$), at low pressure and room temperature, was condensed on a cold finger at -196°C, SO_3F radicals were trapped and observed as a slightly anisotropic doublet in the E.S.R. spectrum. The same radical was observed when a gaseous mixture of the dimer and trichloro-fluoro-methane was condensed at -196°C. The authors also observed that when the above frozen mixture was irradiated with UV light, the E.S.R. spectrum of the radical disappeared. The results of their work are shown in Table 1.1. No interpretation of these results was given by the authors.

The structural analysis of the dimer and the radical was carried out in 1965 by Bauer and Hencher[12] using electron diffraction. They found that the radical has a pyramidal structure as shown in Fig. 1.1. The molecular parameters for both the radical and the dimer are given in Table 1.2.

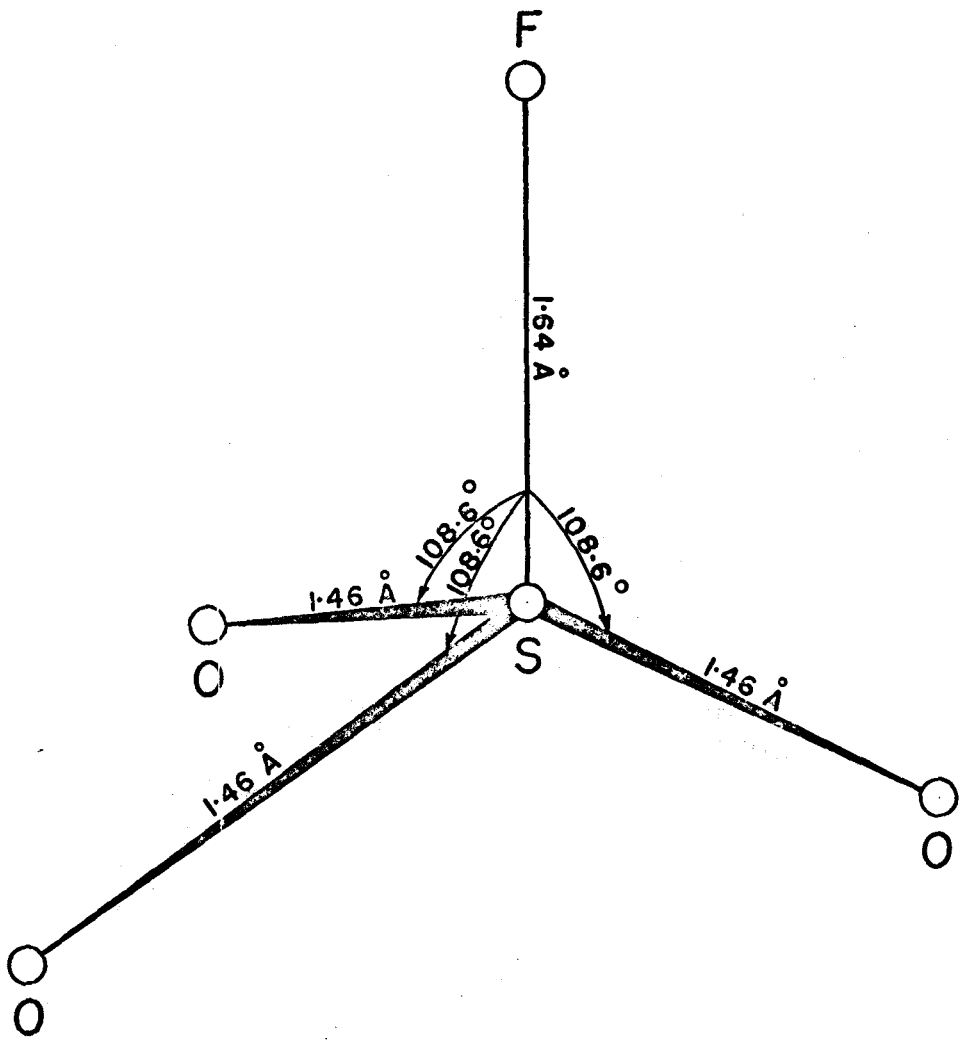

FIGURE 1·1 GROUND STATE GEOMETRY OF THE FLUOROSULFATE RADICAL

TABLE 1.1

E.P.R. DATA OF THE FLUOROSULPHATE RADICAL

Compound, % in CCl_3F	Radical	Temp °C	hfs gauss A	hfs gauss B	Isotropic g VALUE
$S_2O_6F_2$ (Pure)	SO_3F	-196	9.9	0.43*	2.0133
$S_2O_6F_2$ (25%)	SO_3F	-196	9.4		2.0131
$S_2O_6F_2$ (15%)	SO_3F	-132 to -175	9.5		2.0132

* Observed values: hfs $\perp$ = 9.5, hfs $\parallel$ = 10.8, g $\perp$ = 2.0122, g $\parallel$ = 2.0155

TABLE 1.2

MOLECULAR PARAMETERS OF $S_2O_6F_2$ AND SO_3F

SO_3F

S-F = 1.64 ± 0.01 Å

S=O = 1.46 ± 0.01 Å

∠OSF = 108.6° ± 0.4°

$S_2O_6F_2$ *

Oρ—Oρ = 1.49 Å

*Oρ— S = 1.51 Å

O═S = 1.40 Å

S—F = 1.63 Å

∠OρOρS = 102.6°

∠OρSF = 116.9°

∠OSO = 108.3°

∠OSOρ = 120.9°

* Oρ refers to oxygen in the peroxylinkage.

1.4 Symmetry Classification of the SO_3F Radical

Symmetry classifications are of great importance in the theory of molecular structure and spectra.

The symmetry elements of the fluorosulfate radical with the nuclei in their ground state equilibrium configuration are shown in Fig. 1.2. The symmetry operators which interchange identical nuclei in a molecule are described by the same symbols as those given to the corresponding symmetry elements. The symmetry operators are:

i) E, the identity operator which leaves the molecule unchanged,

ii) C_3, C_3^2, the operations of rotation by 120° and 240° about the C_3 axis respectively, (These operators rotate the identical oxygen nuclei into one another.)

iii) σ_{1v}, σ_{2v}, σ_{3v}, the operations of reflection in the vertical planes containing the C_3 axis and each of the oxygen nuclei.

The group of symmetry operations that can be applied to a molecule constitute the point group to which the molecule belongs. The above six symmetry operators comprise the molecular point group C_{3v}*.

---

* Throughout this thesis, an elementary knowledge of group theory will be assumed.[13,14]

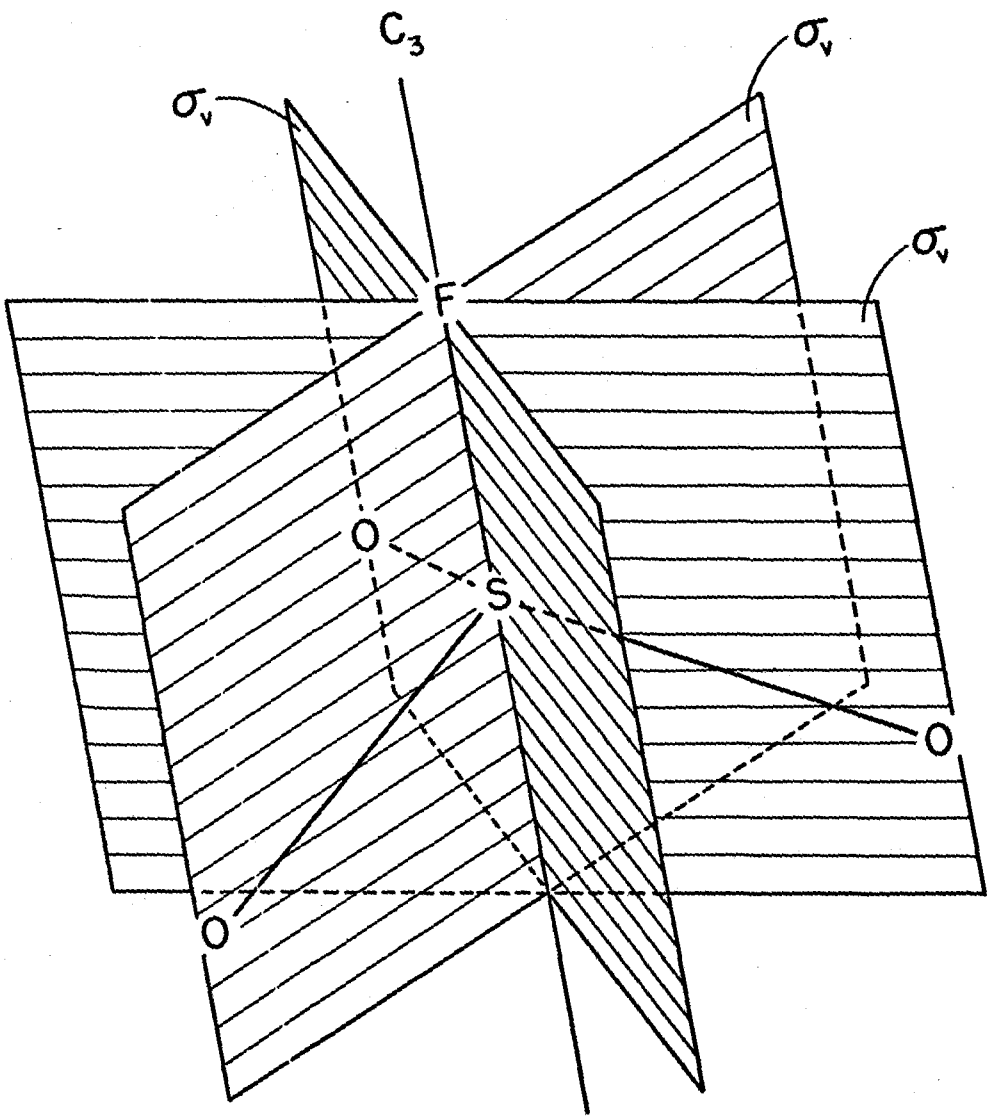

FIGURE 1·2 SYMMETRY ELEMENTS FOR SO_3F^- (C_{3V})

1.5 Double Groups

The irreducible representations of the normal C_{3v} molecular point group can be used to classify states of a molecule in which the total angular momentum is integral; that is, the molecule contains an even number of electrons. The fluorosulfate radical, however, has an odd number of electrons and therefore has states with half integral total angular momentum because the spin of the odd electron is 1/2. To these states there correspond two-valued representations of the molecular point group. To find the two-valued representations, the following artifice is employed.[16] In a purely formal manner, the concept of a new element of the group (denoted by $\bar{E}$) is introduced. This is a rotation through an angle 2π about an arbitary axis, and is not the unit element, but gives the latter when applied twice in succession;

$$\bar{E}^2 = E$$

Accordingly, rotations C_n about the axis of symmetry of the n^{th} order will give identical transformations only after being applied 2n times.

$$C_n^n = \bar{E}, \qquad C_n^{2n} = E$$

Similarily,

$$\sigma_v^2 = \bar{E}, \qquad \sigma_v^4 = E$$

As a result of these operations, a set of elements is obtained which forms some fictitious point symmetry group whose order is twice that of the original group; such groups are called double or extended point groups*.

---

* The theory of double groups is discussed in greater detail by the following authors: Tinkam,[15] Wigner,[16] Landau and Lifshitz[17]

The two-valued representations of the original group will be one-valued representations of the corresponding double group and can be determined by the usual methods of group theory.

Table 1.3 contains the character table for the extended C_{3v} point group. It differs from the normal C_{3v} point group by the addition of the last three columns and last three rows. The irreducible representations are denoted by two sets of notation, Mulliken's and Bethe's. In accordance with Mulliken's notation, doubly degenerate representations are given the letter E and a subscript J to show that they form part of the basis for the representation with angular momentum quantum number J, the chosen value for which this is true.

Table 1.4 contains the multiplication or direct product table for the extended C_{3v} point group.

TABLE 1.3

THE CHARACTER TABLE FOR THE POINT GROUP C_{3v}

Bases for C_{3v}	Representations		E	$2C_3$	$3\sigma_v$	$\bar{E}$	$2\bar{C}_3$	$3\sigma_v$
	*	**						
Tz	Γ_1	A_1	1	1	1	1	1	1
Rz	Γ_2	A_2	1	1	-1	1	1	-1
(x,y) (Rx,Ry)	Γ_3	E	2	-1	0	2	-1	0
ϕ (1/2, -1/2) ϕ (1/2, 1/2)	Γ_4	$E_{1/2}$	2	1	0	-2	-1	0
ϕ (3/2, -3/2) $-i\phi$ (3/2, 3/2)	Γ_5	$E_{3/2}$	1	-1	i	-2	1	i
$-\phi$ (3/2, 3/2) $-i\phi$ (3/2, -3/2)	Γ_6		1	-1	-i	-1	1	i

* Bethe's Notation
** Mulliken's Notation

TABLE 1.4

DIRECT PRODUCT TABLE FOR THE GROUP C_{3v}

	A_1	A_2	E	$E_{1/2}$	$E_{3/2}$
A_1	A_1	A_2	E	$E_{1/2}$	$E_{3/2}$
A_2		A_1	E	$E_{1/2}$	$E_{3/2}$
E			$A_1, [A_2]^*, E$	$E_{1/2}, E_{3/2}$	$E_{1/2}, E_{1/2}$
$E_{1/2}$				$[A_1]^*, A_2, E$	E, E
$E_{3/2}$					$[A_1]^*, A_2, A_1, A_2$

* Species to be omitted in the symmetrical direct product of a degenerate species with itself are put in square brackets. They represent the antisymmetric direct product of a degenerate species with itself.

CHAPTER 2

EXPERIMENTAL WORK

2.1 Preparation of Peroxydisulfuryl difluoride

Peroxydisulfuryl difluoride (called peroxide in this section, for convenience) was prepared by the method of Dudley and Cady[4] in the copper reactor shown in Fig. 2.1. Sulfur trioxide, distilled from Baker and Adamson "Sulfan," and fluorine, each diluted with nitrogen were allowed to mix in the reactor A. The reactor, containing copper wire which had been coated with silver metal from a bath of silver cyanide complex, was electrically heated to a temperature between 120°C and 140°C with externally wound nichrome wire. The fluorine flow rate was maintained slightly in excess of one half the sulfur trioxide flow rate, that is, slightly in excess of the stoichiometric requirement. The flow rates were measured by means of the flow meters B and C. The product was collected in traps D which were cooled with finely crushed dry ice. Final purification of the peroxide was accomplished by distillation at atmospheric pressure in a still. The distillate was protected from atmospheric moisture by a magnesium perchlorate drying tube. The fraction boiling between 66.5 and 67.0°C was taken as pure peroxydisulfuryl difluoride.

In order to establish the purity of the peroxide, the infrared spectrum of the sample was taken using a 10cm. gas cell and Kodak Irtran #2 windows. The only peaks observed were the same as those reported by Dudley and Cady.[4]

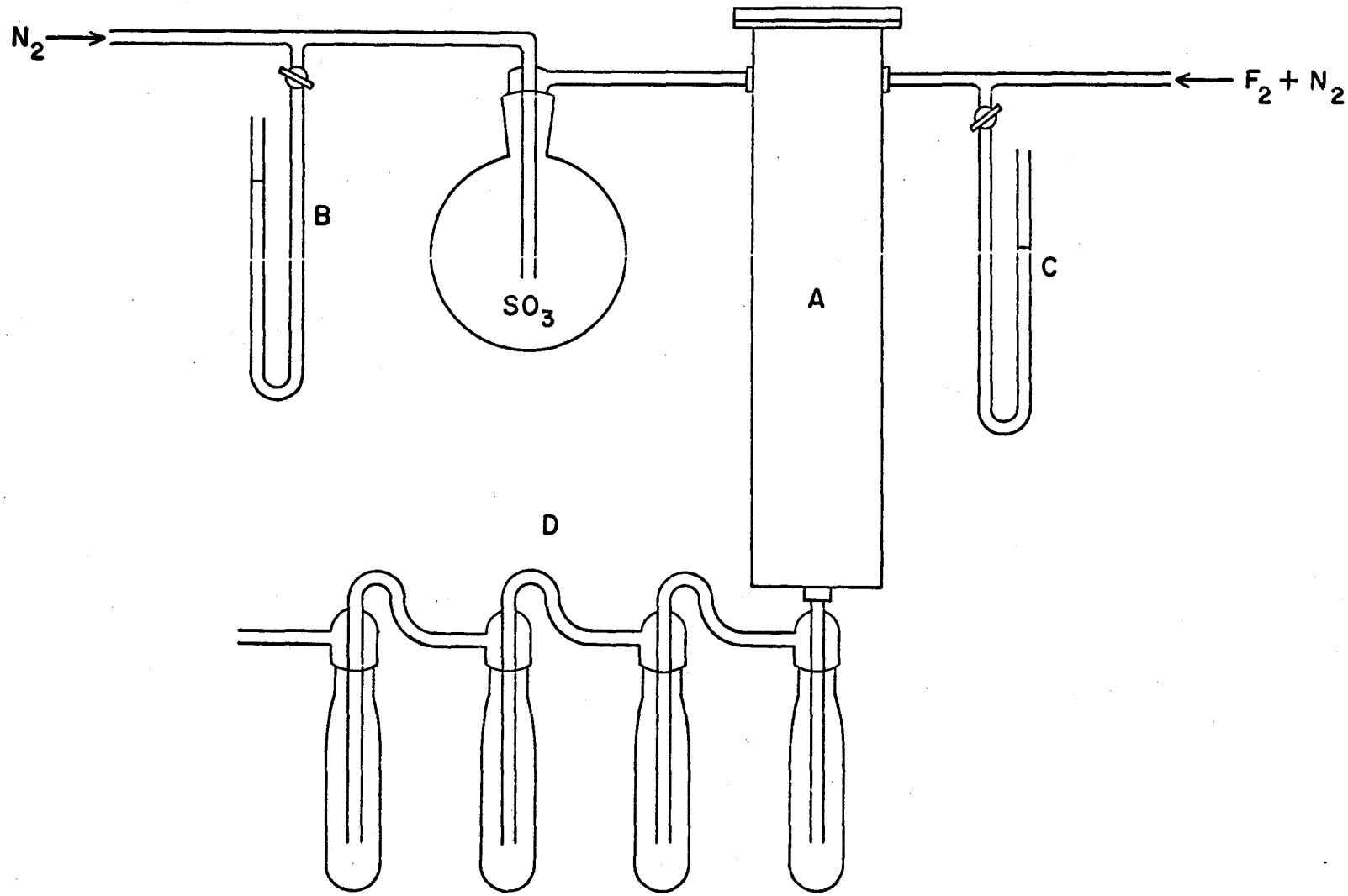

FIGURE 2·1 PREPARATION OF PEROXYDISULFURYL DIFLUORIDE —— $S_2O_6F_2$

Peroxydisulfuryl difluoride readily attacks most vacuum lubricants. Kel-F #90 grease, a halofluorocarbon lubricant, was the least reactive lubricant available and was used on all ground glass joints and stopcocks. Teflon stopcocks with no lubricant were also used.

2.2 Low Resolution Studies of the Electronic Spectrum

A low resolution survey of the spectra of different electronic transitions of the fluorosulfate radical in the gas phase was made using a Cary 14 spectrophotometer. With this instrument the following regions of the spectrum could be scanned: 26,000 - 6500 Å, the near infrared region; 6500 - 4000 Å, the visible region; and 4000 - 2000 Å, the ultraviolet region. A 10 cm. quartz cell with fused silica windows was used in all three regions of the spectrum. A sidearm was attached to this cell. The cell was wrapped with nichrome wire so that it could be heated electrically, and its temperature was determined by means of an iron constantan thermocouple. The thermocouple was placed in contact with the outside of the cell and was separated from the nichrome wire by layers of asbestos paper. The E.M.F. of the thermocouple was measured with a thermocouple potentiometer made by the Croydon Instrument Co. Ltd., England. The reading from the potentiometer, in millivolts, was converted to centigrade degrees by the use of tables in the Handbook of Chemistry and Physics.[18]

A sidearm attached to the cell was cooled with crushed dry ice, and then a few ml. of the peroxide were condensed into it under vacuum. The cell plus the sidearm was then sealed off under vacuum from the rest of the system.

The vapour pressure of the peroxide in the cell was controlled by placing the sidearm of the cell in a Dewar flask which contained a slush bath. The slush bath was a mixture of chloroform, carbon tetrachloride, and liquid nitrogen. The temperature of the slush bath could be varied from -20 to -80°C by changing the ratio of the amount of chloroform to that of carbon tetrachloride in the bath. When higher vapour pressures of the peroxide were required, the sidearm was either placed in an ice bath, left at room temperature, or electrically heated to the same temperature as the cell.

With the cell filled to the saturation vapour pressure of the peroxide at room temperature, the visible spectrum of the radical could just be detected. In order to observe systems of the radical in the near infrared region, the cell plus the sidearm had to be heated to approximately 120°C.

The electronic transition in the visible region was recorded at cell temperatures ranging from 25 to 200°C. For a specific cell temperature, the temperature of the sidearm was adjusted until the absorption was on scale on the spectrophotometer. Before any spectra were recorded, the contents of the cell and sidearm were allowed to reach thermal equilibrium.

2.3 Low Resolution Spectroscopic Studies

The preliminary work on the visible system of the fluorosulfate radical was carried out with a 1.5 meter Bausch and Lomb model 11 spectrograph which has a reciprocal dispersion of 16 Å/mm. in the first order. The slit width was 10 microns.

In order to eliminate the superposition of the Second-order spectrum, from 1850 to 3700 Å, upon the First-order spectrum, from 3700 to 7400 Å, a 2mm. thickness of Chance Bros. glass filter OY10 was placed in the optical path between the lamp and the spectrograph. This cuts off transmitted light below 3500 Å.

2.4 High Resolution Spectroscopic Studies

The visible system of the radical was examined under high resolution in the first order of the twenty foot Ebert spectrograph similar to the one described by King.[19] The plate factor for this spectrograph is 0.72 Å/mm. in the first order. The theoretical resolving power is 150,000 as compared to 32,000 for the Bausch and Lomb spectrograph. The calculated optimum slit width was used for all exposures. This slit width ranged from 40 microns for spectra in the region of 4500 Å to 60 microns for spectra in the region of 5500 Å.

A few selected bands were photographed under still higher resolution in the 10^{th}, 11^{th}, and 12^{th} orders of a thirty-five foot Ebert spectrograph located in the laboratory of Dr. A. E. Douglas at the National Research Council in Ottawa. The theoretical resolving power of this spectrograph was approximately 600,000 in these orders.

Three different light sources were required to photograph the spectra. With the low resolution spectrograph, either a 6V tungsten lamp or a 450 watt Ostram XBO high pressure Xenon lamp was utilized. A striking potential of about 40 Kv., from a Siemens-Schuckert starter, was applied momentarily across the electrodes of the Xenon lamp in order to ignite it. In some regions of the spectrum, the Xenon lamp could not

be employed because of the presence of strong Xenon emission lines in the spectrum.

With the high resolution instruments, either a 110 V tungsten iodide lamp or the 450 watt Xenon lamp was used. The tungsten iodide lamp was much more intense than the 6V tungsten lamp and was particularily useful in conjunction with long path length cells.

The stronger absorption bands of the visible system could easily be photographed when a vapour pressure of 30 mm.Hg of the peroxide was present in a 50 cm. quartz cell heated electrically to approximately 60°C. However, to photograph the weaker bands, path lengths up to 12 meters and pressures from 5 to 100 mm.Hg (peroxide) were found necessary. The long path lengths were attained with a 1.65 meter multiple pass absorption cell of the White type.[20] The construction and alignment of the White cell was essentially the same as that described by Bernstein and Herzberg.[21] The one major difference was that the mirrors were mounted exterior to the cell windows which were sealed to the cell body. This was done to prevent the aluminum surface of the mirrors, the O-rings, and the mirror holders from being attached by the extremely reactive fluorosulfate radical. This external mounting limited the numbers of traversals to twelve. Each time the light passed through the Pyrex cell windows it was refracted such that after a number of traversals the White cell was no longer in optical alignment. Light losses by reflection at the cell windows also contributed to limiting the path length obtainable.

The majority of the absorption bands were photographed on Ilford 35mm. FP3 film. The exposed film was developed with intermittent agitation in complete darkness for four minutes with Kodak D-19 developer.

After the film was carefully rinsed with water, it was fixed in Kodak fixer at 68°F for thirty minutes and then hung to dry in a dust free space.

2.5 Measurement and Calibration of Spectra

Wavelength measurements of the spectra were made by a direct comparision with standard spectral emission lines. An iron emission spectrum from either a Pfund arc or a neon-filled hollow iron cathode discharge tube was recorded adjacent to the absorption spectrum. Accurate wavelengths in air for the iron lines were obtained from the M.I.T. wavelength tables.[22] The weakness of the iron spectrum in the red was compensated for by the presence of strong neon lines in the discharge tube. Accurate wavelengths for the neon lines were taken from "Wavelength Standards" by Lofthus[23].

The positions along the spectrogram of the bands of the fluorosulfate radical spectrum and the adjacent iron lines were measured with a McPherson travelling microscope having a precision of 0.0001 mm. The measured iron lines were then fitted to an equation of the form $Y = A + BX + CX^2$ by means of a least squares program carried out on an IBM 7040 computer. Once the constants A, B and C were determined, the wavelengths of the absorption bands of the fluorosulfate radical were then calculated by substituting the microscope measurements for these bands into the above equation.

The air wavelengths were converted to vacuum wavelengths on the computer by means of a formula derived by B. Edlén[24] from refractivity measurements of H. Barrell and J. E. Sears,[25] W. Traub,[26] and J. Kock.[27]

The vacuum wavelengths were then converted to vacuum wavenumbers. The wavenumbers of some of the weaker broader bands were measured by interpolation from photographic enlargements or from traces made on a Joyce-Loebl MK-III C double beam recording microdensitometer.

2.6 Zeeman Effect

The Zeeman effect on the origin band* of the visible absorption system was carried out at the National Research Council in Ottawa with the electromagnet and 35 foot Ebert spectrograph of Dr. A. E. Douglas.

The dimer, $S_2O_6F_2$, was introduced into a one meter gas cell and since no provisions for heating the cell had been made, a high pressure (~100mm.Hg) of the dimer was required to observe the origin band. The cell was placed in the centre of a long electromagnet (~4 feet) and subjected to a magnetic field of approximately 2000 G. Exposures on the same photographic plate were made with the magnetic field turned alternately on and off.

2.7 The Infrared Spectrum of the Fluorosulfate Radical

A Perkin-Elmer model 521 double-beam spectrophotometer was used to record the infrared spectrum of the fluorosulfate radical in the vapour phase. Peroxydisulfuryl difluoride was introduced into a 10 cm. gas cell which was wrapped with nichrome wire and which had a sidearm with a teflon stopcock.

---

* The origin band is caused by the transition from the vibrationless level of the ground electronic state to the vibrationless level of the excited electronic state.

A variety of window materials were employed in an attempt to find a substance that was inert to the fluorosulfate radical and at the same time a good transmitter of infrared energy. Windows that were used and their range of transmittance are given in Table 2.1.

The NaCl and KBr windows were clamped to the flat ground ends of the cell after a mercury amalgamed lead gasket was placed between the cell and the window. The AgCl windows were directly sealed to the Pyrex glass cell. This sealing was accomplished by heating the AgCl windows to a temperature just below their melting point and then pressing them on to the heated platinized cell ends. Platinization of cell ends enables the silver chloride to bond to the glass. The Irtran windows were attached to the cell as shown in Fig. 2.2. Teflon washers, A and A', were placed on each side of the Irtran window B. This combination was pressed against the ground glass flange C and held in place by the metal washer D and the threaded rods and nuts E. The nuts were gradually tightened until a vacuum could be held in the cell. Since polyethylene is readily attacked by the fluorosulfate radical, a 0.0001 mm. thickness of teflon sheeting was placed over the inner sides of the polyethylene windows before they were clamped to the Pyrex gas cell.

The gas cell was filled with peroxydisulfuryl difluoride and the infrared spectrum was first recorded at room temperature. The sample cell was then heated electrically to temperatures ranging from 40°C to 130°C. When the cell reached thermal equilibrium, the infrared spectrum was again recorded. The gas cell was then allowed to cool to room temperature at which point the infrared spectrum was again recorded.

When the temperature is increased, the equilibrium $S_2O_6F_2 \rightleftharpoons 2SO_3F$. is displaced to the right, which causes an increase in the radical concentration. The infrared spectra of the contents of the gas cell at room temperature and at the higher temperature should be different. The infrared spectra of the contents of the gas cell at room temperature before it was heated and the spectrum after the cell was allowed to cool to room temperature, after it was heated, should be identical.

The results obtained by following the above procedure were very poor. The spectra recorded before heating the cell and after cooling the cell to room temperature were not identical. There were a large number of extraneous absorption peaks present in the infrared spectrum recorded at room temperature after heating. These peaks were not present when the spectrum was first observed at room temperature but appeared in the spectrum recorded at the high temperature. These observations indicate that the cell windows are attacked by the radical. This conclusion was substantiated by the observation of a brownish white deposit on the inside surface of the cell windows.

The NaCl and KBr windows were readily attacked by the fluorosulfate radical even at room temperature. The AgCl and Irtran windows were severely attacked only at the higher temperatures.

Because both the radical and the dimer ($S_2O_6F_2$) have absorption bands in the same regions of the infrared, the observation of vibrational transitions due to the radical was further hindered since the concentration of the dimer was always much greater than that of the radical, even at temperatures of 150°C.

TABLE 2.1

INFRARED WINDOW MATERIALS

Window Material	Range of Transmittance
NaCl	2-15μ
KBr	12-25μ
AgCl	0.6-22μ
Kodak Irtran #2 (Zinc sulphide)	.57-14.7μ
Kodak Irtran #4 (Zinc selenide)	.48-21.8μ
Polyethylene	15-425μ
Teflon	50-425μ

Figure 2.2

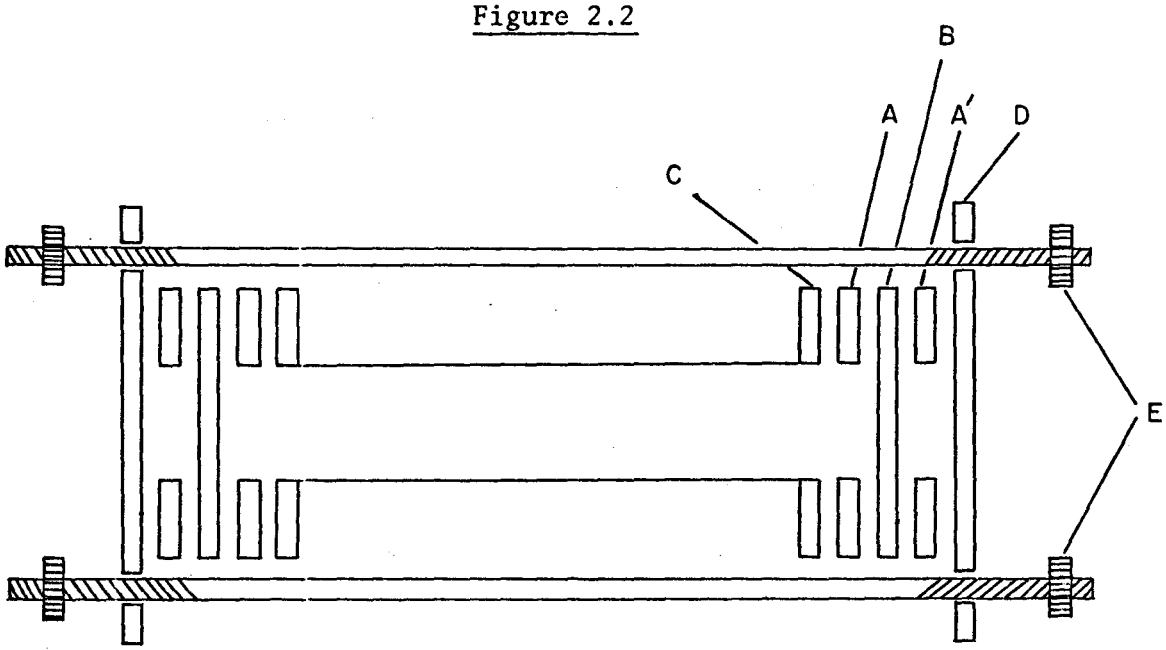

ATTACHMENT OF THE IRTRAN WINDOWS TO THE INFRARED GAS CELL

2.8 The Emission Spectrum

Attempts to observe the emission spectrum of the fluorosulfate radical in the visible region were made using three types of excitation: microwave, radio-frequency, and tesla.

Microwave exciting radiation was supplied by a Raytheon "Microtherm" microwave generator, model CMD4, delivering 100 watts power at 2450 megacycles per second. A half-wave antenna with a cylindrical parabolic reflector, used to focus radiation, was mounted 1 cm. from the outside of the emission cell.

Radio-frequency radiation of approximately 900 kilocycles per second was obtained from a Hewlett-Packard, model 200CD, wide range oscillator. The output of the oscillator was amplified and the circuit was tuned, by means of a 100 picofarad variable capaciter, to resonance in a copper coil three inches in diameter. The discharge tube was placed in the centre of the coil.

The tesla coil, obtained commercially from Edwards High Vacuum Ltd., operated at approximately 300 kilocycles per second. The emission apparatus for the tesla excitation is shown in Fig. 2.3. The peroxide was introduced into the system at trap A. Before each exposure, the peroxide was purified by a trap to trap distillation (B to C). The vapour pressure of the peroxide was controlled by the temperature at which trap B was maintained. Bulb C was heated by means of the heating mantle D to a temperature of approximately 100^{o}C in order to increase the concentration of the radical. The peroxide and the radical were passed through the teflon capillary stopcock E into the emission cell F. This cell, made from quartz, was 25 cm. long and 15 mm. in diameter.

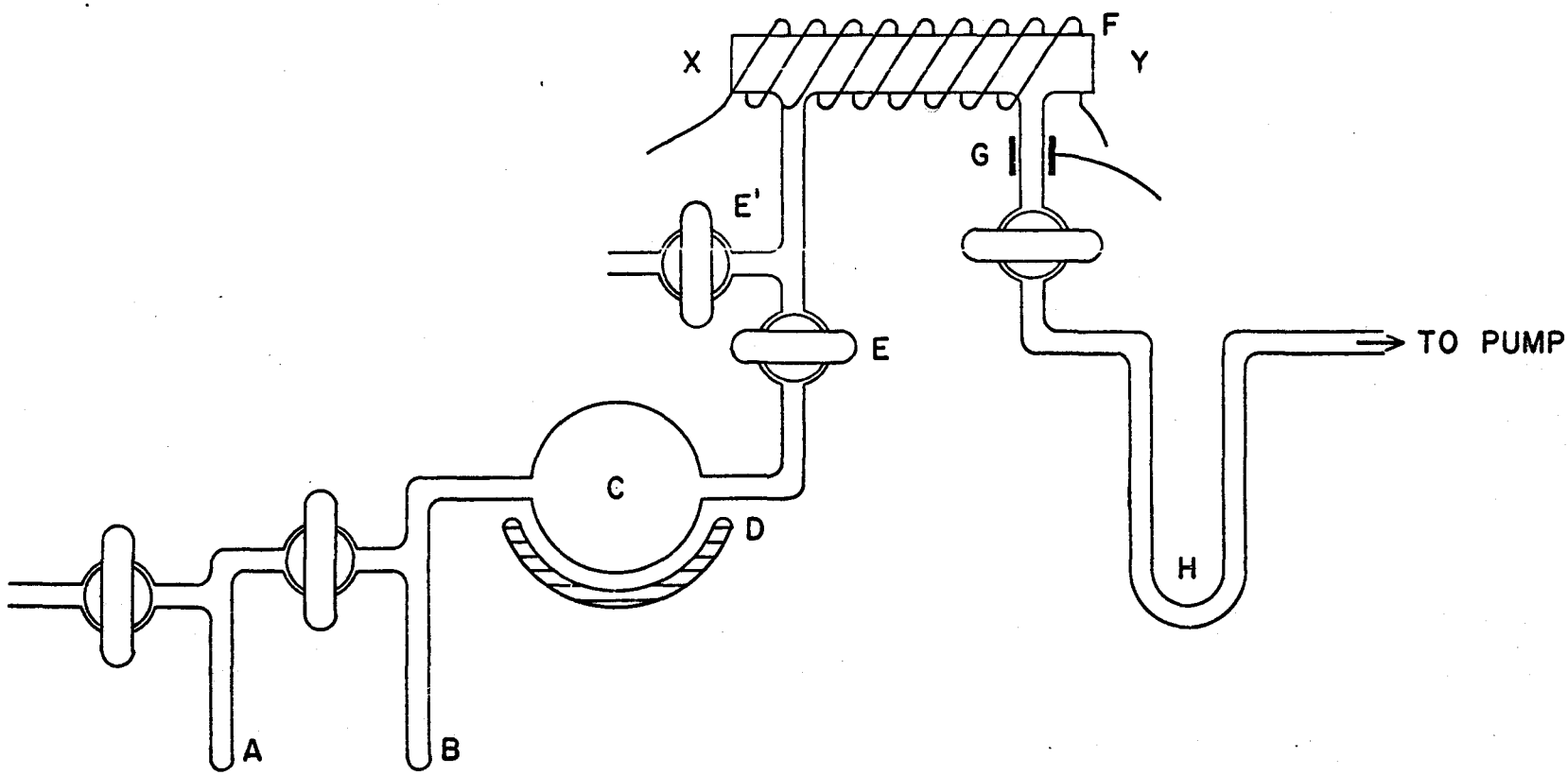

FIGURE 2·3 EMISSION APPARATUS —— TESLA EXCITATION OF THE RADICAL

Quartz windows were sealed to the ends of the cell. Nichrome wire was wrapped around the outside of the cell so that it could be heated electrically. The streaming vapour was excited with the tesla at G and then it was collected in the trap H.

In general, the emission of a particular species, is very dependent upon the means of excitation, the flow rate, and the presence or absence of carrier gases. For these reasons, the emission spectrum of the radical was sought using a range of gas pressures, flow rates, and the previously mentioned various types of excitation. Either neon, argon or helium were employed as carrier gases. Observation of emission was also attempted with no carrier gases present.

The Bausch and Lomb spectrograph model 11 was used to record any emission. Spectra were looked for in the 1^{st} order. A slit width of 60μ and Ilford FP3 film was used. Exposure times ranged from thirty minutes to four hours.

The emission spectra of the radical in the visible region of the spectrum could not be observed by any of the above techniques; only the spectra of miscellaneous molecular fragments were observed.

The visible absorption spectrum of the radical at high sample gas pressures and high emission cell temperatures (~100 ^{o}C) could be observed by placing a tungsten lamp at X and observing the transmitted light at Y with a pocket spectroscope. However, when the exciting radiation was applied to the sample, the visible absorption spectrum of the radical could no longer be detected. This observation indicates that the radical is unstable in the presence of the above excitations and

accounts for the fact that the emission spectrum of the radical could not be seen at high cell temperatures or even if the storage bulb C was at a high temperature. The above behaviour did not occur when both the emission cell and the storage bulb C were at room temperature; however, the emission spectrum could still not be detected.

The reason why the emission spectrum of the radical was not observed is not known for certain. Similarly, the fluorescence of the radical could not be detected even though a number of different optical exciting sources* were tried. Exposure times of up to three days were carried out on high speed Kodak Tri-X panchromatic film whose sensitivity was further enhanced by development in Acufine developer.

The presence of oxygen is known to quench the emission of radiation and the fluorescence of atoms and molecules.[28] Since both peroxydisulfuryl difluoride and the fluorosulfate radical contain oxygen, it is possible that oxygen is produced from the dissociation of either of these molecules by the exciting radiation. Therefore, any emission or fluorescence of the radical would be quenched.

One other explanation which would account for the absence of a detectable emission or fluorescent spectrum of the radical is illustrated in Fig. 2.4.

If the transition labelled 1, E ← G accounts for the observed visible absorption system of the radical (See Chapter 5), then, the transition that must occur if one is to detect the emission of the radical

---

* The optical radiation emitted when either neon, argon, xenon or mercury contained in glass helices was excited electrically, was used to excite the radical.

in the visible region is 2 , E →G. However, if there are low lying states of the radical below E, such as O, then the preferred dissipation of energy from the excited state E could be by the pair of transitions labelled 3, E → O then O→G. In this circumstance, emission of radiation would be detected in the infrared regions of the spectrum and not in the visible region. The results of Chapters 3 and 5 indicate that there are two electronic states of the radical below the state labelled E in Fig. 2.4.

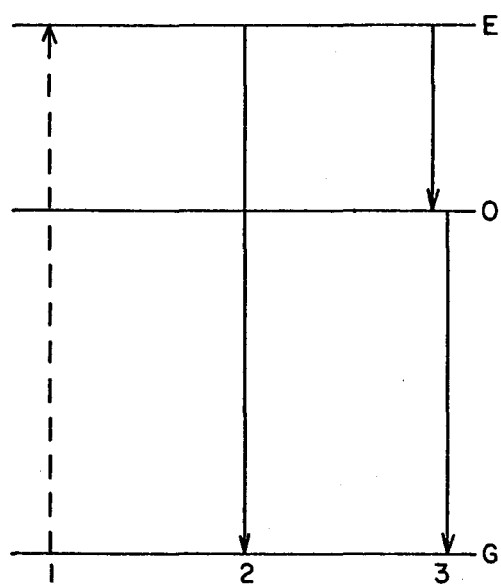

FIGURE 2·4 DISSIPATION OF ENERGY FOR THE EXCITED STATE OF THE FLUOROSULFATE RADICAL·

CHAPTER 3

MOLECULAR ORBITAL CALCULATIONS FOR THE FLUOROSULFATE RADICAL

3.1 Introduction

Molecular orbital calculations on the fluorosulfate radical have not previously been reported in the literature. Information about the electronic symmetry of the ground and excited electronic states, the energy separation of these states, and the nature of the electronic transitions can be obtained from a theoretical calculation. This information aids the interpretation of the observed electronic spectra. In this chapter, the results of calculations for the four lowest energy doublet states of the fluorosulfate radical are presented.

Self consistent field theory attempts to calculate atomic or molecular orbitals using the full many electron Hamiltonian and a single determinantal wavefunction (or the smallest number of determinants required to produce a function with the appropriate symmetry). Optimization of the orbitals by means of the variational principle leads to a set of differential equations[29,30] which are normally intractable. The equations can be solved if the molecular orbitals are approximated as linear combinations of atomic orbitals (LCAO). In this approximation, the i^{th} molecular orbital ψ_i is written as

$$\psi_i = \sum_{\nu} \phi_\nu C_{\nu i} \qquad (3.1)$$

where ϕ_ν are the atomic orbitals. If the orbital coefficients $C_{\nu i}$ are chosen to minimize the total energy, one obtains LCAO/SCF orbitals. These orbitals are the best LCAO approximation to the self-consistent wavefunction. Equations for the LCAO/SCF orbitals were first given by Hall[31] and by Roothaan[30]. However, the use of the LCAO/SCF method without further approximation is limited by computational difficulties.

The simplest approach which overcomes the computational difficulties and still takes detailed account of the Coulomb repulsions is the method described as "complete neglect of differential overlap" (CNDO)[32,33,34,35].

3.2 The method of complete neglect of differential overlap --- CNDO

The original Roothaan equations for a closed shell configuration

$$\bar{F}\bar{C}_i = \bar{S}\bar{C}_i \, \epsilon_i \tag{3.2}$$

become

$$\bar{F}\bar{C}_i = \bar{C}_i \, \epsilon_i \tag{3.3}$$

when overlap between different orbitals is neglected. $\bar{F}$ and $\bar{S}$ are the Fock and overlap matrices respectively. $\bar{C}_i$ is the column vector of the atomic orbital coefficients $C_{\nu i}$ and ϵ_i is the orbital energy for the molecular orbital ψ_i.

In the CNDO approximation, the molecular orbital Coulomb integrals are given by

$$J_{ij} = \sum_A \sum_B D_i^A \, D_j^B \, \gamma_{AB} \tag{3.4}$$

where the summations are over all atoms A and B and

$$D_i^A = \sum_{\mu}^{A} C_{\mu i}^2 \tag{3.5}$$

the summation being over all atomic orbitals centred on atom A. γ_{AB} is an average Coulomb repulsion between an electron in any valence orbital centred on nucleus A and one in any valence orbital centred on nucleus B. Formulae for these integrals are listed by Roothaan[36].

The exchange integrals are given by

$$K_{ij} = \sum_A \sum_B E_{ij}^A \, E_{ij}^B \, \gamma_{AB} \tag{3.6}$$

where

$$E_{ij} = \sum_{\mu} C_{\mu i} \, C_{\mu j} \tag{3.7}$$

The Hartree-Fock matrix elements are approximated as

$$F_{\mu\mu} = U_{\mu\mu} + (P_{AA} - 1/2P_{\mu\mu})\gamma_{AA} + \sum_{B\neq A} (P_{BB} - Z_B)\gamma_{AB} + \sum_{B\neq A} Z_B(\gamma_{AB} - V_{AB})$$

$$F_{\mu\nu} = \beta_{AB}^{o} \, S_{\mu\nu} - 1/2P_{\mu\nu}\gamma_{AB} \quad (\mu\neq\nu) \tag{3.8}$$

$U_{\mu\mu}$ is the energy of a single electron occupying the orbital ϕ_μ in the field of the core* of the atom to which ϕ_μ belongs, that is, its kinetic energy plus its potential energy in the field of the nucleus and inner shells. These matrix elements $U_{\mu\mu}$ were approximated using the following relation[34]:

$$U_{\mu\mu} = -1/2(I_\mu + A_\mu) - (Z_A - 1/2)\gamma_{AA} \tag{3.9}$$

---

* Nucleus plus inner shell electrons.

I_μ and A_μ are the ionization potential and the electron affinity for an electron in the orbital ϕ_μ. These quantities were obtained from atomic spectroscopic data*.

$$P_{\mu\nu} = 2 \sum_{i}^{occ} C_{i\mu} C_{i\nu} \tag{3.10}$$

is the bond order and charge density matrix. The summation is taken over occupied valence molecular orbitals only.

$$P_{AA} = \sum_{\mu}^{A} P_{\mu\mu} \tag{3.11}$$

is the total valence electron density (charge density) on atom A.

Z_B is the magnitude of the resultant charge of the core electrons on atom B and its nuclear charge, in units of +e, and V_{AB} is an average nuclear-attraction integral which represents the potential energy arising from the attraction of an electron in an orbital on atom A by the core (nucleus and inner shell electrons) of another atom B. In the CNDO approximation, V_{AB} is given as

$$V_{AB} = Z_B \gamma_{AB} \tag{3.12}$$

The overlap integrals $S_{\mu\nu}$ were calculated explicitly by means of formulae given by Lofthus[37].

β^o_{AB} is an empirically chosen, bonding parameter which depends only on the pair of atoms bonded. The values of this parameter used in the calculations are given in Appendix I.

---

* These empirical quantities are listed in Appendix I.

A basis set of Slater type valence atomic orbitals was used for the calculation of the molecular orbitals of the fluorosulfate free radical. The valence set for the oxygen and fluorine atoms consisted of 2s, $2p_x$, $2p_y$ and $2p_z$ Slater type orbitals. The valence set of atomic orbitals for sulfur was composed of the 3s, 3p and 3d Slater type orbitals. The orbital exponents of the 2s, 2p, 3s and 3p functions were determined by Slater's rules[38] and are listed in Appendix I. The orbital exponents of the 3d functions were taken to be the same as the 3s and 3p functions.[35]

3.3 Approximations to the Open Shell Problem

The previous equations of the CNDO approximation are only valid for molecules with a closed shell configuration. The fluorosulfate radical, however, has an open shell configuration since it has an odd number of electrons. In order to treat this open shell problem, two approaches were used.

Approximation 1

In this approximation the energy of the radical is determined from the calculated energies and molecular orbitals of the FSO_3^+ and FSO_3^- ions. A pictorial representation of this approximation is shown in Fig. 3.1.

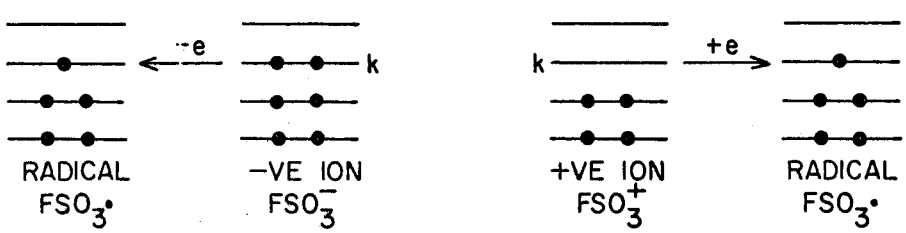

Fig. 3.1 Pictorial Representation of Approximation 1; Electrons in Orbitals shown as dots.

The FSO_3^- ion and the FSO_3^+ ion both have closed shell configurations and therefore the equations of Sec. 3.3 can be used to calculate the molecular orbitals, the orbital energies, and the ground state energy for the ions.

The ground state energy of the FSO_3^- ion is given by

$$W_{ion}^- = 2 \sum_{i}^{occ} H_{ii} + \sum_{i}^{occ} \sum_{j} (2J_{ij} - K_{ij}) \tag{3.13}$$

where H_{ii} are the diagonal core elements.

The ground state energy of the radical, W_{RAD}, is given, according to Koopman's theorem, by the difference between the ground state energy of the ion W_{ion}^- and the energy of highest occupied orbital of the ion ε_k^-.

$$W_{RAD} = W_{ion}^- - \varepsilon_k^- \tag{3.14}$$

If the SO_3F radical is considered to be formed by the addition of an electron to the lowest unoccupied molecular orbital of the FSO_3^+ ion, then the ground state energy of the radical is given as

$$W_{RAD} = W_{ion}^+ + \varepsilon_k^+ \tag{3.15}$$

W_{ion}^+ is the ground state energy of the FSO_3^+ ion and ε_k^+ is the energy of the lowest unoccupied orbital of the FSO_3^+ ion.

$$W_{ion}^+ = 2 \sum_{i}^{\substack{occ \\ \neq k}} H_{ii} + \sum_{i}^{\substack{occ \\ \neq k}} \sum_{j} (2J_{ij} - K_{ij}) \tag{3.16}$$

Approximation II

The second approach uses the "approximate open shell" treatment proposed by Nesbet and Pople[39] in which a single determinantal wave function is used with different molecular orbitals for the electrons with

α and β spins. The incorporation of this approximate open shell method into the CNDO theory has been described by Pople and Segal[36].

The two sets of LCAO molecular orbitals and the corresponding partial charge density and bond order matrices are

$$\psi_i^\alpha = \sum_\mu C_{i\mu}^\alpha \phi_\mu \qquad P_{\mu\nu}^\alpha = \sum_i^{occ} C_{i\mu}^\alpha C_{i\nu}^\beta \tag{3.17}$$

$$\psi_i^\beta = \sum_\mu C_{i\mu}^\beta \phi_\mu \qquad P_{\mu\nu}^\beta = \sum_i^{occ} C_{i\mu}^\alpha C_{i\nu}^\beta \tag{3.18}$$

The total charge density and bond-order matrix is

$$P_{\mu\nu} = P_{\mu\nu}^\alpha + P_{\mu\nu}^\beta \tag{3.19}$$

and the spin density matrix is defined as

$$Q_{\mu\nu} = P_{\mu\nu}^\alpha - P_{\mu\nu}^\beta \tag{3.20}$$

The LCAO coefficients $C_{i\mu}^\alpha$ and $C_{i\mu}^\beta$ are eigenvectors of separate Fock matrices. The Fock matrix elements for orbitals describing α spin states are

$$\begin{aligned} F_{\mu\mu} &= -1/2(I_\mu + A_\mu) + [(P_{AA} - Z_A) - (P_{\mu\mu}^\alpha - 1/2)]\gamma_{AA} + \sum_{B\neq A} (P_{BB} - Z_B)\gamma_{AB} \\ F_{\mu\nu}^\alpha &= \beta_{AB}^\circ S_{\mu\nu} - P_{\mu\nu}^\alpha \gamma_{AB} \end{aligned} \tag{3.21}$$

The corresponding Fock matrix elements for orbitals describing β spin states are obtained from equation 3.21 by replacing α with β.

The solution of the CNDO equations was determined by the following procedure:

1) An initial set of LCAO coefficients $C_{i\mu}$ was obtained from a Hückel type calculation in which

$$F^{(o)}_{\mu\mu} = -1/2(I_\mu + A_\mu)$$
$$F^{(o)}_{\mu\nu} = \beta^o_{AB} S_{\mu\nu} \qquad (3.22)$$

2) Electrons were then assigned to the molecular orbitals. Fifteen electrons were placed in the 15 β orbitals of lowest energy; sixteen electrons were placed in the 16 α orbitals of lowest energy* (the FSO_3 radical has 31 valence electrons).

3) The alpha and beta charge density and bond order matrices were then calculated from equations 3.17 and 3.18. These were used to form new Fock matrices by means of equations 3.21.

4) New ccefficients $C^\alpha_{i\mu}$ and $C^\beta_{i\mu}$ were obtained from solutions of the matrix equations

$$\bar{F}^\alpha \bar{C}^\alpha_i = \bar{C}^\alpha_i \varepsilon^\alpha_i$$
and (3.23)
$$\bar{F}^\beta \bar{C}^\beta_i = \bar{C}^\beta_i \varepsilon^\beta_i$$

The process was then repeated from Step 2 until self-consistency was achieved for the normalized coefficients C^α_i and C^β_i to within a tolerance of 0.0002.

For these calculations, the geometrical symmetry of both the radical and the ions was assumed to be C_{3v} in the ground and excited states. The experimentally determined bond lengths for the radical in the ground electronic state[12] (see section 1.3) were used in the molecular

---

* The odd electron was arbitrarily assigned an α spin.

orbital calculations for both the radical and the ions.

The electronic energies and charge distributions were calculated for each of the four lowest doublet states of the radical for a number of OSF bond angles. The minimum of the molecular energy with respect to the OSF bond angle for each of these doublet states was then determined graphically.

3.4 Theoretical Results

The calculations based on the positive and negative ions (Approximation 1) are first reported since they provide a convenient and useful introduction to the problem of determining the electron configurations of the low-lying doublet states of the radical.

i) Results from Approximation 1 - Ions

The ground states for both the FSO_3^- and the FSO_3^+ ions were found to be of symmetry species A_1. The ground state energy of the FSO_3^+ ion was found to be a minimum at an OSF angle of 107°, whereas the ground state energy of the FSO_3^- ion was a minimum for an OSF angle of 102°. The ordering of the orbital energies as calculated for the ions is shown in Fig. 3.2.

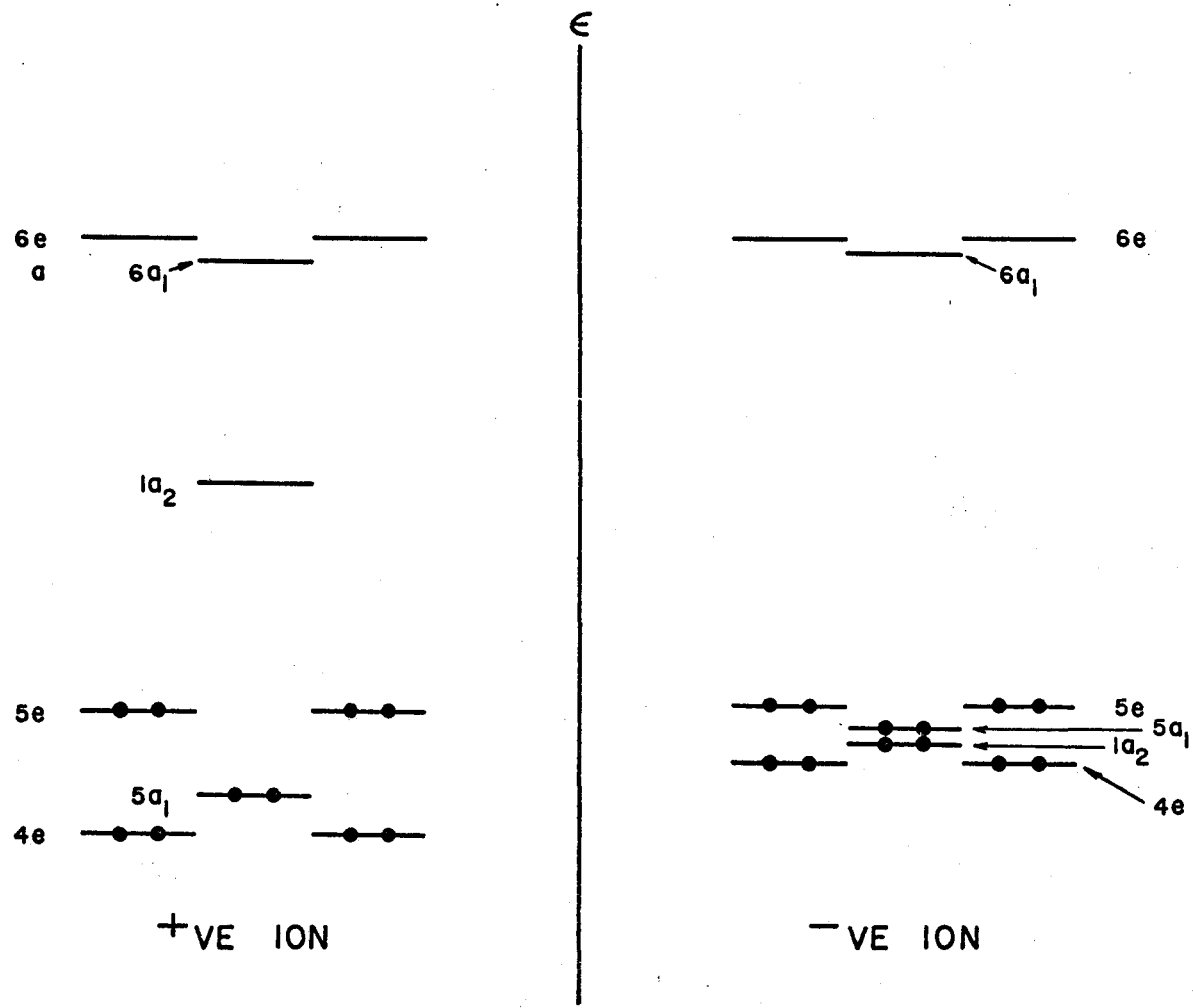

FIGURE 3·2 ORDERING OF THE MOLECULAR ORBITALS FOR THE GROUND STATE OF THE FSO_3^+ AND FSO_3^- IONS; ELECTRONS IN ORBITALS SHOWN AS •

a) SO_3F Radical Treated as an Ionization Product of SO_3F^-

In this approximation, the lowest energy state of the radical is obtained by the removal of an electron from the 5e orbital of the FSO_3^- ion in Fig. 3.2. The configuration of the ground state of the radical is therefore

$$(\ldots\ldots)\ (4e)^4\ (1a_2)^2\ (5a_1)^2\ (5e)^3 \qquad {}^2E$$

With this approximation, the ground state symmetry of the radical is calculated to be ^2E.

The next three lowest excited states in order of increasing energy were calculated to arise from the following electron configurations:

$$(\ldots\ldots)\ (4e)^4\ (1a_2)^2\ (5a_1)^1\ (5e)^4 \qquad {}^2A_1$$

$$(\ldots\ldots)\ (4e)^4\ (1a_2)^1\ (5a_1)^2\ (5e)^4 \qquad {}^2A_2$$

$$(\ldots\ldots)\ (4e)^3\ (1a_2)^2\ (5a_1)^2\ (5e)^4 \qquad {}^2E$$

The energy of the ground electronic state and the three lowest excited states of the radical were calculated using equation 3.14.

The atomic spin density Q_A for atom A was calculated for the radical from the coefficients of the singly occupied orbital k

$$Q_A = \sum_{\mu}^{(A)} C_{\mu k}^2 \qquad A = S,O,F \tag{3.24}$$

where the summation is over only those atomic orbitals centred on atom A.

The total charge density on atom A was also calculated using the relation

$$P_{AA}^{RAD} = P_{AA}^{-ION} - Q_A \qquad A = S,O,F \tag{3.25}$$

where P_{AA}^{-ION} is defined by equation 3.11.

The results of the above calculations are given in Tables 3.2, 3.3 and 3.4.

b) SO_3F Radical Treated as a Product of Electron Capture by SO_3F^+

In this approximation, the lowest energy state of the radical is obtained when an electron is added to the $1a_2$ orbital of the FSO_3^+ ion in Fig. 3.2. This gives the ground state configuration and symmetry of the radical as

$$(.....)\ (4e)^4\ (5a_1)^2\ (5e)^4\ (1a_2)^1\ (6a_1)^0 \qquad {}^2A_2$$

By direct calculation, it is found that the next lowest energy state of the radical is obtained not from the electron configuration

$$(.....)\ (4e)^4\ (5a_1)^2\ (5e)^4\ (1a_2)^0\ (6a_1)^1 \qquad {}^2A_1$$

but from the electron configuration

$$(.....)\ (4e)^4\ (5a_1)^2\ (5e)^3\ (1a_2)^2 \qquad {}^2E$$

This latter configuration for the radical is obtained by first adding an electron to the $1a_2$ orbital of the +ve ion and then promoting an electron from the 5e to the singly occupied $1a_2$ orbital. The next higher excited states are found by direct calculation to result from similar configurations. These are, in order of increasing energy

$$(.....)\ (4e)^3\ (5a_1)^2\ (5e)^4\ (1a_2)^2 \qquad {}^2E$$

and

$$(.....)\ (4e)^4\ (5a_1)^1\ (5e)^4\ (1a_2)^2 \qquad {}^2A_1$$

The energy of the $^2A_2$ ground state of the radical was calculated using equation 3.15. The energy of the above three excited states

obtained from the excitation of an electron from a doubly occupied orbital l to the singly occupied orbital k is given by

$$W_{RAD}^{EXCITED} = W_{ION}^{+} + 2\varepsilon_k^{+} - \varepsilon_l^{+} + J_{kk} - 2J_{jl} + K_{lk} \qquad (3.26)$$

The coulomb and exchange integrals, J and K respectively, in this expression were calculated from the molecular orbitals for the positive ions. The vertical excitation energies, charge densities, and spin densities are given in Tables 3.2, 3.3, and 3.4.

According to the positive ion calculation, the ground state of the radical is of $^2A_2$ symmetry. In this state, the odd electron occupies the $1a_2$ molecular orbital. With the basis set used in this calculation, there is only one a_2 molecular orbital. This orbital is composed of a symmetry-determined combination of oxygen $2p_x$ and $2p_y$ atomic orbitals*. The electron in this molecular orbital is therefore localized on the oxygens and is non-bonding with respect to the sulfur and fluorine atoms.

The next two doublet states of the radical are both of symmetry ^2E and correspond to the odd electron occupying two different e orbitals. The electrons in these e orbitals are mainly localized on the oxygen nuclei* although they do contribute slightly to π-bonding between sulfur and oxygen.

The $^2A_1$ state corresponds to the odd electron occupying the $5a_1$ molecular orbital. This orbital is delocalized over the whole of the

---

* This description is obtained from the calculated magnitudes of the orbital coefficients $C_{i\nu}$; the odd electron occupies the molecular orbital ψ_ν.

molecule*.

The qualitative descriptions of the lowest doublet states of the SO_3F radical which emerge from the two sets of calculations based on the ion approximation are very similar. According to these calculations, the four lowest doublet states of the radical are very close in energy and are well separated from the other excited states. Both treatments yield the same number of low lying states and the same symmetries $^2A_2$, $^2A_1$, ^2E and ^2E. However, the ordering of the levels is significantly different for the two models as shown in Fig. 3.3. In order to distinguish between the two ^2E states, the ^2E state higher in energy will be labeled $^2E(2)$ and the lower energy ^2E state will be labeled $^2E(1)$.

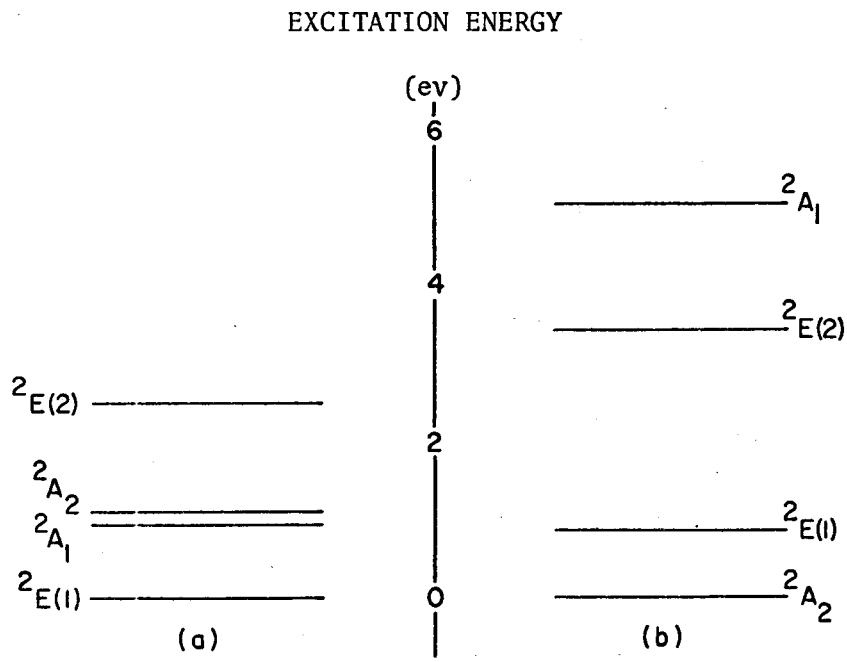

Fig. 3.3 Ordering of the four lowest doublet states of the radical as predicted by a) FSO_3^- ion calculation, b) FSO_3^+ ion calculation.

---

* This description is obtained from the calculated magnitudes of the orbital coefficients $C_{i\nu}$; the odd electron occupies the molecular orbital ψ_ν.

The reordering of the levels of the radical and the difference in the excitation energies between the two calculations is not surprising since the energy differences between these levels is small. The results of the open-shell calculations which are presented in the next section help resolve the problem of the ground state symmetry and the symmetries of the low lying excited states.

ii) Results from Approximation 2 — Open Shell Calculation

With this approximation, the electronic ground state of the radical was found to be of symmetry species $^2A_2$ in agreement with the results of the positive ion calculation. The energy of this state was determined to be a minimum at an OSF bond angle of 105°. This theoretically calculated OSF bond angle for the ground state of the radical agrees quite well with the experimentally determined OSF bond angle of 108.6°.

It is interesting to note that the ground state energy of the radical and the OSF angle at which this energy is a minimum are intermediate between the correspondingly calculated quantities for the ions. This correlation is displayed in Table 3.1.

TABLE 3.1

SOME CALCULATED QUANTITIES FOR FSO_3^+, $FSO_3^\cdot$, AND FSO_3^-

MOLECULAR SPECIES	*DIFFERENCE BETWEEN GROUND STATE ENERGY OF THE IONS AND THE GROUND STATE ENERGY OF THE RADICAL (ev.)	OSF ANGLE AT WHICH THE GROUND STATE ENERGY IS A MINIMUM
FSO_3^+	17.056	107°
$FSO_3^\cdot$	0.00	105°
FSO_3^-	- 6.133	102°

The orbital energies of the levels of the $^2A_2$ ground state are shown in Fig. 3.4. Throughout these calculations, the odd electron has been assigned an α spin. This is just a convenient convention since the same results would be obtained if this electron had been assigned a β spin.

From Fig. 3.4, it can be seen that the lowest excited states of the radical will be obtained by promotions of the electron in the β stack rather than within the α stack. Promotion of an electron from the β stack to the α stack gives a quartet state. The lowest quartet state was calculated to be between five and six electron volts above the $^2A_2$ ground state.

In this approximation, the lowest excited state of the radical is found to have $^2A_1$ symmetry and is obtained by the promotion of the electron in the $5a_1$ orbital of the β stack to the $1a_2$ orbital of the

* The differences are obtained by subtracting the ground state electronic energy of the radical at the potential minimum from the ground state electronic energies of the ions at the potential minima.

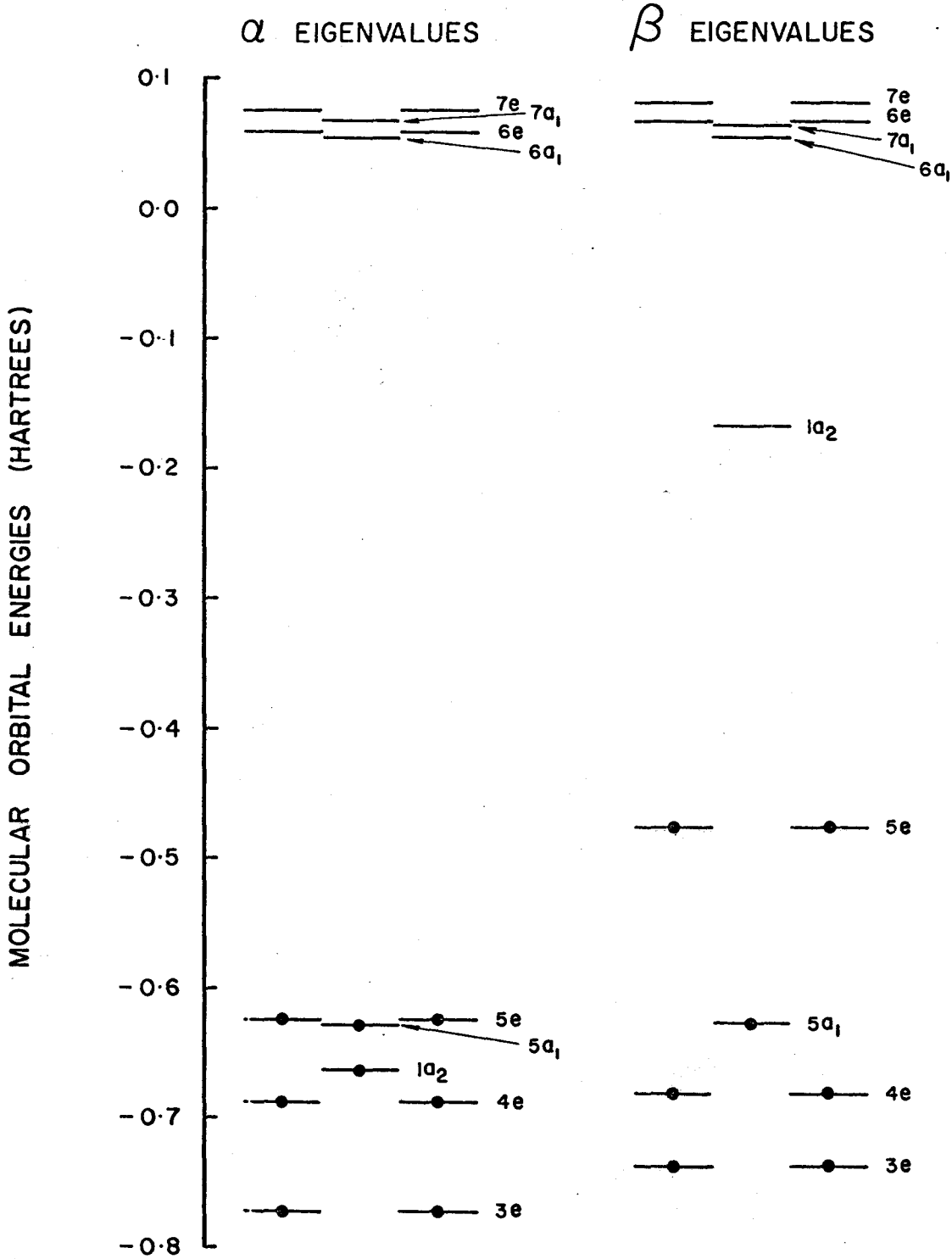

FIGURE 3·4 MOLECULAR ORBITAL ENERGIES FOR THE $^2A_2$ STATE OF THE SO_3F RADICAL

β stack.

The next highest state of the radical is calculated to be of ^2E symmetry. This state results from the transfer of the electron in the 5e orbital of the β stack to the unoccupied $1a_2$ orbital of the β stack.

The energy of the radical was calculated for different values of the OSF bond angle. The results of these calculations for the three lowest doublet states of the radical are shown graphically, as potential curves, in Fig. 3.5.

It can be seen that the energy of the radical is a minimum at OSF bond angles of 97° and 105° for the $^2A_1$ and $^2E(1)$ states respectively.

The open shell calculation does not lend itself to the calculation of more than one state of a given symmetry. Since the C_{3v} point group contains only three irreducible representations A_2, A_1 and E, and since states of the radical transforming as A_2, A_1 and E have already been calculated, the energy of the next lowest excited state above these three states could not be determined by the open shell calculation.

Energies of states higher in energy than the three previously calculated states of the radical were determined by the use of a virtual orbital theory[40] in conjunction with the open shell results of the $^2A_2$, $^2A_1$ and $^2E(1)$ states.

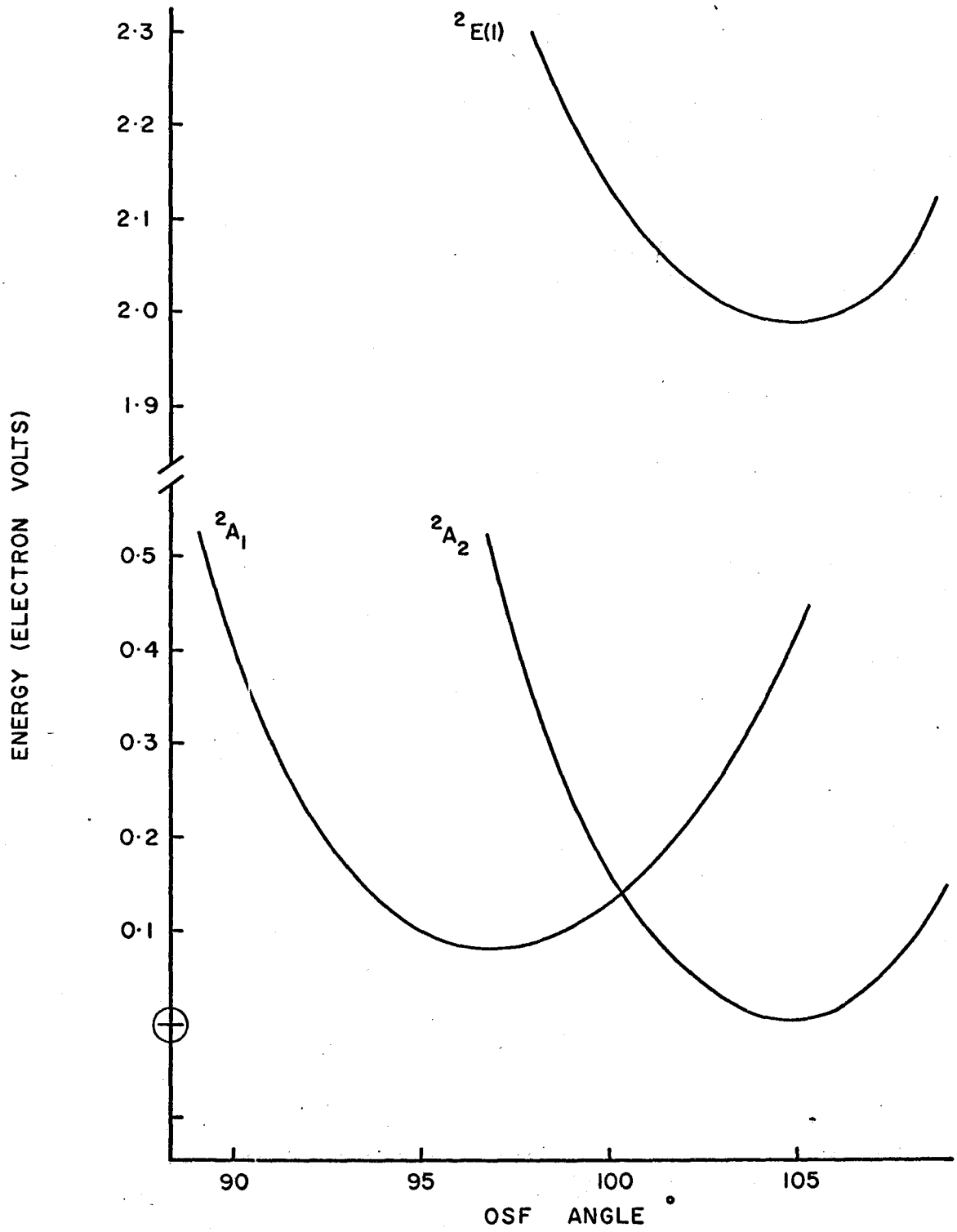

FIGURE 3·5 ENERGY OF THE THREE LOWEST DOUBLET STATES OF THE RADICAL AS A FUNCTION OF THE OSF BOND ANGLE. C_{3v} SYMMETRY IS ASSUMED FOR THE RADICAL.

In the virtual orbital approximation, the excited state is represented by a single determinantal wavefunction constructed using a virtual (unoccupied) orbital obtained by the minimization of the ground state energy. The energy of the excited state is expressed in terms of the energy of the $^2A_2$ ground state (or in terms of the calculated energy of one of the excited states, $^2A_1$ or $^2E(1)$) and a contribution which results from the reorganization of the electrons on excitation. The energy of an excited state obtained by the promotion of an electron in the kth molecular orbital of the β stack to the $1a_2$ orbital of the β stack is given in terms of the ground state energy by

$$W_{RAD}^{k\rightarrow a_2} = W_{RAD}^{^2A_2} + \varepsilon_{1a_2}^{\beta} - \varepsilon_k^{\beta} - (J_{1a_2,k}^{\beta\beta} - K_{1a_2,k}^{\beta\beta})$$

where $W_{RAD}^{^2A_2}$ is the open shell energy of the $^2A_2$ state and $\varepsilon_{1a_2}^{\beta}$ is the open shell energy for the $1a_2$ molecular orbital of the β stack.

The application of the virtual orbital open shell approximation to the results of the open shell calculation for the $^2A_2$, $^2A_1$ states gives $^2E(2)$ as the symmetry of the next lowest excited state above the $^2E(1)$ state and also gives approximately the same value for the electronic energy of the $^2E(2)$ state. The energy of the $^2E(2)$ state is found to be a minimum at an OSF bond angle of 105°. All other doublet states of the radical above the $^2E(2)$ state are found to be significantly higher in energy (at least 5-6 ev. above the $^2A_2$ state).

The calculated vertical transition energies between the ground electronic state and the three lowest excited states are given in Table 3.2.

The formal charge and spin density distributions for the three lowest doublet states of the radical are shown in Fig. 3.6. The formal charge on atom A is defined as

$$Z_A - P^{\alpha}_{AA} - P^{\beta}_{AA}$$

where P_{AA} is defined by equation 3.11 and Z_A is the net charge of the core of atom A. The formal charge is given in units of $|e|$, the magnitude of the charge of the electron.

The spin density on atom A is defined as

$$Q_{AA} = P^{\alpha}_{AA} - P^{\beta}_{AA}$$

since the odd electron was arbitrarily assigned an α spin.

The formal charge on the oxygen and fluorine atoms is negative and the formal charge on sulfur is positive for all three doublet states of the radical. The charge distributions for the $^2A_2$ and $^2E(1)$ states are quite similar. The only difference is a slight transfer of negative charge, relative to the $^2A_2$ state, from the sulfur to the oxygen and fluorine nuclei in the $^2E(1)$ state. The spin density distributions for these two states are also similar.

The charge and spin density distributions for the $^2A_1$ state are different from those of the other two states. In the $^2A_1$ state there is very little negative charge on the fluorine nucleus. Most of the negative charge on fluorine in the $^2A_2$ state has been transferred to the oxygen nuclei in the $^2A_1$ state of the molecule. This extra electronic charge on the oxygen nuclei leads to a greater electronic repulsion between them and it is not surprising that the OSF angle in the $^2A_1$ state (97°) is decreased with respect to the OSF angle

	FORMAL CHARGE DISTRIBUTION	SPIN DENSITY DISTRIBUTION
$^2A_2$	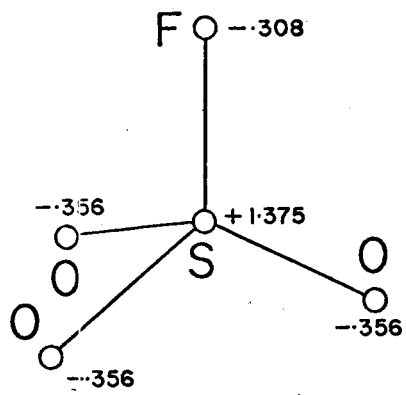	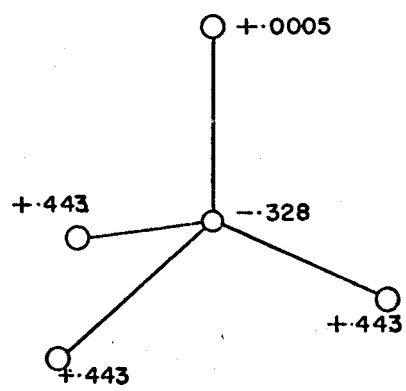
$^2A_1$	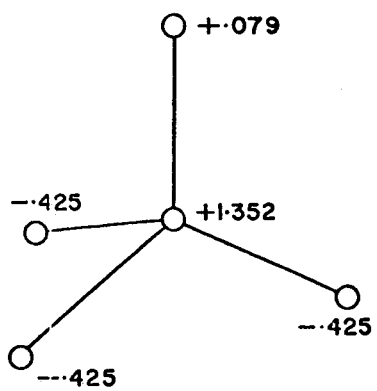	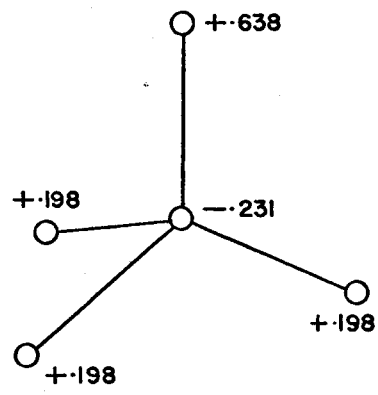
^2E	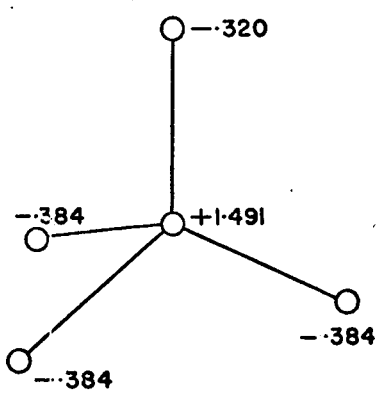	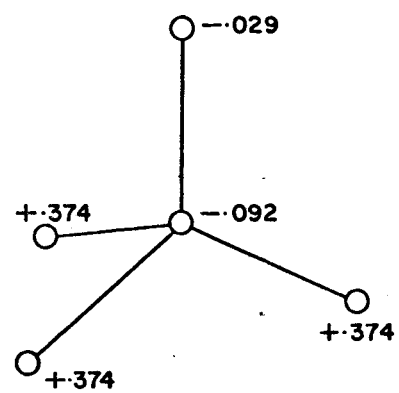

FIGURE 3·6 FORMAL CHARGE AND SPIN DENSITY DISTRIBUTIONS FOR THE LOWER ELECTRONIC STATES OF SO_3F·

of the $^2A_1$ state (105°).

The spin density on the fluorine nucleus is approximately 1000 times larger in the $^2A_1$ state than in the $^2A_2$ state. Since the isotropic fluorine hyperfine splitting is proportional to the electron density at the fluorine nucleus,[41] one would expect to observe a much larger fluorine hyperfine splitting for the radical in a $^2A_1$ ground electronic state than in a $^2A_2$ ground electronic state. The small isotropic fluorine hyperfine splitting observed in the E.S.R. spectrum of the FSO_3 radical[11] (~ 9.5 gauss) indicates that the ground state of the radical is not of symmetry $^2A_1$.

An interesting comparison can be made between the three approximate calculations by examining the charge and spin density distributions predicted by each of them for the $^2A_2$, $^2A_1$ and $^2E(1)$ states of the radical. These electron distributions are given in Tables 3.3 and 3.4.

The atomic charge densities calculated by all three methods agree fairly well, at least at a qualitative level. An exception to this is found with the positive ion calculation of the charge densities for the $^2A_1$ state of the radical. This model predicts an abnormally high charge density for the oxygens at expense of the charge on fluorine. In fact, fluorine is predicted to have a positive charge. It is not surprising that the energy predicted by the model for the transition $^2A_1 - {}^2A_2$ is so high. (See Table 3.2).

In general, the most serious discrepancies between the results of the three approximations are to be found in the calculated spin densities. For example, the large negative spin density found for the sulfur nucleus in the $^2A_2$ state of the radical by the open shell

calculation is not reproduced by the positive or negative ion approximations.

The vertical transition energies from the ground electronic state to the three lowest excited states of the radical, which were calculated from the three approximations, are summarized in Table 3.2. The experimentally observed vertical electronic excitation energies of the fluorosulfate radical are also given in Table 3.2.

The calculations suggest that the electronic symmetry of the ground state is $^2A_2$ and that there are three low lying states to which transitions from the ground state can occur. The agreement between the theoretically calculated excitation energies, determined from the open shell and negative ion approximations, and the experimentally observed vertical excitation energies, is quite reasonable. The agreement between the calculated energy of the lowest transition, determined from the positive ion calculation, and the corresponding experimentally observed transition is also quite good, whereas, the agreement between the energies of the next two higher transitions is poor.

All of the approximations predict that, for the four low lying states of the radical, one state has symmetry species $^2A_2$, one has $^2A_1$ and two have ^2E. However, the results of the calculations for each of the three approximations predict a different ordering of the levels.

The vibrational and rotational analyses of the third electronic transition (vertical excitation energy equals 2.422 ev.) are reported in detail in Chapters 5 and 6. The results of these analyses indicate that the observed transition is either $^2E - {}^2A_2$ or $^2E - {}^2A_1$. It is therefore proposed, in accordance with the predictions of the open shell approximation, that the three observed low energy transitions are $^2A_1 - {}^2A_2$,

$^2E(1) - {}^2A_2$ and $^2E(2) - {}^2A_2$ in order of increasing energy. These assignments are discussed further in Chapter 5.

The reliability of the results presented in this chapter is dependent upon three factors: the validity of the CNDO approximation, the approximate nature of the open shell method, and the unusual proximity of the four lowest doublet states.

The CNDO approximation has been used very successfully to calculate the ground state properties of a large number of molecules and also to calculate the excited states of a smaller number of molecules. The symmetries predicted for the ground state have always been found to be in agreement with experimental observations.

Since the open shell results appear to be simply refinements of the closed shell results, the open shell approximation appears to be valid.

The most serious problem is the small energy separation between the four low lying states of the radical under consideration. This small energy separation makes the determination of their order difficult. The order of the states which is predicted by the open shell calculation gives the best agreement with the observed results.

TABLE 3.2

Results from -VE ION		Results From +VE ION		Results From Open Shell Calculation		Experimental Results
ASSIGNMENT	ENERGY (ev)	ASSIGNMENT	ENERGY (ev)	ASSIGNMENT	ENERGY (ev)	ENERGY (ev)
$^2A_1$-^2E	0.996	^2E-$^2A_2$	0.832	$^2A_1$-$^2A_2$	0.419	0.870
$^2A_2$-^2E	1.020	^2E-$^2A_2$	3.403	^2E-$^2A_2$	1.983	1.619
^2E-^2E	2.530	$^2A_1$-$^2A_2$	5.152	^2E-$^2A_2$	2.851	2.422

Table 3.2 THEORETICAL AND EXPERIMENTAL EXCITATION ENERGIES

TABLE 3.3

ELECTRONIC STATE OF RADICAL / Approx. ATOM	$^2A_2$			$^2A_1$			^2E		
	OPEN SHELL	POSITIVE ION	NEGATIVE ION	OPEN SHELL	POSITIVE ION	NEGATIVE ION	OPEN SHELL	POSITIVE ION	NEGATIVE ION
OXYGEN	-0.3556	-0.4278	-0.3062	-0.4169	-0.5999	-0.4453	-0.3936	-0.4763	-0.3568
FLUORINE	-0.3077	-0.1500	-0.4586	-0.0993	+0.2581	-0.1078	-0.3205	-0.1500	-0.4498
SULPHUR	+1.3745	+1.4340	+1.3771	+1.3502	+1.5411	+1.4438	+1.4714	+1.5792	+1.5201

TABLE 3.3 Net Atomic Charge Densities for the Three Lowest Doublet States of the SO_3F Radical. The oxygen charge densities have been averaged over the three atoms.

TABLE 3.4

ELECTRONIC STATE OF RADICAL / APPROX. ATOM	$^2A_2$			$^2A_1$			^2E		
	OPEN SHELL	POSITIVE ION	NEGATIVE ION	OPEN SHELL	POSITIVE ION	NEGATIVE ION	OPEN SHELL	POSITIVE ION	NEGATIVE ION
OXYGEN	0.4425	0.3333	0.3333	0.2250	0.1618	0.1942	0.3737	0.2849	0.2827
FLUORINE	0.0005	0.0000	0.0000	0.5739	0.4081	0.3508	-0.0287	0.0000	0.0088
SULPHUR	-0.3278	0.0000	0.0000	-0.2488	0.1071	0.0667	0.0924	0.1453	0.1430

TABLE 3.4 Atomic Spin Density Distributions For The Three Lowest Doublet States Of The SO_3F Radical. The Oxygen Density Is The Average Over Three Atoms.

CHAPTER 4

VIBRATIONAL STRUCTURE OF ELECTRONIC STATES

4.1 Vibrational Structure of a Non-Degenerate Electronic State

4.1.1 Normal Modes of Vibration, Symmetry Classification

Only a brief summary of the theory of the vibrational structure of a non-degenerate electronic state is presented in this section. More detailed accounts of the theory are given by King,[42] Herzberg,[43,44] and Wilson, Decius and Cross.[45]

Molecules are assemblies of nuclei and electrons held together by electrostatic forces. A molecule, composed of N atoms, has 3N degrees of freedom. Six of these, for non-linear molecules, constitute the translational and rotational degrees of freedom of the whole system; the remaining 3N-6 represent the internal vibrations of the framework.

The complex vibrational motion of the molecule can be decomposed in terms of normal modes. A normal mode is a mode of vibration in which each nucleus reaches its position of maximum displacement at the same time, and each nucleus passes through its equilibrium position at the same time. Each normal mode is associated with a normal coordinate for the vibration.

The normal coordinates of vibration for a molecule can be determined by applying the proper similarity transformation to a set of Cartesian displacement coordinates with origins at the nuclei of the molecule. The procedure for obtaining this similarity transformation is described by Wilson, Decius and Cross.[46]

The symmetry classification and degeneracy of each of the normal modes, however, can be determined without an explicit knowledge of their form. By applying each of the symmetry operations of the molecular point group in turn to the set of Cartesian displacement coordinates, the matrices for their transformations under the operations can be determined. The set of matrices form a reducible representation of the molecular point group. Since the character of a matrix is invariant under a similarity transformation, the decomposition of this reducible representation into the irreducible representations of the molecular point group will give the irreducible representations to which the normal modes belong.

The fluorosulfate radical has $3N - 6 = 9$ fundamental vibrations of which three are doubly degenerate and transform as the e representation of the C_{3v} molecular point group. The remaining three transform as the a_1 representation.

A diagram representing the normal vibrations of a ZYX_3 type molecule is given by Nielsen.[47] From the diagram, reproduced in Fig. 4.1, a qualitative picture of the normal vibrations of the fluorosulfate radical can be obtained.

4.1.2 Vibronic Energies

The energy of a vibrating molecule is quantized. In a given electronic state, a polyatomic molecule may be excited to any of the possible vibrational levels. Each of these levels may be called a vibrational-electronic state or following Mulliken, a vibronic state. The energy of a vibronic level of a non-degenerate electronic state may be

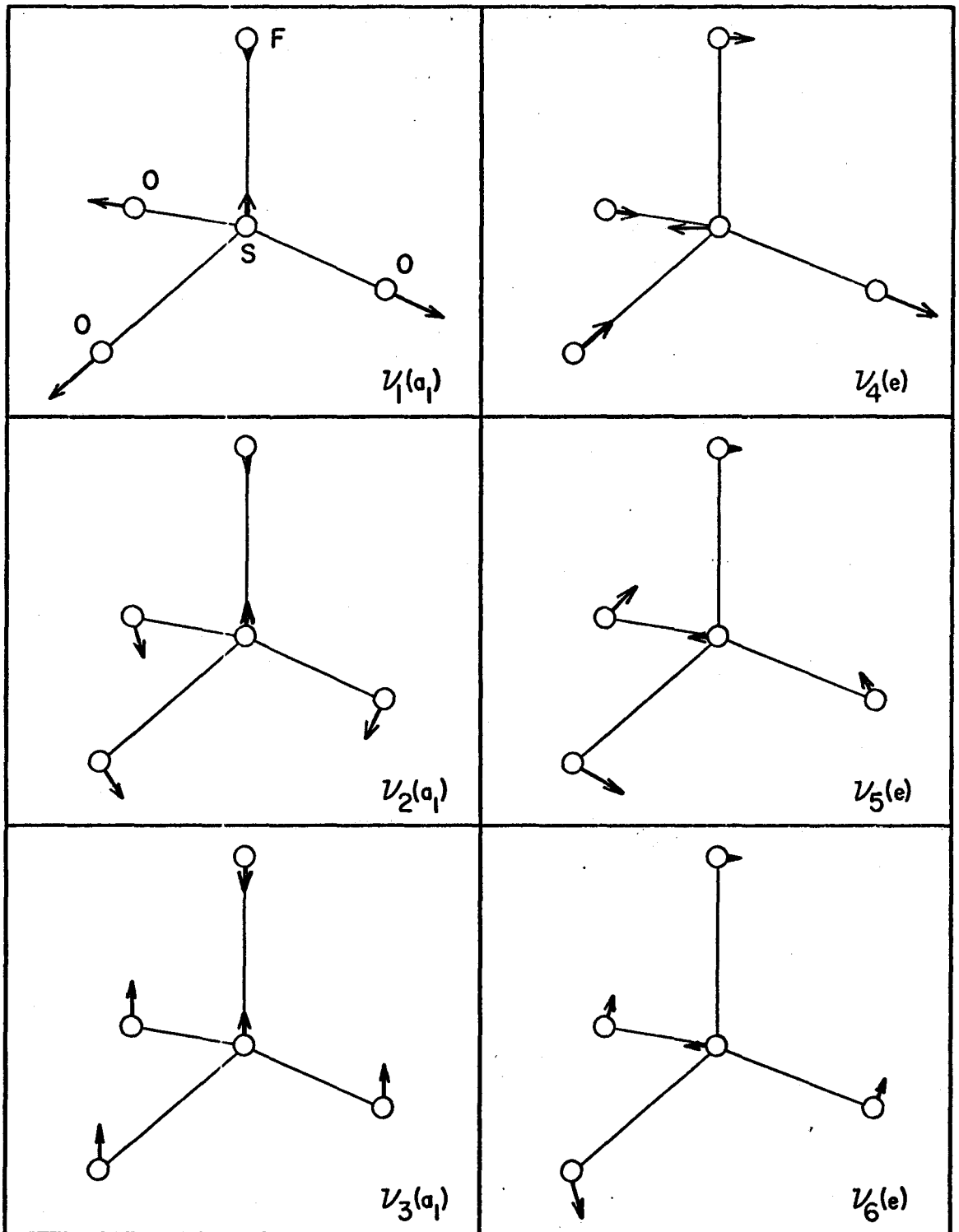

FIGURE 4·1 NORMAL MODES OF THE FLUOROSULFATE RADICAL

written as,

$$T = T_e + G(v_1,v_2,v_3\ldots) \tag{4.1}$$

where T and T_e are the term values of the vibronic level and the minimum of the potential surface of the electronic state respectively. $G(v_1,v_2,v_3\ldots)$ is the term value of the vibrational level and an empirical formula is given by Herzberg[48] as

$$G(v_1,v_2,v_3\ldots) = \sum_i \omega_i\,(v_i + d_i/2) + \sum_i \sum_{k\geq i} x_{ik}\,(v_i + d_i/2)\,(v_k + d_k/2)$$

$$+ \sum_i \sum_{k\geq i} g_{ik}\,l_i l_k \tag{4.2}$$

In this equation, v_i and v_k are the vibrational quantum numbers, ω_i are the vibrational frequencies for infinitesimal amplitudes, x_{ik} and g_{ik} are anharmonicity constants, d_i and d_k are the degeneracies (1,2 or 3) of the vibrations i and k, and l_i and l_k are vibrational angular momentum quantum numbers if either the i^{th} or k^{th} mode is doubly degenerate and excited with v quanta.

$$l_i = v_i, v_i-2, v_i-4, \ldots\ldots, 1 \text{ or } 0 \tag{4.3}$$

and similarly for l_k. For non-degenerate vibrations, $l_i = 0$ and $g_{ik} = 0$.

The first term on the right of equation 4.2 can be obtained from the solution of the time independent Schrödinger equation in which the molecule is assumed to "vibrate" in a quadratic potential well. The vibrational eigenfunctions obtained, using this approximation, are each a product of Hermite polynomials and an exponential function. The

remaining terms in equation 4.2 account for the fact that the vibrations of the molecule are in reality not harmonic, but anharmonic.

The symmetry of the vibrational eigenfunctions are determined by the manner in which the Hermite polynomials transform under the group symmetry operations.[49]

The vibrational wavefunction for the vibrationless ground state, the state in which $v_i = v_2 = \ldots = 0$, always transforms as the totally symmetric group representation. The vibrational wavefunction for the state in which $v_i = 1$ and all the remaining v_j's are zero generates an irreducible representation that transforms as the corresponding normal coordinate Q_i under the group symmetry operations. Vibrational wavefunctions for overtones of non-degenerate vibrations transform as the totally symmetric representation, if an even number of quanta are excited. If an odd number of quanta are excited, the resulting wavefunction transforms in the same way as the corresponding normal coordinate for that vibration. The symmetry of the vibrational wavefunction for the k^{th} overtone of a degenerate vibration is much more complex to determine and is found by taking symmetrical direct products. Symmetry species of the higher vibrational levels of degenerate vibrations are given by Herzberg.[50]

The symmetry species of the vibrational wavefunction for any level of the fluorosulfate radical can be obtained by application of the above theory. The symmetry species of the vibronic wavefunction is given by the direct product of the symmetry species of the vibrational wavefunction and the symmetry species of the electronic wavefunction.

4.1.3 Selection Rules and Intensities

The quantum mechanical probability of a transition between the states ψ' and ψ'' is proportional to the square of the transition moment integral defined by equation 1.11.

$$\bar{M} = \int \psi' \, \bar{P} \, \psi'' \, d\tau \tag{1.11}$$

where $\bar{P}$ is the electric dipole moment operator.

In the analysis of transitions between different electronic states, two approximations are generally made. The first approximation, the Born-Oppenheimer approximation, allows the total eigenfunction* to be written as the product

$$\psi = \psi_e \, \psi_v \tag{4.4}$$

The dipole moment operator $\bar{P}$ can be divided without approximation into

$$\bar{P} = \bar{P}_e + \bar{P}_n \tag{4.5}$$

where $\bar{P}_e$ and $\bar{P}_n$ are the electric dipole moment operators associated (classically) with the charge distributions of the electrons and nuclei respectively. Thus, equation 1.11 can now be written as the sum of two terms

$$\bar{M} = \int \psi_v' \, \bar{P}_n \, \psi_v'' \, d\tau_n \int \psi_e' \, \psi_e'' \, d\tau_e + \int \psi_v' \, \psi_v'' \, d\tau_n \int \psi_e' \, \bar{P}_e \, \psi_e'' \, d\tau_e \tag{4.6}$$

The single and double primes refer to the upper and lower states respectively for a given transition.

---

* The rotational portion of the total wavefunction is assumed to have been previously factored out and is disregarded.[51]

Since the electronic eigenfunctions for different electronic states are orthogonal the first term of equation 4.6 vanishes.

The square of the second term of equation 4.6 gives the probability of a transition arising from a vibronic level of the ground electronic state $\psi''_e \psi''_v$ and terminating on a vibronic level of an excited electronic state $\psi'_e \psi'_v$. The second part of this equation

$$\bar{M}_e = \int \psi'_e \bar{P}_e \psi''_e \, dT_e \qquad (4.7)$$

depends upon the nuclear coordinates R since the electronic eigenfunctions contain these coordinates as parameters. Therefore, the second approximation made is that the electronic eigenfunctions are calculated at the equilibrium position of the nuclei in the initial state. As a result of this approximation, $\bar{M}_e$ becomes independent of the nuclear coordinates. The advantage achieved by this is the fact that the force field of the nuclei in which the electronic motion takes place generally has greater symmetry in the equilibrium position than the force field upon random displacement of the nuclei. When $\psi_e (R_o)$ is used, more selection rules are obtained which are violated to the extent to which the symmetry of the molecule is lost in a nuclear vibration. This latter point will be discussed in Sec. 5.2.

For the fluorosulfate radical, $\bar{M}_e$ is zero only for transitions between an electronic state of symmetry species A_1 and an electronic state of symmetry species A_2. All other electronic states can combine spectroscopically with each other. This rule, however, can break down if

the vibrational and electronic motions are not separable. See Sec. 4.2 and 5.2.

The quantity

$$\int \psi'_v \, \psi''_v \, d\tau_n \tag{4.8}$$

in equation 4.6 gives the magnitude of the overlap for the vibrational eigenfunctions in the two combining electronic states. This term is non-zero only if the direct product for ψ'_v and ψ''_v contains a component that transforms like the totally symmetric representation of the point group for the molecule.

4.2 Vibronic Interaction

The results of the previous section are obtained by assuming that there is no interaction between the electronic and vibrational motions. This assumption is generally a good approximation for non-degenerate electronic states but is inadequate for a discussion of degenerate electronic states. The results of Chapter 3 indicate that at least one of the upper states of the fluorosulfate radical is a degenerate E state. The theory of vibrational-electronic (vibronic) interactions must now be examined. The problem is further complicated by the fact that the radical has an odd number of electrons and hence non-zero resultant spin angular momentum. The electronic states are doublets* Spin-orbit coupling is more likely to have an appreciable magnitude in a ^{2}E state since, in a degenerate electronic state, there is a component of electronic angular momentum[52]

* Quartet states are also possible but since they occur at high energy with respect to the ground state (Chapter 3), they will not be considered.

$$\zeta_e \hbar \tag{4.9}$$

along the figure axis of the molecule with which the spin angular momentum of the odd electron can couple magnetically.

$$\zeta_e = \int \psi_e \mid L_z \mid \psi_e \, dT_e \tag{4.10}$$

where L_z is an angular momentum operator which projects out of the electronic wavefunction the component of electronic angular momentum along the z axis. The value of ζ_e can be non-integral.[52]

For non-degenerate electronic states, the electronic angular momentum is zero and hence there will be no simple first order coupling of the spin and electronic angular momenta.

The effect of the above interactions on the potential function of a ^2E electronic state has been discussed qualitatively by Herzberg[53] but as yet no quantitative calculations have been carried out. In order to analyse the bands resulting from a ^2E - $^2A_2$ electronic transition, a calculation with these interactions present is desirable and the remainder of this chapter is devoted to a treatment of this.

Two types of vibronic interaction can occur in polyatomic molecules:

1) The coupling of vibrational and electronic motions in a degenerate electronic state whereby the electronic orbital degeneracy is removed to an extent depending on the strength of the interaction. Approximation 1 of Sec. 4.1.3 is no longer a good one.

2) The mixing of zeroth order electronic states, $\psi_e(R_0)$ by totally or non-totally symmetric vibrations. When this interaction is large, approximation 2 of Sec. 4.1.3 breaks down.

The first type of interaction is known as the dynamical* Jahn-Teller effect[54] for non-linear molecules. The second type of interaction, known as the Herzberg-Teller effect[51] is responsible for the partial breakdown of symmetry selection rules in polyatomic spectra and is of major importance in causing "forbidden" electronic spectra to appear by intensity borrowing. This latter effect will be discussed further in Sec. 5.2. Since the transition $^2E - {}^2A_2$ is electronically allowed only the effects of the first interaction will be treated in this chapter.

4.3 Jahn-Teller - Spin-Orbit Interaction

Jahn and Teller[54] in 1937 and Jahn[55] in 1938 proved theorems which state that a geometrical configuration in which the electronic state is degenerate cannot be stable except in the following cases:

i) The configuration of the degenerate electronic state is linear.

ii) The system contains an odd number of electrons and the degeneracy is the two-fold Kramer's degeneracy[56] which cannot be removed by any non-magnetic interaction such as a change in the electrostatic field of the molecule by the excitation of a non-totally symmetric vibration.

A $^2A_1$ or a $^2A_2$ state of the fluorosulfate radical is doubly degenerate with respect to the spin of the odd electron. This, however, is a Kramer's degeneracy and because of ii) the molecule can be stable in the symmetrical configuration. A ^2E state of the fluorosulfate radical

* The "dynamical" Jahn-Teller effect is concerned with the vibronic interaction itself while the "static" Jahn-Teller effect has to do with energetic considerations concerning the nonvibrating molecules.

on the other hand is four-fold degenerate (two-fold due to orbital degeneracy and two-fold due to spin degeneracy). In order to describe this state, the effect of both a Jahn-Teller and a spin-orbit perturbation must be considered. These two perturbations compete against one another in the following way. For large spin-orbit coupling, the ^2E state will split into two states of symmetry species $^2E_{1/2}$ and $^2E_{3/2}$. The introduction of a small vibronic interaction will introduce no further splittings, and will not lead to instability of the molecule in these states since the $^2E_{1/2}$ and $^2E_{3/2}$ states are both Kramer's doublets. For a large vibronic interaction and a small spin-orbit interaction the molecule is not stable in the symmetrical configuration and distorts in order to remove the orbital degeneracy. This distortion quenches the electronic angular momentum and thus there is no large component of orbital angular momentum present in the molecule with which the spin can couple or interact.

For the intermediate case, the case in which both interactions are of equal magnitude, both perturbations must be considered simultaneously.

A cross-section of the potential surface of the molecule in a ^2E state is shown in Fig. 4.2 for each of the three above cases. In this diagram, the abscissa is one of the components of a degenerate e-type normal coordinate, Q_{e_+}. It can be seen that two potential surfaces are obtained for the intermediate case. The upper surface has a single minimum in the symmetrical configuration ($Q_{e_+} = 0$); the lower surface has two minima off the axis ($Q_{e_+} \neq 0$) and a maximum in the symmetrical configuration. For large displacements of the nuclei in a non-totally symmetric degenerate vibration ($Q_{e_+} >> 0$) it can be seen that the two Jahn-Teller-spin-orbit potential functions approach the two Jahn-Teller potential functions.

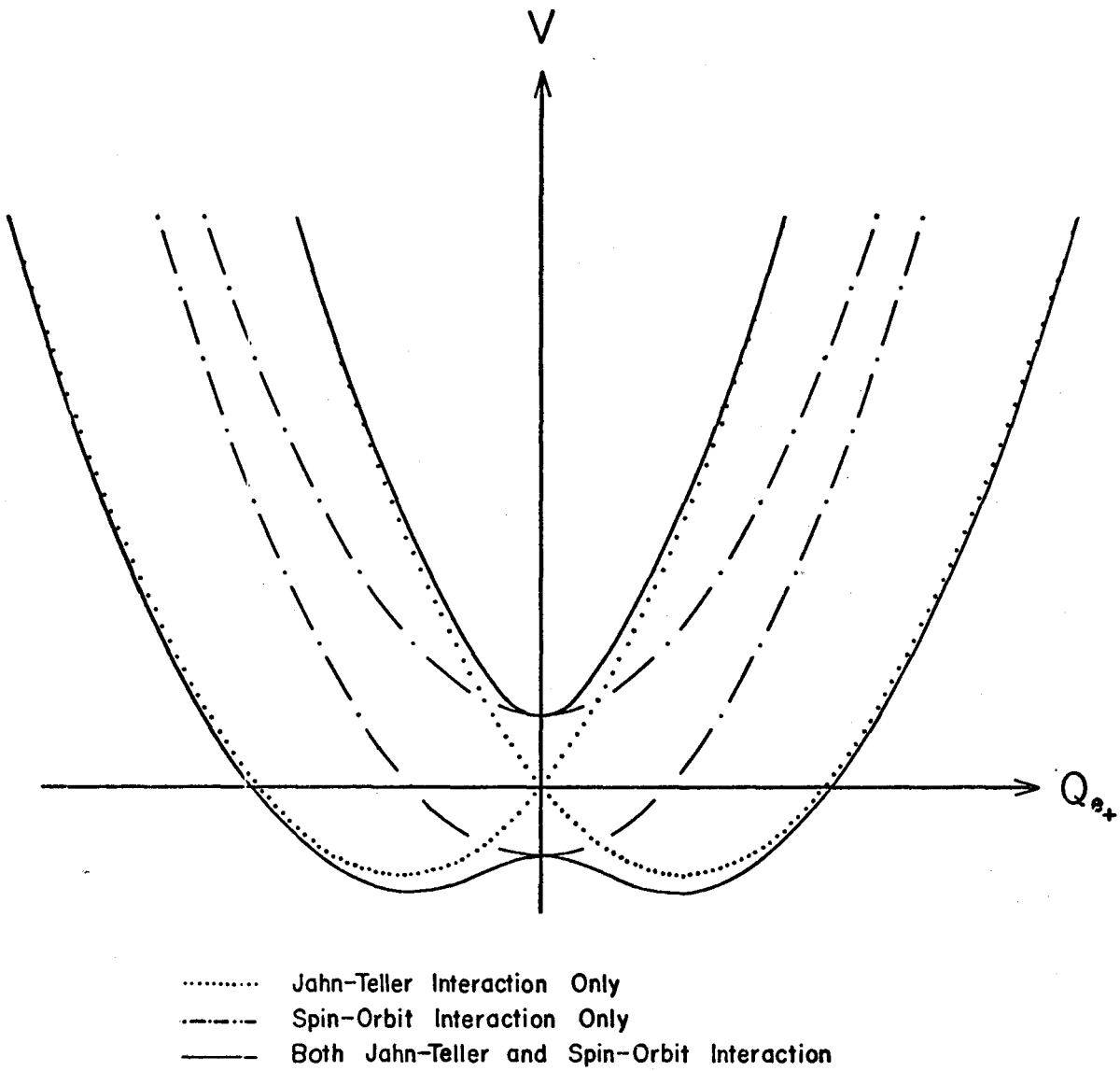

FIGURE 4·2 CROSS-SECTIONS THROUGH THE POTENTIAL SURFACES OF A DOUBLET ELECTRONIC E STATE

In effect, the spin-orbit interaction for half-integral spin reduces the instability, produced by the orbital degeneracy, of a molecule in its symmetrical configuration ($Q_{e_+} = 0$).

The species of the normal vibration that causes a molecule to be unstable in a degenerate E state of C_{3v} molecule is e.[57] There are three e-type vibrations for the fluorosulfate radical. Each of these can theoretically lead to instability of the molecule with respect to the symmetrical configuration of the nuclei.

The calculation of the Jahn-Teller effect in which a doubly degenerate electronic state interacts with three doubly degenerate vibrations is very complex and introduces too many unknown parameters. Hence, the first assumption made in this calculation is that only one of the degenerate e type vibrations is effective in removing the instability. The validity of this assumption for SO_3F can be checked by examination of the observed spectrum since the strength of the interaction of a degenerate vibration with the degenerate electronic state can be approximately determined by the ratio of the intensity of the 1-0 transition to the intensity of the 0-0 transition.[58] See Sec. 5.3(v)

The calculation of the energy levels for this Jahn-Teller-spin-orbit interaction was modeled on the method used by H.C. Longuet-Higgins, U. Öpik, M.H.L. Pryce and R.A. Sacks[59] and Moffitt and Thorson[60] to calculate the effect of a pure Jahn-Teller interaction.

These authors[59] assumed as a model an elliptically deformable ring on which an electron was constrained to move. They then showed that this model faithfully represented the essentials of the problem, so that mathematical results obtained from it could be used to interpret

the properties of physical systems of which the model was only an abstract representation. A diagram representing the model is given in Fig. 4.3.

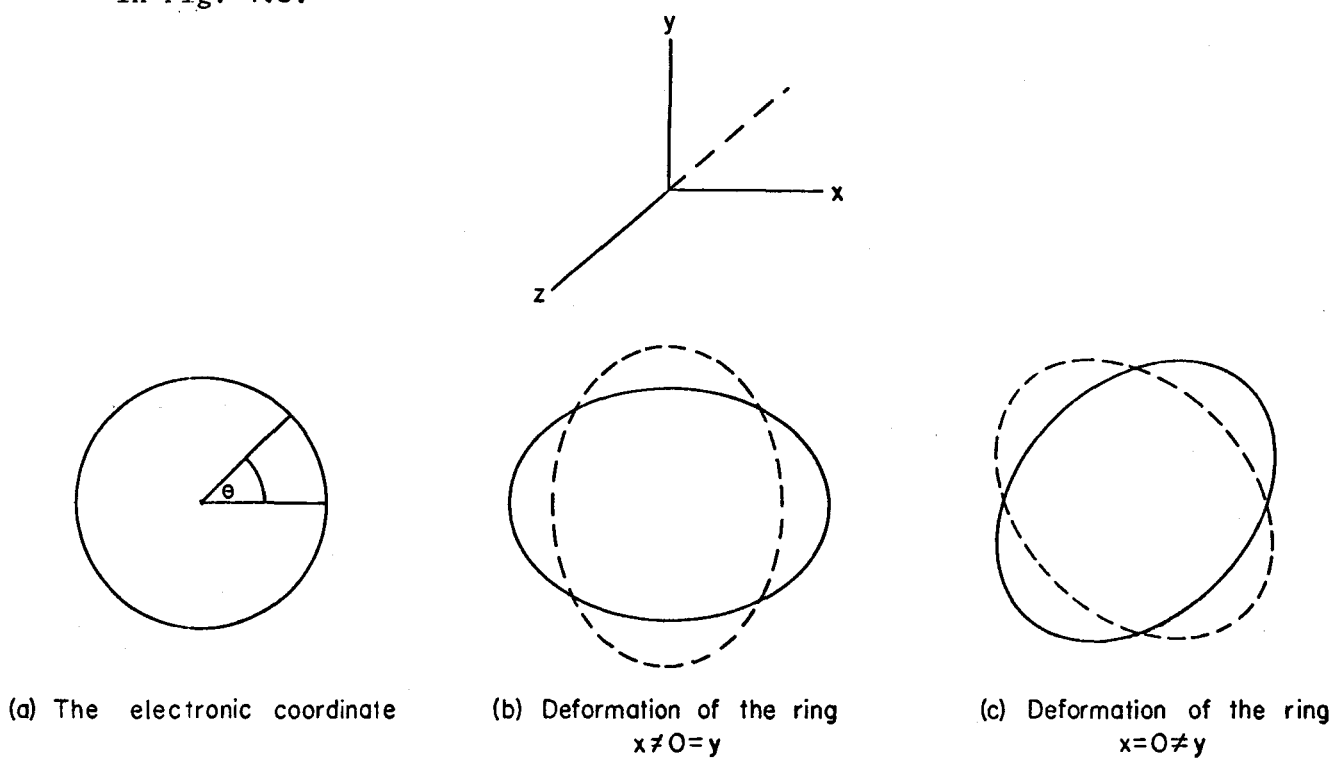

(a) The electronic coordinate

(b) Deformation of the ring $x \neq 0 = y$

(c) Deformation of the ring $x = 0 \neq y$

FIGURE 4·3 MODEL SYSTEM EXHIBITING THE JAHN–TELLER EFFECT.

The electron moves on a circular ring about the z-axis and Θ is the angular coordinate of the electron relative to a fixed direction. The ring can undergo an elliptical deformation in its plane and this deformation is represented as doubly degenerate vibration with normal coordinates x and y. In terms of the corresponding polar coordinates r, ϕ, defined by

$$x+iy = re^{i\phi} \tag{4.11}$$

the magnitude of the deformation is r and the direction of its major axis is 1/2 ϕ. In order to include spin-orbit interaction, their model has to be extended. This was done by including the spin angular momentum of the electron.

If there is no coupling between the orbital motion of the electron, its spin, or motion of the ring, the wavefunction for the combined system takes the form

$$\Psi = \psi_{n1}\ (r,\phi)\ e^{i\Lambda\theta}\psi_{\substack{\alpha \\ \beta}} \tag{4.12}$$

where $\psi_{n_1}(r,\phi)$ is assumed to satisfy the wavefunction for an isotropic two-dimensional harmonic oscillator. The solutions to this equation are given by Pauling and Wilson[61] as

$$\psi_{n1}(r,\phi) = \rho_{n|1|}(r)e^{im\phi} \tag{4.13}$$

$$E_{n1} = n \tag{4.14}$$

where n = 1, 2,..., and 1 = n-1, n-3, ..., n+1.

n and 1 are vibrational and vibrational angular momentum quantum numbers respectively. $\rho_{n|1|}(r)$[62] are polynomials related to the associated Laguerre polynomials.

The term $e^{i\Lambda\theta}$ represents the orbital motion of the electron and the electronic angular momentum quantum number Λ equals

$$\Lambda = 0,\ \pm 1,\ \pm 2\ .... \tag{4.15}$$

$\psi_{\substack{\alpha \\ \beta}}$ are the electron spin functions defined by the equations

$$\hat{S}_z \psi_\alpha = + 1/2 \psi_\alpha$$

$$\hat{S}_z \psi_\beta = - 1/2 \psi_\beta \qquad (4.16)$$

The coupling between the orbital motion of the electron and the ring is given by

$$H' = kr \left[e^{i(2\theta-\phi)} + e^{-i(2\theta-\phi)} \right] + gr^2 \left[e^{i(4\theta-2\phi)} + e^{-i(4\theta-2\phi)} \right] + \ldots . \qquad (4.17)$$

where k and g are constants.

If terms higher than first-order terms in r are neglected, then the only non-vanishing matrix elements of the form

$$\left\langle \psi^{\Lambda}_{n,l} \left| H' \right| \psi^{\Lambda'}_{n'l'} \right\rangle \qquad (4.18)$$

are those for which

$$\begin{aligned} \Lambda' &= \Lambda+2 \quad ; \quad l' = l-1 \\ \Lambda' &= \Lambda-2 \quad ; \quad l' = l+1 \end{aligned} \qquad (4.19)$$

If interactions between different electronic states are ignored then $|\Lambda| = |\Lambda'|$. This restriction and the above restrictions are only satisfied if $|\Lambda| = 1$.

The levels which interact under the perturbation H' are shown in Fig. 4.4. Each dashed line joins a pair of interacting levels and the symbols + and - indicate values of +1 and -1 respectively. From the diagram, it can be seen that only those levels with $j = l + 1/2$ Λ interact. In this calculation, 2j is the total angular momentum

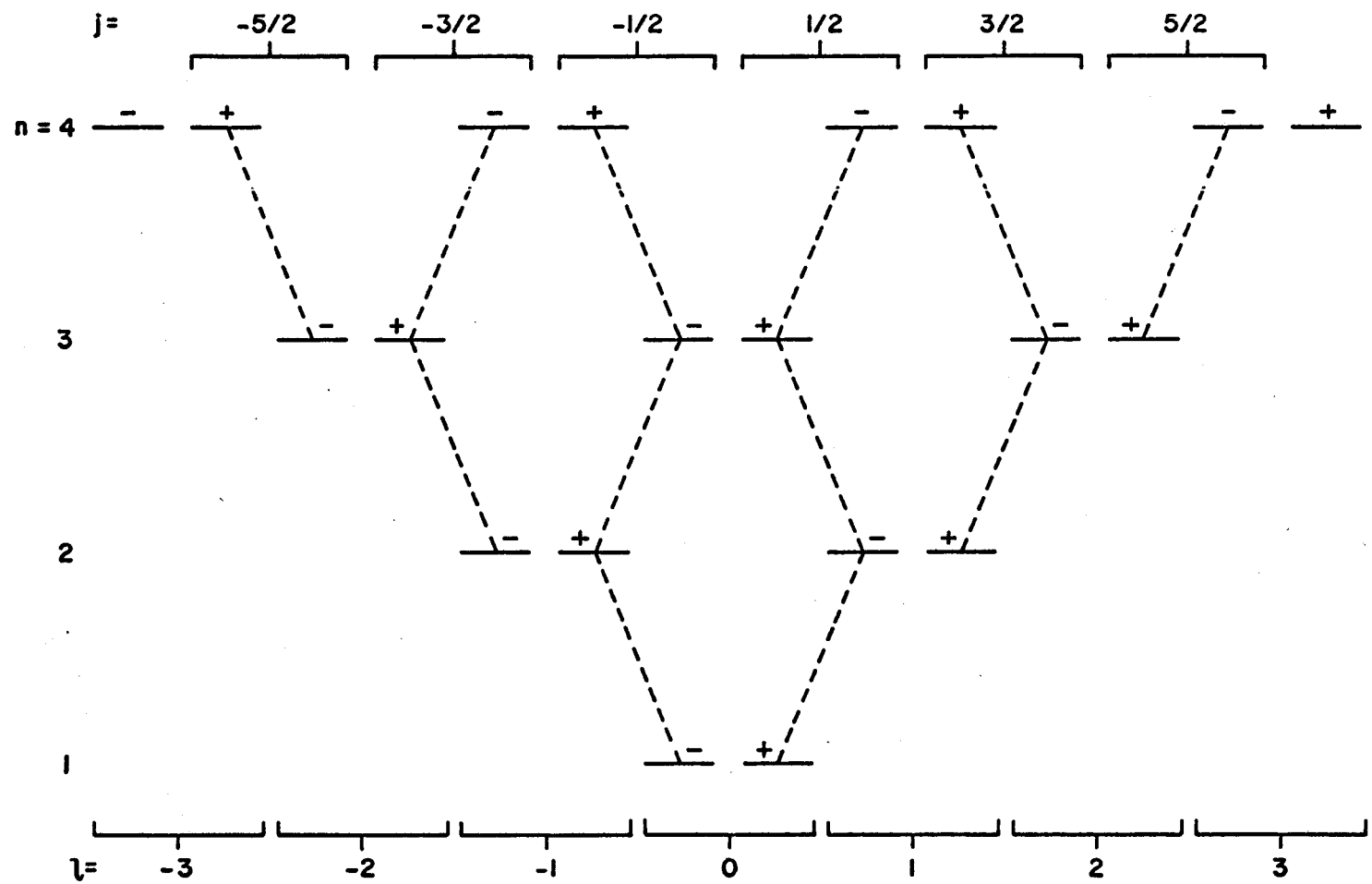

FIGURE 4·3 LEVELS WHICH INTERACT UNDER THE PERTURBATION H'

(excluding spin).

A perturbing Hamiltonian of the form

$$H'' = A\,\Lambda\hat{S}_z \tag{4.20}$$

where A is the spin-orbit coupling constant, introduces a coupling between the orbital motion of the electron and its spin. Since components of orbital angular momentum perpendicular to the C_3 axis of a C_{3v} molecule are largely quenched, a Hamiltonian of this form takes into account the most important part of the spin-orbit coupling.

Since the perturbation H' mixes together levels whose values are +1 and -1 respectively, the correct wavefunction will be of the form

$$\begin{aligned}\Psi_\alpha &= \psi^+(r,\phi)\, e^{i\theta}\, \psi_\alpha + \psi^-(r,\phi)\, e^{-i\theta}\, \psi_\alpha \\ \Psi_\beta &= \psi^+(r,\phi) e^{i\theta}\, \psi_\beta + \psi^- (r,\phi)\, e^{-i\theta}\, \psi_\beta\end{aligned} \tag{4.21}$$

Application of variational theory in the same manner as was done by Longuet-Higgins and others[59,63] leads to a set of equations for ψ^+ and ψ^-. These functions are coupled together by H' and may be written in the compact form

$$\begin{bmatrix} H_o + A\hat{S}_z - E, & kre^{-i\phi} \\ kre^{i\phi}, & H_o - A\hat{S}_z - E \end{bmatrix} \begin{bmatrix} \psi^+(r,\phi)\,\psi_{\alpha\atop\beta} \\ \psi^-(r,\phi)\,\psi_{\alpha\atop\beta} \end{bmatrix} = 0 \tag{4.22}$$

where H_o is the unperturbed two-dimensional oscillator Hamiltonian.

In order to solve the above equations, ψ^+ and ψ^- are expanded in terms of two-dimensional oscillator functions $\psi_{nl}(r,\phi)$ defined by equation 4.13

$$\psi_j^+ = a_1 \psi_{l+1,1} + a_3 \psi_{l+3,1} + a_5 \psi_{l+5,1} + \cdots$$

$$\psi_j^- = a_2 \psi_{l+2,l+1} + a_4 \psi_{l+4,l+1} + a_6 \psi_{l+6,l+1} + \cdots \qquad (4.23)$$

The matrix elements of $re^{\pm i\phi}$ between the functions $\psi_{n,l}$ and $\psi_{n,l+1}$ which enable equation 4.22 to be converted into matrix form are given by Longuet-Higgins and others.[59] Multiplying on the left by $\psi_{n,l+1}$ or $\psi_{n,l}$ and integrating, the matrix equation 4.24 given in Table 4.1 is obtained.

In this treatment, dimensionless units have been employed. The unit of energy is the zero-point energy of the two-dimensional harmonic oscillator in the absence of any coupling ($\hbar\omega$). In a physical system, k^2 equals twice the depression of the nuclear potential minimum, measured from the value of the potential function at the symmetrical configuration of the nuclei, divided by the zero-point energy of the unperturbed vibration.

The previous matrix equation, Table 4.1, is unbounded and contains two unknown parameters, k and A. However, since the results are to be compared with experiment, ω must also be known and therefore the number of unknowns is really three.

In this calculation, no attempt was made to determine an analytical solution. Trial values were inserted for the unknown parameters and the

TABLE 4·1

MATRIX EQUATION 4·24

$$
\begin{bmatrix}
l+1\pm A/2-E & k\sqrt{l+1} & & & & \\
k\sqrt{l+1} & l+2\mp A/2-E & k\sqrt{l} & & & \\
 & k\sqrt{l} & l+3\pm A/2-E & k\sqrt{l+2} & & \\
 & & k\sqrt{l+2} & l+4\mp A/2-E & k\sqrt{2} & \\
 & & & k\sqrt{2} & l+5\pm A/2-E & \cdots
\end{bmatrix}
\begin{bmatrix}
a_1^{\alpha,\beta} \\ a_2^{\alpha,\beta} \\ a_3^{\alpha,\beta} \\ a_4^{\alpha,\beta} \\ a_5^{\alpha,\beta} \\ \vdots
\end{bmatrix}
= 0
$$

eigenvalues were determined by numerical methods using an IBM 7040 computer. The size of the matrix was increased until convergence was obtained for the lower eigenvalues and eigenvectors. A further check on the diagonalization was obtained by comparing the results in the limit of zero spin-orbit coupling with those obtained by Moffitt and Thorson[60] in their treatment of a pure Jahn-Teller interaction. The results were identical to six significant figures for the first ten eigenvalues. The trivial calculation in the limit for zero Jahn-Teller interaction also gave the correct results.

Fig. 4.5 shows the variation of the energy levels as a function of k^2 for a fixed spin-orbit coupling constant of 30 cm^{-1}. For these results, ω was arbitrarily chosen to be 300 cm^{-1}. It can be seen that as the Jahn-Teller interaction parameter k^2 increases, the spin-orbit splitting decreases. This spin-orbit splitting would be expected to decrease because as the coupling of the vibrational and electronic motions increases, the molecule tends more and more away from its symmetrical C_{3v} configuration. This leads to a quenching of the electronic angular momentum and hence a reduction in the spin-orbit splitting.

From the diagram, it can also be seen that the splitting of each level for a particular value of k^2 is not a constant. The inclusion of spin-orbit coupling leads to a very complicated ordering of the energy levels.

The previous calculation is an approximate one. Interactions with the other degenerate vibrations should also be considered but were not because their inclusion would increase the number of unknown parameters to seven. For the same reason, only the linear term of the perturbing Hamiltonian H' was used in the calculation.

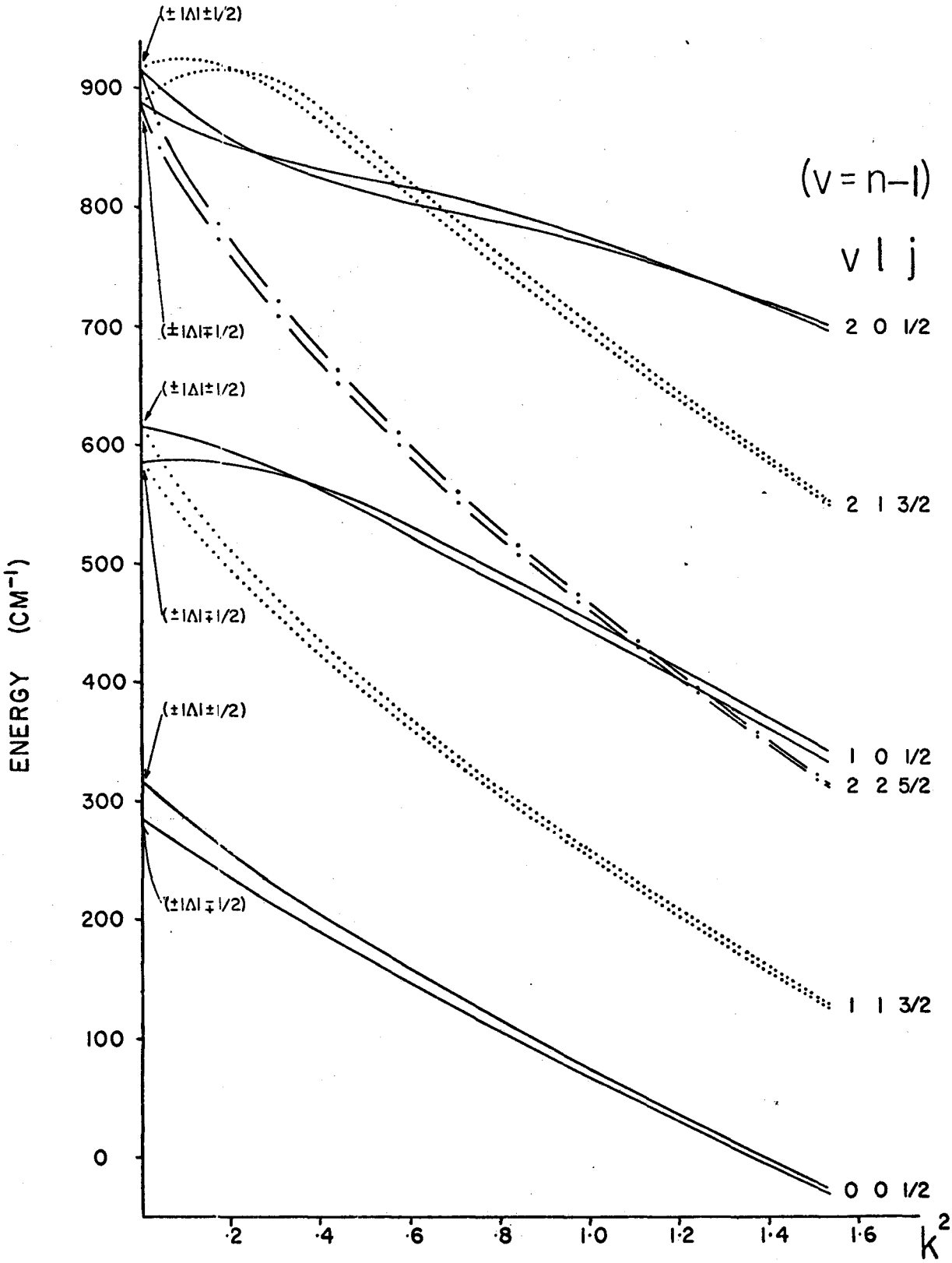

FIGURE 4·5 Variation of the energies of the lower vibronic levels of a degenerate vibration of a ^2E electronic state as a function of the JAHN-TELLER parameter k^2 for a fixed spin-orbit coupling constant of 30 cm^{-1}. A freq. of 300 cm^{-1} is assumed.

Although derived from a rather simple theory, the results should at least be qualitatively correct and helpful in the assignment of the visible spectrum of the fluorosulfate radical. The comparison of the theoretical results with the experimental results is given in the following chapter.

CHAPTER 5

ANALYSIS OF THE FLUOROSULFATE RADICAL SPECTRA

5.1 Electronic Transitions

The results that will be discussed in this section were obtained from a low resolution spectral study of the equilibrium mixture of peroxydisulfuryl difluoride and the fluorosulfate free radical using the Cary 14 spectrophotometer. Henceforth, these two species will be referred to as the dimer and the radical respectively.

Since the equilibrium

$$S_2O_6F_2 \rightleftharpoons 2SO_3F$$

is temperature dependent, the observed spectra are assigned to the radical or the dimer according to the temperature dependence of the absorbance for each system of absorption. As the temperature is increased, the above equilibrium is shifted to the right. Thus, an increase in temperature will increase the radical concentration, and hence will lead to an increase in any absorbance caused by the radical.

Three absorption systems were observed in the near infrared and visible regions of the spectrum. These systems have been labelled 1,2, and 3. The range of absorption, the wavelength region of the most intense absorption, and the oscillator strength* is given in Table 5.1 for each of these systems.

---

* The oscillator strengths were calculated by means of equations given by Robinson.[64]

TABLE 5.1

ELECTRONIC ABSORPTION SYSTEMS OF THE FLUOROSULFATE RADICAL

System	Range of Absorption	Region of Intense Absorption	Oscillator Strengtl
1st	20,000-10,000 Å	14,000-13,000 Å	$5X10^{-4}$
2nd	10,000- 5,700 Å	8,400- 7,200 Å	$2X10^{-3}$
3rd	5,500- 3,600 Å	5170 Å	$5X10^{-2}$

The third absorption system has previously been reported by Dudley and Cady[5] and also by Schumacher.[10] Both groups assigned this observed spectrum (3^{rd}) to the radical. Schumacher also noted that the third system was overlapped by a relatively strong continuum which begins at approximately 4600 Å. Our results confirm this observation. The intensity of the continuous absorption gradually decreases from this point to 3700 Å, and then rapidly decreases in intensity to 3300 Å. From 3300 to 2700 Å, the intensity of the absorption is constant. From 2700 Å downwards, the intensity of the absorption rises strongly to 2000 Å.

The strong continuous absorption between 2700 and 2000 Å is present even when the partial pressure of the radical is so small, that the absorption system of the radical in the visible region (3^{rd}) cannot be detected. Furthermore, the variation of the intensity of the absorption with changes in the temperature of the contents of the 10 cm. gas cell is not as large in this continuous absorption system as in the visible absorption system. These two experimental results indicate that the continuous absorption (2700-2000 Å) is mainly caused by the dimer and

not the radical which is in equilibrium with the dimer.

The intensity of the continuous absorption (4700-3300 Å) which overlaps the high wavenumber portion of the visible absorption system (3^{rd}) is found to be temperature dependent. The intensity of the continuous absorption is the least intense in the regions where the visible absorption is the most discrete and appears, at a fixed temperature, to form a continuation of the discrete spectrum. The conclusion drawn from these results is that this continuous absorption is part of the visible system (3^{rd}) and that it is not caused by a separate electronic transition of the radical.

The two absorption systems in the near infrared region of the spectrum have not previously been reported. In order to establish whether these systems were the result of the absorption of radiation by the radical or the dimer, the maximum absorption of these systems was measured at different temperatures. The results, corrected for background absorption of the cell, are given in Table 5.2. The results are accurate to ±0.03 absorbance units.

TABLE 5.2

TEMPERATURE DEPENDENCE OF THE ABSORPTION SYSTEMS

ABSORBANCE

Temp	System #1 (20,000-10,000 Å)	System #2 (10,000-5700 Å)	System #3_o (5500-3600 Å)
25°C	0.00	0.00	0.04
78°C	0.01	0.02	0.96
112°C	0.14	0.20	≯2.0
145°C	0.60	0.75	>2.0

From the above table it can be seen that the absorbance of all three systems is very small at room temperature, where the concentration of the radical is very low, and that the absorbance increases rapidly as the temperature is raised.

Beer's Law states that the fraction of light absorbed is proportional to the number of absorbing molecules through which the light passes. Mathematically, this is expressed as

$$A = abc$$

where A is the absorbance, c is the concentration of the absorbing species, b is the path length, and a is the absorptivity (a molecular property independent of concentration).

In the previous table, the increase in absorbance with an increase in temperature means that the concentration of the absorbing species must have increased since the variables a and b were constant throughout the experiment. Since an increase in temperature will increase the radical concentration and hence lead to an increase in the absorbance, the results of the previous table provide strong evidence for the fact that the absorption in the near infrared regions of the spectrum is caused by the radical.

The above experiment, however, was not conclusive since it was carried out with excess dimer present in the liquid state. As the temperature is increased, the equilibrium

$$S_2O_6F_2 \underset{\text{(liquid)}}{\rightleftharpoons} S_2O_6F_2 \text{ (vapour)}$$

is also shifted to the right. Therefore, at higher temperatures there will also be a greater number of dimer molecules in the optical path than at lower temperatures. If the previous absorption systems were caused by the dimer, then the absorbance would also show a temperature dependence. The results of Table 5.2 for all three systems are consistent with the interpretation that the absorbing species is either the radical or the dimer.

The second interpretation was ruled out by the following experiment. The 10 cm. quartz gas cell was filled with the dimer at a pressure equal to its saturation vapour pressure at zero degrees C. When the contents of the cell are heated, only the concentration of the radical can increase. The absorbance for the three systems was measured at different temperatures and was again found to increase as the contents of the cell were heated.* Therefore, the absorbing species for the three absorption systems must be the radical and not the dimer. This conclusion is also in agreement with the results of the CNDO calculation for the fluorosulfate radical. The theoretical calculation predicted that there would be three low lying energy states above the ground electronic state to which electronic transitions from the ground state could occur. Three low energy transitions were observed.

5.2 Assignment of the Absorption Systems

The absorption profile for each of the systems is shown in Fig. 5.1. It should be noted that in this diagram the systems in the near infrared region are not reproduced on the same wavelength scale as the visible system and that the absorption profile is different for each of the absorption systems.

* The experimental results are given in the appendix. See Table A.12.

The first system, labelled 1^{st} in Fig. 5.1, has a very broad absorption profile with some vibrational structure superimposed upon it. The absorption profile is symmetrical about the intensity maximum and according to the Frank-Condon principle,[65,66] this symmetrical shape is characteristic of an electronic transition between two states for which the geometry* or symmetry of the molecule at its equilibrium position is quite different for each of the two combining states. The electronic transition of lowest energy is predicted to be a $^2A_1$-$^2A_2$ transition by the molecular orbital calculations of Chapter 3. The $^2A_2$ state has a minimum of energy for an OSF angle of 105° while the $^2A_1$ state has a minimum of energy for an OSF angle of 97°. Thus the geometry of the radical, with respect to the OSF angle, at the energy minimum for each of these states is significantly different. On the basis of the results of the molecular orbital calculations and the observed intensity distribution of the 1^{st} absorption system, this absorption has been tentatively assigned as arising from the $^2A_1$-$^2A_2$ electronic transition. It should be noted that the geometry of the radical, with respect to the OSF angle, in the two lowest ^2E states is predicted to be almost the same as the geometry of the $^2A_2$ ground state by the molecular orbital calculations

* In this thesis, a change in geometry will refer only to changes in bond lengths or bond angles that preserve the ground state symmetry of the molecule. A change in symmetry means that the molecule can no longer be classified under the same molecular point group that it was originally classified under in its ground electronic state equilibrium configuration.

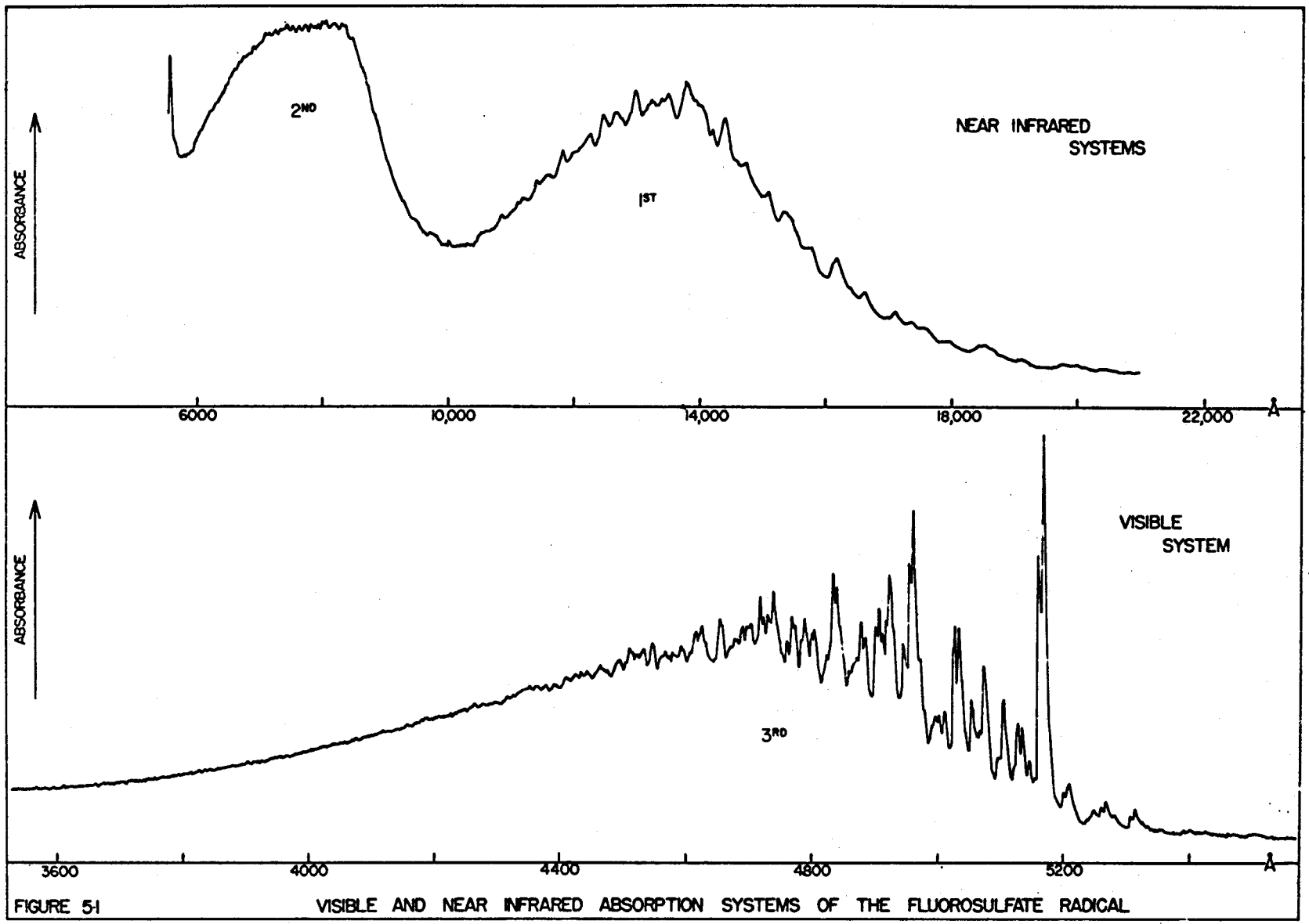

FIGURE 5-1 VISIBLE AND NEAR INFRARED ABSORPTION SYSTEMS OF THE FLUOROSULFATE RADICAL

The $^2A_1$-$^2A_2$ transition, however, is unallowed by equation 4.7 and thus should not be detected experimentally. However, two approximations were used in deriving this equation. The second approximation assumes that R_e is independent of the nuclear coordinates. This assumption is only valid if the molecule retains its assumed symmetry during a vibration, and therefore the approximation will break down when antisymmetric or degenerate vibrations are excited in either of the combining states. A breakdown of this approximation leads to the appearance of transitions which are forbidden by the above equation if the following conditions are fulfilled:

1. A perturbing electronic state is in the vicinity of one of the two participating states, that is, the states for which an electronic transition is forbidden by equation 4.7.

2. The transition between the perturbing state c and the lower state a is allowed by equation 4.7 (See Fig. 5.2).

3. The symmetry species to which the states a and c belong differ by the symmetry species of one, and only one, non-totally symmetric normal coordinate.

Herzberg and Teller[51] further state that if the energy of the two mutually perturbing states (b and c) differs by less than 1 ev. then the forbidden transition can have an intensity comparable to that of a weakly allowed transition.

On the basis of the molecular orbital calculations, the 2nd transition observed at 7000 Å is assigned as a ^2E-$^2A_2$ transition. Condition 1

is therefore satisfied for the 1st transition since the ^2E state is approximately 0.7 ev. above the $^2A_1$ state. The transition ^2E-$^2A_2$ is also fully allowed by equation 4.7. The third condition is satisfied since

$$A_1 \times e = E$$

that is, the symmetry species A_1 and E of the two electronic states (a and c) differ only by the symmetry species of one of the degenerate e-type normal coordinates of which there are three for the fluorosulfate radical.

Since the above conditions are satisfied, the $^2A_1$-$^2A_2$ transition (1st) is not strictly forbidden and therefore could be observed.

One alternative explanation which would account for the presence of this normally forbidden electronic transition is that the molecule may not have the same symmetry at equilibrium in both the upper and lower electronic states. For example, the molecule in the upper state, denoted as $^2A_1$, may be distorted such that it transforms according to the symmetry

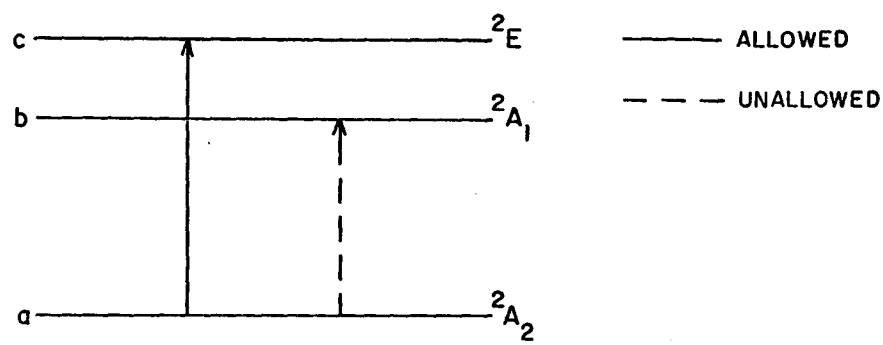

FIGURE 5·2 FORBIDDEN ELECTRONIC TRANSITION $^2A_1$—$^2A_2$

operations of the C_s or C_1 molecular point groups. The question as to whether the transition is allowed or forbidden must now be decided on the basis of the behaviour of $\int \psi_e' \bar{P}_e \psi_e \, dT_e$ with respect to the symmetry operators of the point groups C_s or C_1, not C_{3v}. The correlation between the irreducible representations of the C_{3v} group and those of the C_s or C_1 groups is given in Table 5.3.

TABLE 5.3

CORRELATION TABLE BETWEEN THE IRREDUCIBLE REPRESENTATION OF THE C_{3v} MOLECULAR POINT GROUP AND THE IRREDUCIBLE REPRESENTATION OF THE C_s AND C_1 MOLECULAR POINT GROUPS

C_{3v}	C_s	C_1
A_1	A'	A
A_2	A''	A
E	A'+A''	A+A

If the upper $^2A_1$ state of the molecule is distorted from C_{3v} symmetry such that it now has the symmetry C_s or C_1 then the transition denoted as $^2A_1$-$^2A_2$ under the C_{3v} point group will now be denoted as $^2A'$ (C_s) - $^2A_2$ (C_{3v}) or ^2A(C_1) - $^2A_2$ (C_{3v}). These latter transitions are both fully allowed according to group theoretical arguments. Similarly, the transition is allowed if the ground state is distorted instead of the upper state or if both the upper and the lower states are distorted such that they have C_s or C_1 symmetry. The results of the electron diffraction study[12] of the radical, however, indicate that the radical has C_{3v} symmetry in its ground state. Thus, if the transition is allowed because of a permanent distortion of one of the states of the fluorosulfate radical

from C_{3v} symmetry, then it must be the upper state which is distorted. Transitions of the type $^2A_1'(C_s)$ - $^2A_2$ and $^2A(C_1)$ - $^2A_2$ would be predicted to exhibit long progressions in some of the vibrational fundamentals in accordance with the Franck-Condon principle.

Two explanations have been presented to account for the presence of the normally forbidden $^2A_1$-$^2A_2$ transition. A detailed vibrational analysis or possibly even a rotational analysis would have to be carried out in order to decide which of the above explanations accounts for the observation of this normally forbidden transition.

The vibrational analysis of the 1st system was not attempted. It could not be examined in great detail since it occurs in a very awkward region of the spectrum and appears to have a rather diffuse structure; that is, on the Cary it certainly appears quite diffuse by comparison with the sharp bands of the 3rd system. High resolution photographic plates and films are not available commercially for this region of the spectrum and the absorption of the 1st system could only be detected with the low resolution Cary spectrophotometer. This low resolution is not sufficient for a detailed vibrational analysis.

The 2nd system (10,000-5700 Å) has been assigned as the ^2E-$^2A_2$ transition on the basis of the results of the molecular orbital calculations. This system overlaps the 1st system in the region of 10,000 Å and overlaps the 3rd system at 5700 Å. The absorption profile of the 2nd system is not symmetrical as that for the 1st system; there is a sharp drop in intensity at the high wavelength side of the absorption. The absorption is broad and no resolvable structure is detected with the low resolution Cary spectrophotometer.

The molecular orbital calculations predict that the 3rd absorption system (5500-3600 Å) is the result of a second ^2E-$^2A_2$ electronic transition. The results discussed in the remainder of this thesis confirm this assignment.

The absorption profile for the visible system (3rd) is very unsymmetrical. Sharp discrete structure is observed at the high wavelength end of the absorption. As one progresses to low wavelengths, the number of sharp band heads multiplies until they gradually merge into a continuous background. The most intense band of the system consists of a sharp doublet at approximately 5170 Å. To the low frequency side of this band, much weaker bands are present. Other intense bands occur to the high frequency side of this band. No long progressions are evident and the discrete structure appears quite complex. The low resolution visible spectrum is shown in Figs. 5.1 and 5.3.

The magnitudes of the experimentally determined oscillator strengths* for the absorption systems of the radical (See Table 5.1) are consistent with the assignment of the three lowest transitions of the radical as $^2A_1$-$^2A_2$, $^2E(1)$-$^2A_2$ and $^2E(2)$-$^2A_2$ in order of increasing energy. An oscillator strength between 10^{-3} and 1 is generally observed for a fully allowed electric dipole transition such as the $^2E(1)$-$^2A_2$ or the $^2E(2)$-$^2A_2$ transitions of the radical; the observed oscillator strengths for these two transitions were $2X10^{-3}$ and $5X10^{-2}$ respectively. The observed oscillator strength of $5X10^{-4}$ for the 1st system (assigned to the transition $^2A_1$-$^2A_2$ of the radical)is consistent with a weakly (vibronically) allowed electric dipole transition.

---

* The oscillator strength is a measure of the intensity of absorption (or emission) of an electronic transition. This quantity has a maximum value of 1.

5.3 Vibrational Analysis of The Third System

i) Introduction

With the majority of the vibrational analyses of the electronic spectra of polyatomic molecules, the frequencies of the ground state fundamentals are known in advance. Generally, these frequencies have been determined from the infrared and Raman spectra of the molecules. The infrared and Raman spectra of the radical, however, have not been previously reported in the literature. Our attempts to detect the Raman spectrum of the radical in the liquid phase were unsuccessful. Also, the infrared spectrum of the radical could not be observed with any degree of certainty. The reasons that these investigations were unsuccessful are that the concentration of the dimer was always much greater than the concentration of the radical and that the radical is so reactive that it attacked the window materials which were used with the infrared cells.

These factors, which prevented the observation of the infrared and Raman spectra of the radical, do not interfere with the observation of the visible spectrum. Since the dimer is a colourless liquid, it does not have absorption bands in the visible region of the spectrum. Therefore, the presence of undissociated dimer molecules in the gas cell is immaterial when the visible spectrum of the radical is observed. When the infrared spectrum of the radical is under examination, however, the ratio of the concentration of the radical to the dimer is extremely critical because of the proximity of the wavenumbers of the absorption bands of the radical and the dimer. For the visible absorption studies, a quartz cell was used; the radical is fairly inert towards quartz.

Thus, the problems which plagued the observation of the infrared and Raman spectra, are of no importance for the observation of the visible spectrum of the radical.

Theoretically, the wavenumbers of the ground state fundamentals can be extracted from the vibrational analysis of the electronic spectrum. It is felt that this is the most fruitful means of obtaining the ground state frequencies of the radical.

ii) Assignment of the Origin Band

In Fig. 5.3, a low resolution spectrogram of the visible absorption system of the radical is shown. A large number of discrete double-headed bands with accompanying rotational structure can be seen. Single-headed bands are also observed.

The intense double-headed band with components at 19383.1 and 19353.7 cm^{-1} has been assigned as the origin band. This band, caused by the transition from the vibrationless level of the ground electronic state to the vibrationless level of the excited electronic state, is the most intense band of the visible absorption system. All the bands to the low frequency side of this band are very much weaker and are attributed to transitions from vibrational levels of the ground electronic state to levels of the excited electronic state. The intensity of these bands, called hot bands, is not only determined by the magnitude of the overlap integral (equ't 4.8) but is also dependent upon the Boltzmann population factor for the vibrational levels in the ground state

$$g_{v''} e^{-G(v'') hc /kT} \qquad (5.1)$$

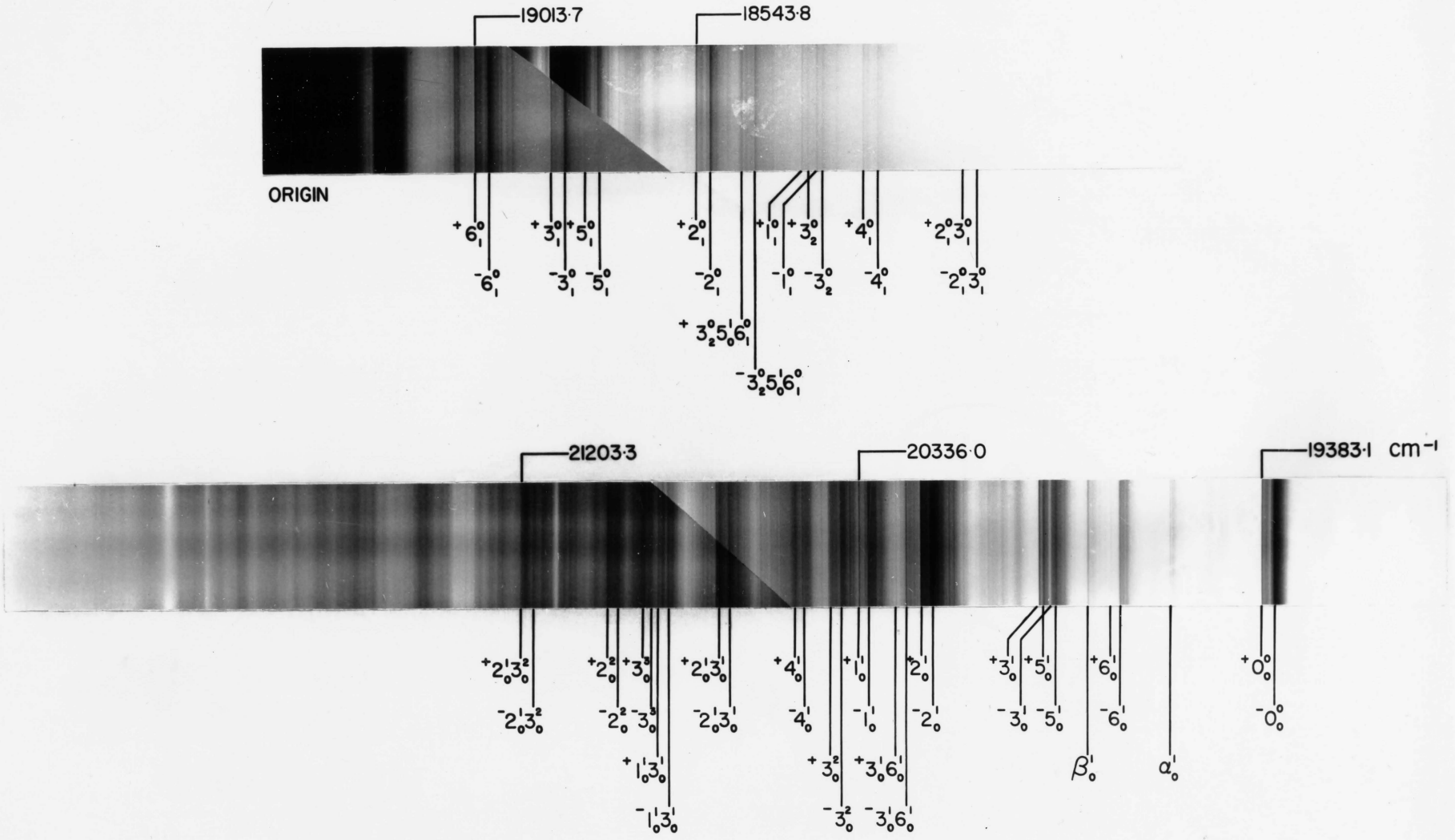

FIGURE 5·3 LOW RESOLUTION SPECTROGRAMS OF THE VISIBLE (3RD) ABSORPTION SYSTEM OF THE FLUOROSULFATE RADICAL

where $g_{v''}$ is the degeneracy of degenerate vibrations of the ground electronic state, k is the Boltzmann factor, $G(v'')$ is the term value of the vibrational energy from which the transition originates and is defined by equation 4.2, h is Planck's constant and c is the velocity of light.

Unless $G(v'')$ is very small, the Boltzmann population factor is so small at room temperature that the intensity of the hot bands is much weaker than the intensity of the origin band. From the above expression, it can be seen that the intensity of the hot bands will be enhanced by an increase in temperature.

The two components of the origin band are separated by 29.4 $cm.^{-1}$ The majority of the bands to the low frequency side of the origin band are doublets whose splitting is also approximately 29 $cm.^{-1}$ A large number of bands to the high frequency side of the origin band are also doublets but the separation of the two components is not constant. The component of the origin band at the lower wavenumber is slightly more intense than the component at the higher wavenumber. Under high resolution, both components have very well developed rotational structure. The splitting of 29 cm^{-1} is, however, too large to be explained as the separation between two rotational band heads of the same vibronic transition. This conclusion will be discussed more fully in Chapter 6.

There are three ways in which the splitting of the origin band can be accounted for. These three explanations are shown in Fig. 5.4.

In Case I, the upper state is either split by 29 cm^{-1} via a spin-orbit coupling mechanism (analagous to Hund's case (a)[67] coupling for diatomics) or there is a low lying vibronic level 29 cm^{-1} above the vibrationless excited state level. The ground electronic state is not

split in Case I and hence the spin of the odd electron must be coupled to the molecular system as it is in Hund's case (b)[67] coupling* for diatomics. Case II is identical to Case I except that the 29 cm^{-1} separation occurs in the ground electronic state. In Case III, both states are split by spin-orbit coupling (Hund's case (a)) such that the splitting of one of the states minus the splitting of the other state equals 29 cm^{-1}, or there is a vibronic level Δ_u cm^{-1} above the vibrationless excited state level and a vibronic level Δ_g cm^{-1} above the vibrationless ground state level such that

$$| \Delta_u - \Delta_g | = 29 \text{ cm}^{-1}$$

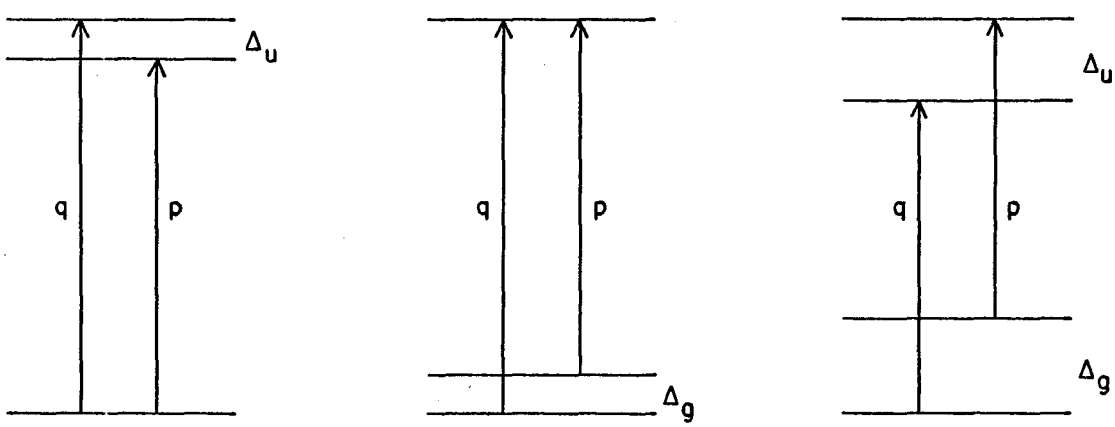

FIGURE 5·4 POSSIBLE EXPLANATIONS FOR THE TWO COMPONENTS OF THE ORIGIN BAND·

* The two Hund's coupling schemes, (a) and (b) will be discussed further in Chapter 6.

The transitions p and q are responsible for the two components of the origin band. The ratio of the intensities of these two transitions will be temperature dependent for Cases II and III because of the Boltzmann population factor in the intensity expression. In Case I, transitions p and q both arise from the vibrationless ground state and therefore the ratio of their intensities will be temperature independent in absorption.

The ratio of the number of molecules in level 1 to that of level 2, in the ground electronic state, is given according to Boltzmann statistics by

$$\frac{n_1}{n_2} = \frac{g_1}{g_2} e^{-\Delta_g hc/kT} \qquad (5.2)$$

where n_i equals the number of molecules populating the i^{th} level of degeneracy g_i. The ratio of the intensities of the transitions p and q at different temperatures will be dependent upon the population ratio of levels 1 and 2 at different temperatures. The calculated change in the population ratio n_1/n_2 as a function of temperature is illustrated in Fig. 5.5 for several values of Δ_g.

The absorbance for each component of the origin band was measured at different temperatures on the Cary 14 spectrophotometer. These measurements are given in Table 5.4.

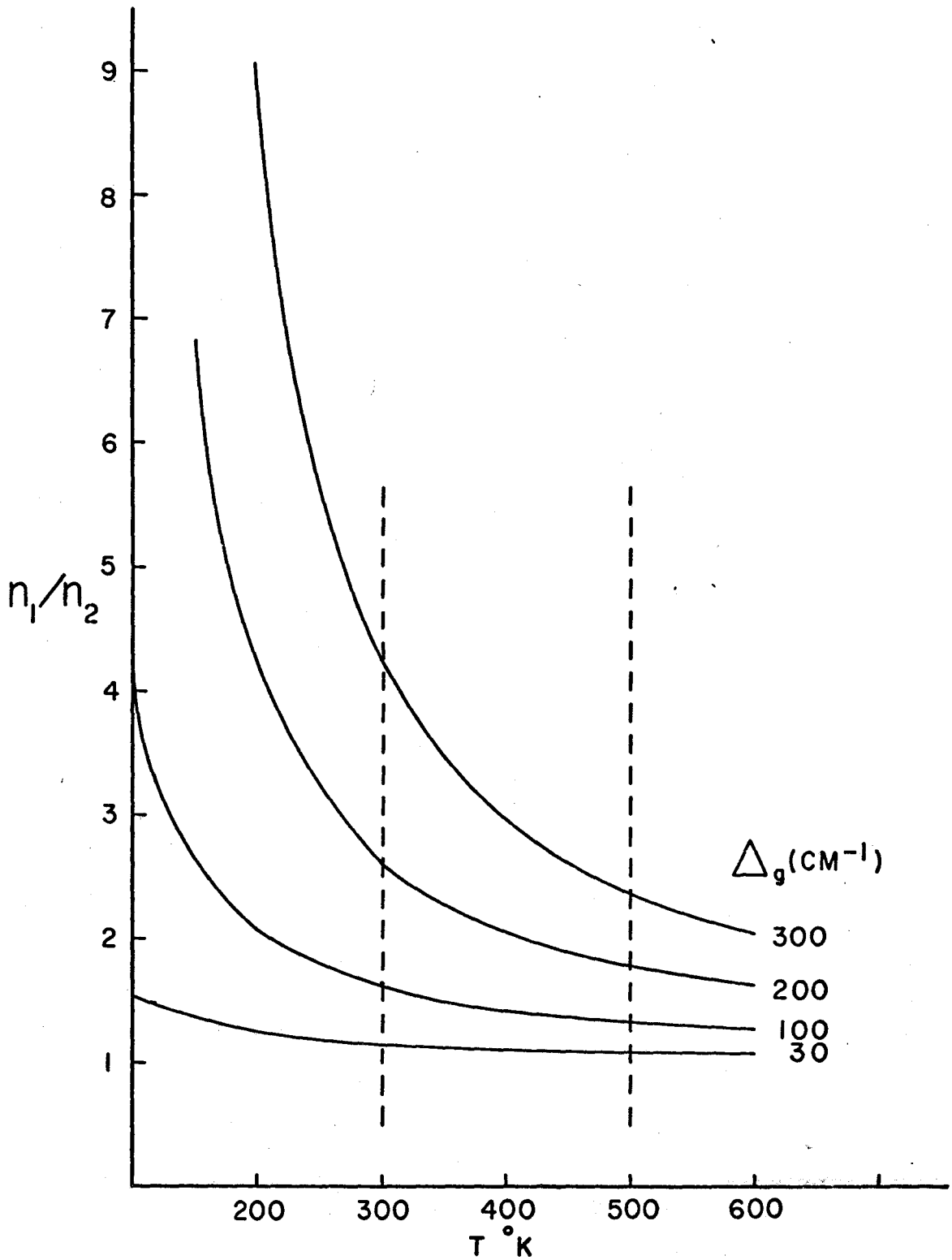

FIGURE 5·5 POPULATION RATIO n_1/n_2 AS A FUNCTION OF TEMPERATURE FOR VARIOUS VALUES OF Δ_g

Table 5.4

Ratio of the Absorbances For The Two Components

of The Origin Band As A Function Of Temp.

TEMPERATURE	ABSORBANCE OF 19383.1 CM^{-1} COMPONENT A_q	ABSORBANCE OF 19353.7 CM^{-1} COMPONENT A_p	RATIO A_p/A_q
24°C	0.035	0.042	1.20 AVERAGE
	0.036	0.041	1.16 =
	0.036	0.042	1.20 1.19
60°C	0.292	0.347	1.19 AVERAGE
	0.296	0.354	1.19 =
	0.289	0.360	1.25 1.21
80°C	0.365	0.435	1.19 AVERAGE
	0.367	0.439	1.19 =
	0.360	0.425	1.18 1.19
108°C	0.292	0.344	1.18 AVERAGE
	0.312	0.367	1.18 =
	0.346	0.403	1.16 1.18
137°C	0.228	0.250	1.10 AVERAGE
	0.251	0.295	1.18 =
	0.282	0.326	1.16 1.15
196°C	0.225	0.272	1.21 AVERAGE
	0.238	0.302	1.26 =
	0.230	0.254	1.10 1.19

From Table 5.4 it can be seen that the ratio A_p/A_q is almost a constant over the temperature range 24 - 196°C; the observed intensity ratio of the two transitions appears to be temperature independent. However, if Δ_g equals 29 cm^{-1} (Case II), the experimental results would also indicate a constant absorbance ratio since from Fig. 5.5 it can be seen that there is very little change in the population ratio n_1/n_2 over the range of temperatures used in the above experiment. In Case III, a Δ_g greater than 100 cm^{-1} would lead to a detectable change in the absorbance ratio as the temperature was increased from 24°C to 196°C. The above experiment eliminates the possibility that one of the components of the origin band is a sequence band. This conclusion is also supported by the observation that there are no higher members of such a sequence present. If one of the components was the first member of a sequence in 29 cm^{-1}, then other members of the sequence extending to higher or lower frequencies would be expected to be seen since the two observed components are of almost equal intensity.

If the ground electronic state is split by spin-orbit coupling (Hund's case (a)) then, this state must be a ^2E state since a $^2A_2$ or $^2A_1$ state has no component of electronic angular momentum along the figure axis (C_3 axis) of the molecule with which the spin can couple.* The results of the Jahn-Teller-spin-orbit calculation, (See Chapter 4), show that the intervals between and the spin splitting of the vibronic levels associated with a ^2E electronic state are very irregular. The observed wavenumber

* The $^2A_1$ and $^2A_2$ states of a C_{3v} molecule are analagous to $^2\Sigma$ states of diatomic molecules in which the spin of the odd electron cannot couple according to Hund's case (a) coupling.

between the doublet components of bands to the high wavenumber side of the origin band is not constant; in fact, some of the bands are single-headed. Also, the spectrum is much more complicated to the high wavenumber side of the origin band than to the low wavenumber side. Most of the bands to the red of the origin band can be assigned as transitions from some vibronic level of the ground state to the vibrationless level of the excited state. If this excited state level were split or if there werea separate level lying just above it, then all transitions from the vibronic levels of the ground electronic state of the two lowest levels of the excited state should consist of doublets with a constant wavenumber separation. Doublets with a constant wavenumber separation are observed to the low wavenumber side of the origin band. If the ground state were ^2E, a constant separation of the doublet components should not be observed in the hot bands. It is felt that the above observations rule out electronic transitions of the type $^2E \leftarrow {}^2E$, $^2A_1 \leftarrow {}^2E$, and $^2A_2 \leftarrow {}^2E$. The assignment of the electronic transition as $^2E \leftarrow {}^2A_1$ or $^2E \leftarrow {}^2A_2$ gives the best agreement with the experimental observations.

iii) Assignment of the Totally Symmetric Ground State Fundamentals

The vibronic transitions are labelled $A_i^j B_m^n \ldots$ where A, B, ... refer to the vibrational modes which are active in a given vibronic transition. The right subscripts and superscripts refer to the number of quanta of this vibration which are excited in the upper and lower states respectively. Since the majority of bands are doublets, a left superscript (+ or -) is used to denote the high and low frequency components respectively. The high frequency component of the origin band is denoted $^+0_0^0$. $^+\nu_{00}$ represents the wavenumber at which it is found.

The band found at $^{+}\nu_{oo}$ - 839.3 cm^{-1} to the low frequency side of the origin band is assigned as 2_1^o. In the fluorosulfate radical, ν_2'' is the symmetric S - F stretch. The assignment of the frequency of this mode as 839.3 cm^{-1} agrees quite well with the frequency of the S - F stretching mode observed in other molecules. The frequency of the S - F stretch for some of these molecules is listed in Table 5.5. (This fundamental, whose frequency generally occurs between 740 and 850 cm^{-1}, is usually observed as a strong band in the infrared region.) The band of the visible absorption system of the radical at $^{+}\nu_{oo}$ - 839.3 cm^{-1} is a fairly intense band with respect to the other bands to the red of the origin band. Since the ν_2'' vibration is a totally symmetric vibration, the structure of this band should be the same as that of the origin band. This was found to be the case. There are no other strong bands with the same structure as the origin band within 700 - 900 cm^{-1} to the low frequency side of the origin band.

From Table 5.5, it can be seen that the S -O symmetric deformation fundamental ν_3'' usually occurs between 450 and 550 cm^{-1}. ν_3'' is a totally symmetric vibration, and therefore the rotational envelope of the band corresponding to the 3_1^o transition should be the same as that of the origin band. A strong double-headed band whose structure is very similar to that of the origin band is found at $^{+}\nu_{oo}$ - 533.5 cm^{-1}. The high frequency component of this band has been assigned to the $^{+}3_1^o$ transition.

ν_1'' designates the symmetric S - O fundamental stretching frequency. The band corresponding to the transition $^{+}1_1^o$ was much harder to assign. From Table 5.5 it can be seen that this fundamental can occur within the range 1000 - 1300 cm^{-1}. In the region 1000 - 1300 cm^{-1} to the red of the

Table 5.5

COMPOUND	ν_1(S-O) (cm^{-1})	ν_2(S-F) (cm^{-1})	ν_3(δSO) (cm^{-1})
$NaSO_3F$[68]	1095	740	566
KSO_3F[68]	1073	782	565
$CsSO_3F$[68]	1071	728	
NH_4SO_3F[68]	1072	737	
$AgSO_3F$	1057	767	
$RbSO_3F$[68]	1072	729	
OSF_2[69,70]	1308	801	526
F_2S_2[71]		745	
O_2SF_2[69,72,73,74]	1269	848	544
SF_6[75-78]		775	
$S_2O_6F_2$[4]	1246	848	
SO_2[79]	1147		521
SO_3[80,81]	1069		652
$[SSO_3]^{2-}$ [82,83]	995		446

Frequencies of the S-O stretch, S-F stretch, and the S-O sym. bend for some molecules.

origin band, there are three prominent double-headed bands whose structure is very similar to the structure of the origin band. These bands occur at

$$^{+}\nu_{oo} - 1177.5 \text{ cm}^{-1}$$
$$^{+}\nu_{oo} - 1067.0 \text{ cm}^{-1}$$
$$^{+}\nu_{oo} - 1055.5 \text{ cm}^{-1}$$

and are all of approximately the same intensity.

One of these bands could be assigned as 3_2^o.

$$^{+}\nu_{oo} - 1067.3 = {}^{+}3_2^o \ (533.5 + 533.8)$$

or

$$^{+}\nu_{oo} - 1055.5 = {}^{+}3_2^o \ (533.5 + 522.0)$$

There is also a double-headed band found at $^{+}\nu_{oo} - 1587.1 \text{ cm}^{-1}$. If the band at 1055.5 cm^{-1} to the red of the origin band is assigned as 1_1^6 then

$$^{+}\nu_{oo} - 1587.1 = {}^{+}1_1^o \ 3_1^o \ (1055.5 + 531.6)$$

This assignment is preferred to the following assignments

$$^{+}\nu_{oo} - 1587.1 = {}^{+}3_3^o \ (533.5 + 533.8 + 519.8)$$

where $^{+}\nu_{oo} - 1067.3 = {}^{+}3_2^o$

or

$$^{+}\nu_{oo} - 1587.1 = {}^{+}3_3^o \ (533.5 + 522.0 + 532.1)$$

where $^{+}\nu_{oo} - 1055.5 = {}^{+}3_2^o$

In summary, the most consistent analysis is obtained if the following assignments are made

$$^{+}\nu_{oo} - 1055.5 = {}^{+}1^{o}_{1}$$
$$^{+}\nu_{oo} - 1067.3 = {}^{+}3^{o}_{2}$$
$$^{+}\nu_{oo} - 1587.1 = {}^{+}1^{o}_{1}\ 3^{o}_{1}$$

The band at $^{+}\nu_{oo}$ - 1177.5 cm^{-1} remains to be assigned.

Gillespie and Robinson[84] have shown that the length of an S - O bond and the bond angle of an SO_2 group can be correlated with the S-O stretching frequency which is defined in terms of the symmetric and asymmetric S-O fundamental stretching frequencies. Lehmann[85] has shown for an AB_x group, where the asymmetric S-O fundamental has degeneracy (x-1), that the A-B stretching frequency is given by

$$\nu_{A-B} = (1/x)\ [\nu_{sym} + (x-1)\ \nu_{asym}\ ] \qquad (5.3)$$

Therefore, for the fluorosulfate radical

$$\nu_{S-O} = (1/3)\ [\ \nu_1'' + 2\nu_4''\ ] \qquad (5.4)$$

where ν_4'' is the S-O asymmetric fundamental stretching frequency.

Equation 5.3 is a good approximation to ν_{A-B} if the bending force constant is small, the symmetric fundamental stretching frequency is appreciably larger than the bending frequency, and the coupling of the AB_x group with the rest of the molecule is small.

Gillespie and Robinson examined approximately twenty compounds containing S-O bonds and showed that there was a reasonably good correlation between the S-O bond length and the S-O stretching frequency which is defined by equation 5.3.

The S-O bond length for the fluorosulfate radical in the ground state is 1.46 ± 0.02 Å.[12] The above correlation predicts that a molecule with an S-O bond length of 1.46 Å will have a S-O stretching frequency of approximately 1159 cm^{-1}. If we assume this correlation holds for the radical then

$$\nu_{S-O}(SO_3F) = 1159 \text{ cm}^{-1}$$

Gillespie and Robinson also derived an equation which relates the OSO bond angle to the magnitude of the symmetric and asymmetric S-O fundamental stretching vibrations.

$$\nu_{sym} / \nu_{asym} = [(1+\cos^2\delta) / (1+\sin^2\delta)]^{1/2} \qquad (5.6)$$

where 2δ is defined as the OSO bond angle. They find that there is very good agreement between the bond angles determined from this equation and the bond angles determined by experimental methods. From the electron diffraction results of Hencher and Bauer,[12] the OSO bond angle for the radical in its ground state is determined to be 110°.

By solving the following two equations in two unknowns,

$$\nu_{S-O}(SO_3F) = 1159 \text{ cm}^{-1} = 1/3\ [\nu_1'' + 2\nu_4'']$$

and $$\nu_1'' / \nu_4'' = \left[[\ 1 + \cos^2\ (110/2)] / [1 + \sin^2\ (110/2]\right]^{1/2}$$

ν_1'' and ν_4'' are found to be

$$\nu_1'' = 1072 \text{ cm}^{-1}$$

$$\nu_4'' = 1202 \text{ cm}^{-1}$$

ν_1'' was determined to be 1055.5 cm^{-1} from the analysis of the visible absorption system of the radical. The experimentally and theoretically determined frequencies for ν_1'' agree to within 2%. The most interesting aspect of this calculation is that ν_4'' is predicted to be 1202 cm^{-1}. A relatively strong band is observed at 1177.5 cm^{-1} to the red of the origin band. This hot band could not be assigned as a sequence or combination band and because of the agreement (~ 2%) with the above calculation it was assigned to the transition 4_1^o. The consequences of this assignment will be discussed later.

iv) Assignment of the Totally Symmetric Excited State Fundamentals

There is a very strong double-headed band at $^+\nu_{oo}$ + 515.0 cm^{-1} to the high frequency side of the origin band. This band has been assigned to the transition $^+3_o^1$. There is a difference of 18 cm^{-1} between the frequency of the S-O symmetric bend in the ground and excited states.

The $^2E(2)$ state of the radical is formed when an electron in an e-type molecular orbital is promoted to the a_2 molecular orbital. Both of these orbitals are localized on the oxygen nuclei. The a_2 molecular orbital is composed of a linear combination of the P_x P_y atomic orbitals of the oxygen nuclei and is non-bonding with respect to the sulfur and fluorine nuclei. The e molecular orbital, on the other hand, is partially delocalized over sulfur and fluorine. Thus, when an electron is removed from this orbital and placed in the a_2 orbital, the S-O and S-F bond strengths should decrease. This decrease would reflect itself in a lowering of the S-O and S-F symmetric stretches. Thus, the strong bands observed at $^+\nu_{oo}$ + 800.5 and $^+\nu_{oo}$ + 952.9 cm^{-1} were assigned to the transitions $^+2_o^1$ and $^+1_o^1$ respectively. The rotational structure of these bands is very similar to that of the origin band.

The wavenumber of the three totally symmetric fundamentals for the ground and excited states of the fluorosulfate radical, which have been obtained from the analysis of its visible spectrum, are tabulated in Table 5.6. The percentage change in wavenumber between the fundamentals on going from the ground to the excited state is also included in this Table.

Table 5.6

TOTALLY SYMMETRIC FUNDAMENTALS OF THE GROUND AND EXCITED ELECTRONIC STATES

GROUND STATE	EXCITED STATE	% DECREASE ON EXCITATION
$\nu_1'' = 1055.5\ cm^{-1}$	$\nu_1' = 952.9\ cm^{-1}$	10%
$\nu_2'' = 839.3\ cm^{-1}$	$\nu_2' = 800.5\ cm^{-1}$	5%
$\nu_3'' = 533.5\ cm^{-1}$	$\nu_3' = 515.0\ cm^{-1}$	3%

A large part of the visible spectrum can now be assigned to transitions which can be represented as combinations or overtones of the totally symmetric ground and excited state fundamentals. These assignments are listed in Table 5.7. Transitions which originate from a common ground state level and which are observed as absorption bands give the same difference in energy ($\pm$ 0.3 cm^{-1}) between this common ground state level and the vibrationless ground state level.

Long progressions in the totally symmetric fundamentals of the ground or the excited electronic state are not observed. The longest assigned progression has three members in ν_3'. The lack of long progressions and the fact that the origin band is the most intense band indicates that the geometry of the molecule in the upper and lower state is similar.

Very few sequence bands involving totally symmetric fundamentals are observed.

v) Assignment of the Degenerate Fundamentals

One of the most intense bands to the red of the origin band occurs at $^{+}\nu_{oo}$ - 369.4 cm^{-1}. This band is composed of two well-defined components whose separation is 29.4 cm^{-1}. This splitting is exactly the same as the splitting of the origin band and this fact suggests that the transition responsible for this band arises from some vibronic level of the ground state and terminates on the split vibrationless excited state level. Under high resolution, the rotational structure of this band and that of the origin band is very similar. This band could not be assigned to a transition which originates on a ground state vibrational level of a totally symmetric fundamental or a combination of totally symmetric fundamentals, and terminates on an excited state vibronic level.

The infrared analysis of the FSO_3^- ion[68] assigns the band found at 409 cm^{-1} as the ν_6'' fundamental—a rocking mode involving the SO_3 group. A pictorial representation of this mode is shown in Fig. 4.1. In other molecules which contain the SO_3 group, such as, $[SSO_3]^{2-}$,[82,83] $CH_3SO_3^-$,[86] $NH_2SO_3^-$,[86] $OHSO_3^-$,[86] and $CH_3OSO_3^-$,[86] the ν_6'' fundamental is observed between 335 and 438 cm^{-1} in the infrared.

The most reasonable assignment for the band at $^{+}\nu_{oo}$ - 369.4 cm^{-1} is $^{+}6_1^o$. Two bands have now been assigned to transitions which arise from degenerate vibrational levels of the ground electronic state.

$$\nu_6'' = 369.4 \text{ cm}^{-1}$$
$$\nu_4'' = 1177.5 \text{ cm}^{-1}$$

The transitions designated as $^{\pm}6_1^o$ and $^{\pm}4_1^o$ are unallowed according to equation 4.8. The appearance of these transitions indicates that the approximation in which the total eigenfunction Ψ is factored into the product

$$\Psi = \psi_e \psi_v$$

does not hold rigidly. If there is an interaction between the vibrational and electronic motions (Jahn-Teller effect) so that the molecule distorts slightly in the degenerate electronic state, then the transitions 6_1^o and 4_1^o are no longer forbidden. The left hand diagram of Fig. 5.6 shows the transitions that are allowed when no vibronic interaction is present in the molecule, that is, the transitions for which the vibrational overlap integral, equation 4.8, does not vanish. The symbol K in Fig. 5.6 represents one of the degenerate vibrations ν_K. The transition K_1^o is unallowed since ψ_v'' transforms as e, ψ_v' transforms as a_1, and their direct product transforms as e under the C_{3v} group. In order for the overlap integral to be non-zero, the direct product of ψ_v'' and ψ_v' must contain the totally symmetric representation. A similar explanation applies to the K_o^1 transition. The transitions K_o^2 and K_2^o are allowed but the intensity of these transitions is generally very low.

The Jahn-Teller interaction mixes vibronic states with the same value of the quantum number j.* The upper state defined by $v_K' = 1$,** $j' = 1/2$

---

* See Fig. 4.4.

** The quantum number v_K equals the quantum number n of Fig 4.4 minus one.

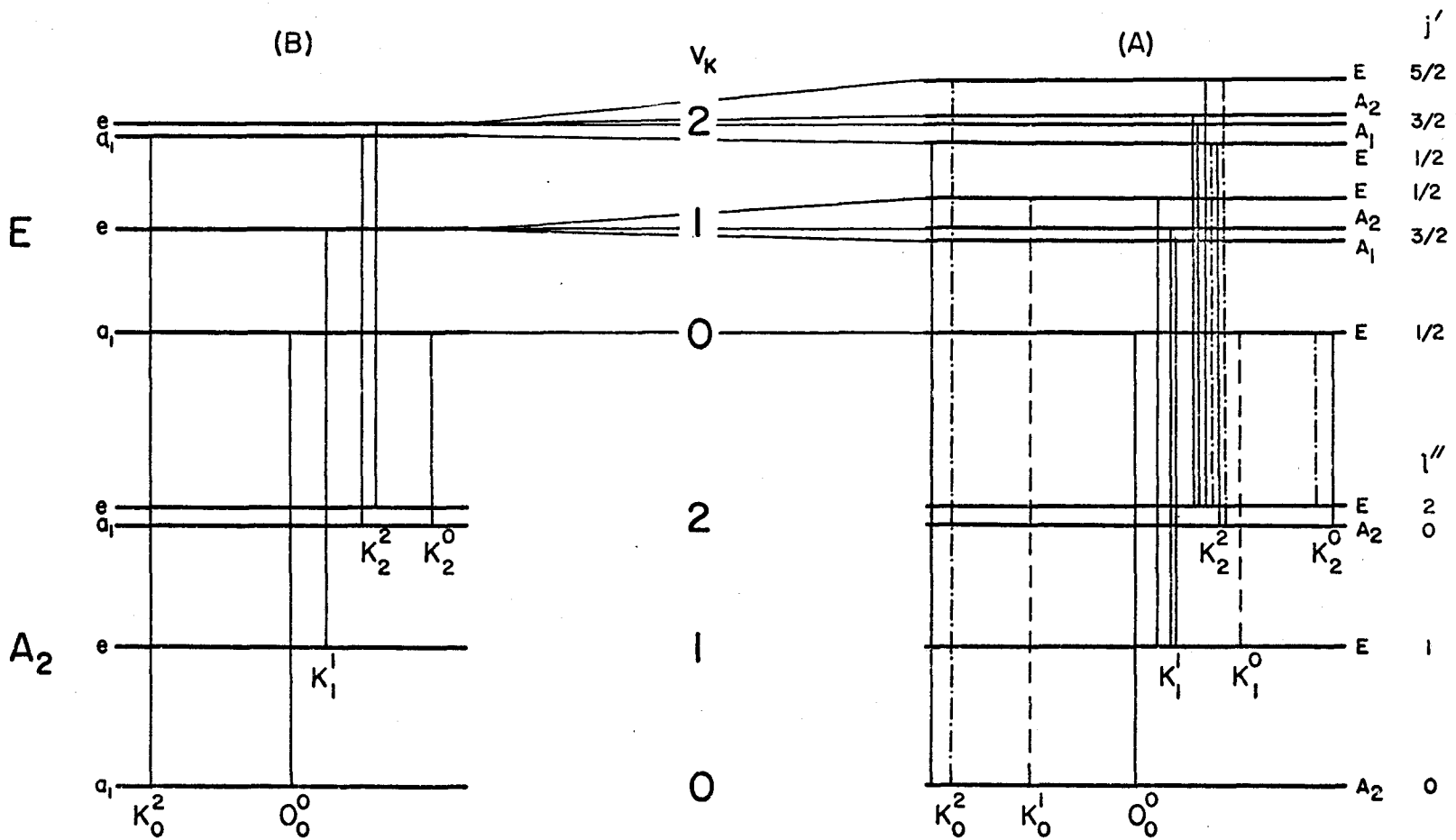

FIGURE 5·6 VIBRONIC TRANSITIONS IN A DEGENERATE VIBRATION V_K FOR AN $^1E—^1A$ ELECTRONIC TRANSITION OF A C_{3V} MOLECULE, (A) WITH AND (B) WITHOUT VIBRONIC INTERACTION

will be mixed with the vibrationless excited state level $v'_K = o$, $j' = 1/2$ by the linear term of the perturbing Hamiltonian equation 4.17. Since the transition from the vibrationless ground electronic state to this latter state ($v'_K = o$, $j' = 1/2$) is allowed (the vibrational overlap integral does not vanish) the mixing of the above two states will now lead to a non-zero transition moment for the transition from the vibrationless ground electronic state to the state $v'_K = 1$, $j' = 1/2$, that is, the transition K_o^1 is now allowed. For similar reasons, the transition K_1^o is also allowed when vibronic interactions are present. The intensity of these transitions depends upon the degree of mixing between the vibronic states, that is, upon the magnitude of the Jahn-Teller parameter k. The transitions which are indicated by dashed lines in Fig. 5.6 are allowed when only the linear term of the perturbing Hamiltonian H' of equation 4.17 is used in the Jahn-Teller calculation. The transitions represented by dashes and dots are allowed when the second order term is also included in the perturbing Hamiltonian. This term mixes states which differ in their j quantum numbers by ±3; that is, the state with $j = 5/2$ will be mixed with the state $j = -1/2$ etc.

The selection rule for vibronic transitions between an E and an $A_{1 \text{ or } 2}$ electronic state has been given by Longuet-Higgins[63] as

$$j' - 1'' = \pm 1/2 \tag{5.9}$$

The intensities of the members of an excited state progression in v'_K can be estimated from the square of the coefficients a_i in the expansion of $\psi_j^{\pm}$. See equation 4.23. ψ_j^+ and ψ_j^- are eigenfunctions of the operator $H_o + H'$ where H_o is the unperturbed two dimensional harmonic oscillator Hamiltonian. If the progression involves transitions arising

from the vibrationless ground state to excited state levels which are associated with vibronic states having j' = 1/2, then the intensity of a member of this progression will be proportional to the square of the coefficient of the zeroth order harmonic oscillator eigenfunction $\psi_{v=o,\ l=o}$, in the expansion of the vibronic wavefunction, equation 4.23, which approximates the vibronic state attained by the transition.

The variation in intensities of the members of a progression in ν_K' as a function of the Jahn-Teller parameter k are shown in Fig. 5.7. The eigenvectors for the upper state vibronic levels were obtained from the numerical solution of the matrix equation 4.24. This equation was solved for various values of k. The spin-orbit coupling constant was set equal to zero and ω_K was arbitrarily set at 300 cm^{-1}.

From Fig. 5.7, it can be seen that for k^2 less than 0.5, the 0_o^o transition is the most intense transition. The intensities of higher members of the progression in ν_K' are much weaker and long progressions in ν_K' would not be observed experimentally. As K^2 increases, the 0_o^o transition is no longer the most intense transition and long progressions in ν_K' would be observed experimentally. When k^2 is very large, two maxima appear in the intensity distribution of the progression.

Similar results will be observed with progressions in the ground state fundamental ν_K''. However, the intensity of these transitions will also depend on the Boltzmann population factor for the ground state vibronic level. For small values of k^2 the intensity distribution for the progression in ν_K'' will be similar to the intensity distribution for ν_K' except that the intensity of higher members will fall off much more rapidly.

No long progressions in ν_6'' (369.4 cm^{-1}) are observed in the absorption

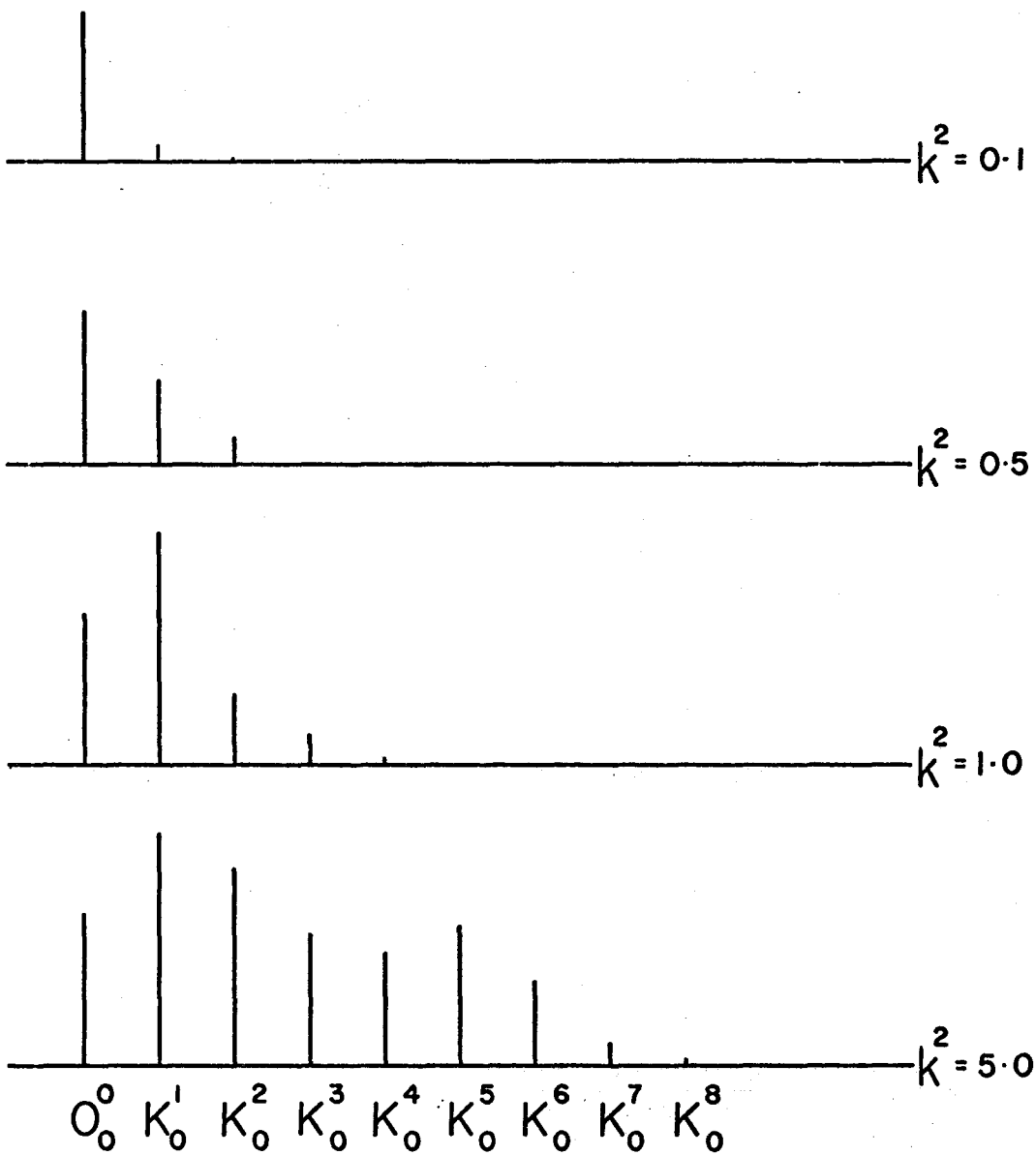

FIGURE 5·7 INTENSITY DISTRIBUTION OF THE MEMBERS OF A PROGRESSION IN ν_K'

spectrum of the fluorosulfate radical. Although 6_1^o is quite intense with respect to the intensity of the other hot bands, the second member of a progression in ν_6'', 6_2^o, could not be assigned with any certainty. In any case, the experimentally observed transition 6_2^o must be very weak.

Progressions in ν_4'' (1177.5 cm^{-1}) were not observed. This is not surprising since the intensity of higher members of a progression in ν_4'' would be very weak because of the Boltzmann population factor.

The band at $^+\nu_{oo}$ - 604.1 cm^{-1} has been assigned as 5_1^o. This transition originates from the degenerate vibrational level $\nu_5'' = 1$, $v_i'' = o$ (i=1,2,3,4,6) of the ground electronic state. In other related molecules, ν_5'' is observed in the infrared (as a strong band) at 583 cm^{-1}, 566 cm^{-1}, for $Na^+SO_3F^-$ [68] and $K^+SO_3F^-$ [68] respectively and at 562, 591, 594, 615, 541 and 611 cm^{-1} for $CH_3SO_3^-$ [86], $NH_2SO_3^-$, $OHSO_3^-$ [86], $CH_3OSO_3^-$ [86], $[SSO_3]^{2-}$ [82,83], $[SO_4]^{2-}$ [87] respectively. The band $^+5_1^o$ is approximately half as intense as $^+3_1^o$. The separation between $^+5_1^o$ and $^-5_1^o$ is 29.0 cm^{-1}. Although the assignment of 5_1^o is quite tentative, the frequency of ν_5'' that is obtained from this assignment agrees quite well with the frequency of ν_5'' in other related molecules.

In summary, the three degenerate e-type fundamentals of the ground state have been assigned the following wavenumbers

$$\nu_4'' = 1177.5 \text{ cm}^{-1}$$
$$\nu_5'' = 604.1 \text{ cm}^{-1}$$
$$\nu_6 = 369.4 \text{ cm}^{-1}$$

Each of these "hot" bands, in which a quantum of ν_K'' is excited, consists of two components whose splitting is the same as the separation of the two components of the origin band. These fundamentals are observed in combination with the totally symmetric fundamentals of the ground and excited states and also in combination with each other. The wavenumbers for these transitions are given in Table 5.7. Only the first members of progressions in the degenerate vibrations of the ground state have been definitely identified.

This fact indicates that if these transitions (K_o^1) are allowed because of a Jahn-Teller interaction then k^2 is not large ($\sim$0.5).

For small values of k^2 it is found from the theoretical calculations of Chapter 4 that the level ($v = o$, $l = o$, $j = 1/2$, $\Lambda = +1$, $\Sigma = 1/2$) is mixed more strongly with the other levels having $j = 1/2$, $\Sigma = +1/2$ by the Jahn-Teller perturbation H' than the level ($v = o$, $l = o$, $j = 1/2$, $\Lambda = +1$, $\Sigma = -1/2$) is mixed with the levels having $j = 1/2$, $\Sigma = -1/2$. The unequal mixing of the states for these above two levels will cause the intensities of the transitions to these two levels, from a common ground state, to be unequal. From this calculation, the low frequency component of the origin band is predicted to be more intense than the high frequency component for small values of k^2. The ratio of the intensities of the components of the origin band have been determined as a function of k^2. For each value of k^2, the spin-orbit coupling parameter A was varied until a splitting of 30 cm^{-1} was obtained for the separation of the two lowest levels of the excited state. The ratio of the squares of the coefficients of the zeroth order eigenfunctions ($v = o$, $l = o$, $j = 1/2$

$\Lambda = +1$, $\Sigma = -1/2$) and ($v = o$, $l = o$, $j = 1/2$, $\Lambda = +1$, $\Sigma = +1/2$) in the expansion of the wavefunctions for the two lowest states (4.23) were plotted as a function of k^2. The ratio of the intensities of the two transitions will be proportional to the above ratio. The results of this calculation are displayed in Fig. 5.8.

When $k^2 \cong o$, the transitions ${}^{+}0_{o}^{o}$ and ${}^{-}0_{o}^{o}$ will have equal intensities. As k^2 increases, the intensity of the ${}^{-}0_{o}^{o}$ transition becomes greater than the ${}^{+}0_{o}^{o}$ transition. It can be seen that the ratio of their intensities as a function of k^2 is linear.

The ratio of the intensities of the components of the origin band is experimentally found to be 1.17. This is the average value of the ratio's of the intensities given in Table 5.4. The value of k^2 which corresponds to this intensity ratio is determined from the graph of Fig. 5.8 to be approximately 0.6.

The above calculation has been carried out on the assumption that only one of the degenerate vibrations interacts in turn with the electronic motion. The fluorosulfate radical has three degenerate fundamentals which can all, in principle, interact with the electronic motion. The theoretical intensity ratio's are qualitatively correct but probably not quantitatively correct.

The results of the above calculation also show that for small values of k^2 the following relationship is valid.

$$\text{Intensity} \left(\frac{{}^{+}K_{o}^{1} + {}^{-}K_{o}^{1}}{{}^{+}0_{o}^{o} + {}^{-}0_{o}^{o}} \right) \cong k^2$$

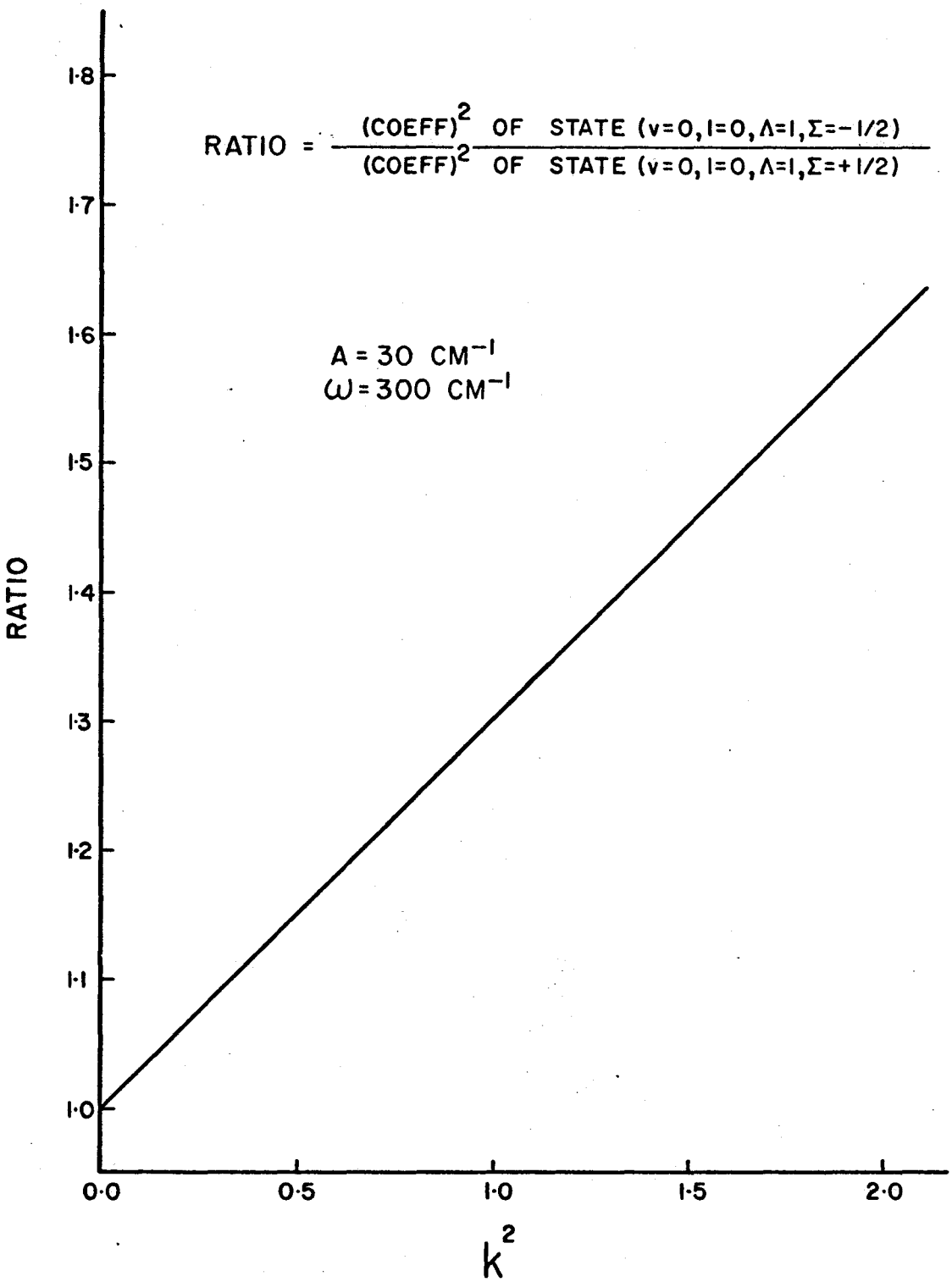

FIGURE 5·8 THEORETICAL INTENSITY RATIO OF $I(^{-}0^{\circ}_{o})/I(^{+}0^{\circ}_{o})$

Since transitions involving the degenerate fundamentals of the ground electronic state are observed in the absorption spectrum, one would also expect to observe transitions to levels involving the degenerate fundamentals of the excited state, that is, transitions of the type K_o^1. The assignment of bands to these transitions is not as definite as the previous assignments.

The band at $^+\nu_{oo}$ + 346.9 cm^{-1} has been assigned as $^+6_o^1$. The other component of this band $^-6_o^1$ is found at $^+\nu_{oo}$ + 346.9 - 22.9 cm^{-1}. The splitting of this band is 6.5 cm^{-1} less than the splitting of the origin band. When the above relationship is applied to the experimentally observed intensities of the transitions $^+6_o^1$, $^-6_o^1$, $^+0_o^o$, and $^-0_o^o$, k^2 is determined to be 0.3.

The sequence band $^+6_1^1$ was difficult to identify. The intense well-developed rotational structure of each of these components made the identificati of any weaker bands in this region very uncertain. However, once the rotational analysis of the origin band was carried out, it was possible to identify a series of lines which begin at $^+\nu_{oo}$ - 21.0 cm^{-1} and which could not be assigned to rotational transitions which accompany the 0_o^o vibronic transition. (See the series of lines labelled Z in Fig. 6.1.) The other component of the sequence, $^-6_1^1$, could not be positively identified. The sequence $^+6_1^1$ is also observed in combination with other fundamentals and these assignments are listed in Table 5.7.

The bands at $^+\nu_{oo}$ + 505.7 and $^+\nu_{oo}$ + 1114.5 cm^{-1} have been assigned to the transitions $^+5_o^1$ and $^+4_o^1$. Combinations of these vibrational frequencies account for a number of previously unassigned bands whose double-headed structure is similar to that of the origin band. These assignments are listed in Table 5.7.

A number of strong bands remain to be assigned. Many of these unassigned bands have a structure completely different from that of the origin band. For example, compare the structure of the bands denoted as α_o^1 and β_o^1 with those denoted as 0_o^o, 2_o^1 and 3_o^1 in Fig. 5.3. These bands are not impurity bands since they are found in combination with the ground and excited state fundamentals. Under high resolution, the rotational structures of α_o^1 and β_o^1 appear to be that of a parallel band (transition moment parallel to the C_3 axis) whereas the rotational structure of the origin band has been analysed as a perpendicular band (transition moment perpendicular to the C_3 axis). (See Chapter 6.) All attempts at assigning these as combination bands involving previously assigned frequencies have failed.

A number of these bands are separated by an interval of 191 cm^{-1}. A hot band is observed at 191 cm^{-1} to the red of the origin band. One puzzling feature of this band is that the spacing of the rotational sub-heads is approximately 3/2 times the spacing of the rotational sub-heads of the origin band. The 191 cm^{-1} interval could not be accounted for.

One possible assignment for the bands labelled α_o^1 and β_o^1 in Fig. 5.3 necessitates the breakdown of the selection rule $j' - 1'' = \pm 1/2$. If this rule is not strictly valid for the radical, then the band labelled α_o^1 could be assigned to the transition 6_o^1 ($j' = 3/2$), that is, the transition from the vibrationless ground electronic state of symmetry $^2A_2$ to the upper vibronic state $v_6' = 1$, $j' = 3/2$ of symmetry A_2. The above selection rule could break down under the following circumstances: strong vibronic interaction,[63] or the presence of a nearly electronic state with which the $^2E(2)$ state or the $^2A_2$ ground electronic state could strongly interact.[51]

The results of Sec. 5.2 and Chapter 3 indicate that there is a state of symmetry ^2E within 0.50 ev. of the $^2E(2)$ state. The former electronic state has been previously labelled $^2E(1)$.

Thus, α_o^1 and β_o^1 have been tentatively assigned as 6_o^1 ($j' = 3/2$) and 5_o^1 ($j' = 3/2$). Both of these transitions ($^2A_2 - {}^2A_2$) should be parallel bands. The observed bands appear to have a parallel structure. Only one of the spin-orbit components is observed for each of these transitions. The other component is either too weak to detect or it is forbidden. Combinations with the above transitions are reported in Table 5.7. A number of other unassigned bands are probably caused by transitions from the vibronic levels of the ground state to the numerous components of the overtones of degenerate vibrations of the excited electronic state. No detailed interpretation of these bands could be made.

It was originally hoped that members of progressions in excited state degenerate fundamentals and sequence bands of the type K_1^1, K_2^2,..., which should consist of several components (Fig 5.6), could be assigned in conjunction with the quantitative results of the Jahn-Teller-spin-orbit calculation. The results of this approach, however, were quite discouraging. It is felt that the qualitative aspects of this calculation are valid but that the quantitative results suffer from the fact that the radical has three degenerate modes of vibration and there is a nearby electronic state, $^2E(1)$, which can perturb the $^2E(2)$ electronic state. A calculation which includes the simultaneous interaction of the three degenerate vibrational modes with the electronic motion was not feasible since at least seven unknown parameters would enter the calculation. Similarily, second order terms in the Hamiltonian H' equation 4.17, should be

considered.*

The paucity of the experimental data and the magnitude of the theoretical calculation restricts the treatment to the interaction of the electronic motion with one degenerate vibrational mode only. This approximation reduces the unknown parameters to three. This restriction however does not appear to be valid for the fluorosulfate radical.

The presence of bands involving transitions of the type K_o^1 and K_1^o have been explained on the basis of a weak Jahn-Teller spin-orbit interaction (k^2,≈ 0.3 - 0.6). These transitions, however, would also be observed if the radical were permanently distorted in either or both the upper and lower states. If the molecule is distorted such that it has C_s symmetry and if the resulting off-axis potential minima are sufficiently deep (See Fig 4.2) then the vibrational levels result from the excitation of the two bending vibrations ν_{K_1} and ν_{K_2} which correspond to the single degenerate vibration ν_K of the symmetric conformation. The correlation of the vibronic levels of a degenerate vibration of a C_{3v} molecule with those of the two non-degenerate vibrations of the deformed molecule of symmetry C_s are given by Herzberg[90] for the E and A_1 electronic states. This diagram has been reproduced in Fig. 5.9 with the exception that the correlation for the A_1 state has been replaced by the correlation for the A_2 electronic state. The effects of spin-orbit coupling have been neglected since the electronic angular momentum will be quenched in the distorted conformation. At the extreme left of each diagram, the vibronic levels are shown for zero or small Jahn-Teller interaction; at the extreme right, they are shown for

---

* The effect of second-order terms of a pure Jahn-Teller interaction on the vibronic energy levels is discussed by Child.[88,89]

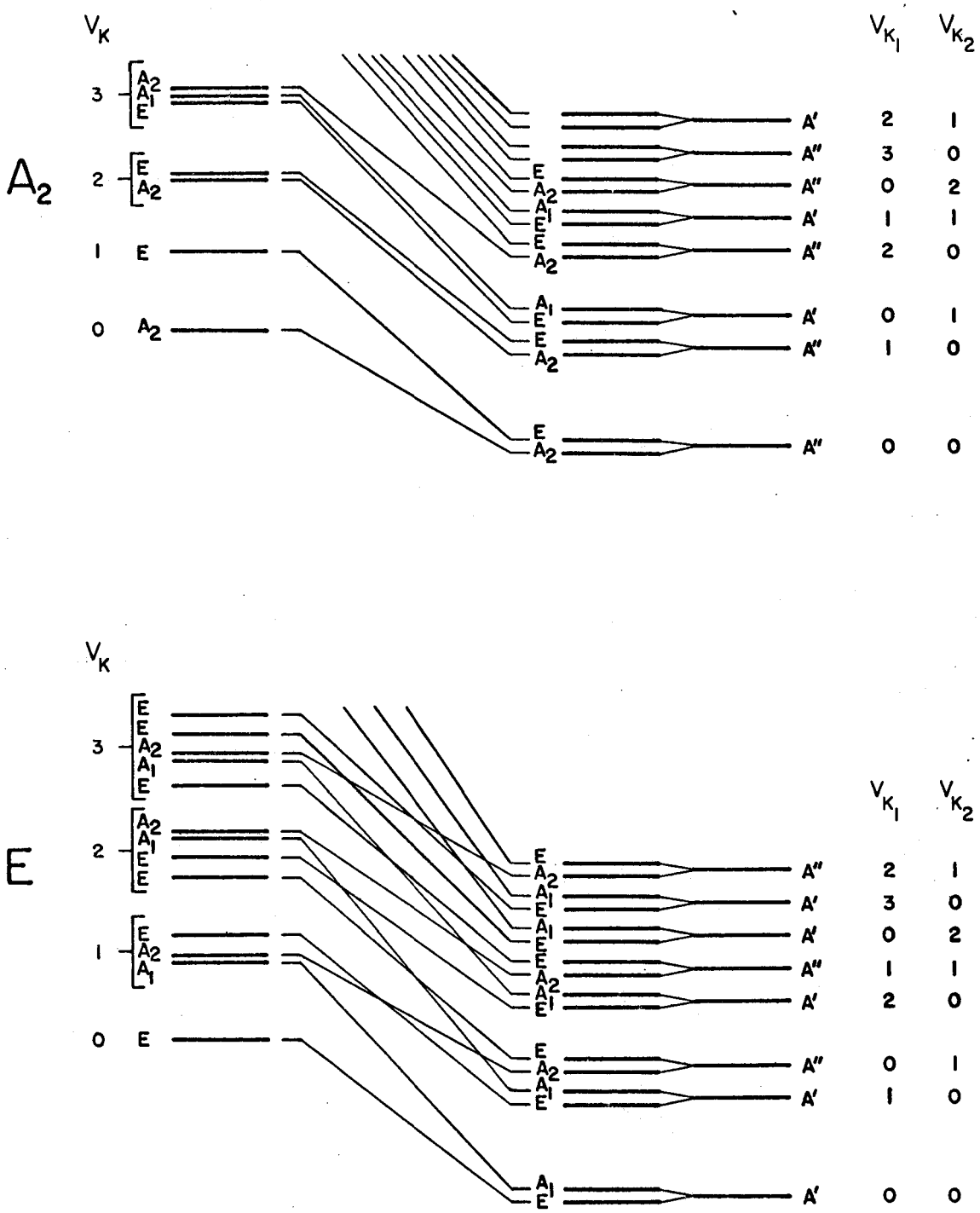

FIGURE 5·9 CORRELATION OF THE VIBRONIC LEVELS OF A C_{3V} MOLECULE WITH THOSE OF A DEFORMED MOLECULE OF SYMMETRY C_S

a corresponding molecule of symmetry C_s. A gradual deformation of the potential function from one of C_{3v} to one of C_s symmetry brought about by a hypothetical deformation of the electronic orbitals (in the case of the A_2 electronic state) or by increasing vibronic interaction (in the case of the E electronic state) is assumed from left to right. The levels at the extreme right are triply degenerate because of the necessary existence of three C_s conformations for the distorted molecule. If the coupling conditions are gradually changed so that the three potential minima are less and less deep, each of the triply degenerate levels at the extreme right will split into a doubly degenerate and a non-degenerate level. The main difference between the correlation of the $^2A_2$ electronic state and the E state is that there are actually twice as many levels to correlate for the degenerate state. It should be noted that the positions of the energy levels cannot be obtained by a simple interpolation between the two extreme cases. The intermediate case for the correlation of the ^2E state corresponds to large values of the parameters k and g and possibly even higher terms in the expansion of H' (4.17).

Absorption bands corresponding to the excitation of degenerate vibrations (or more accurately, vibrations correlating with the degenerate vibrations in the symmetrical configuration) should be observed if either the upper or the lower state were distorted from a C_{3v} configuration.

The results of the rotational analysis for the origin band indicate that there is very little change between the geometry of the upper and lower states (See Chapter 6). This conclusion is supported by the intensity distribution of the vibrational transitions. It is concluded that if one of the states is permanently distorted, then both states must be permanently

distorted by approximately the same amount. Therefore, either both states are permanently distorted or neither are permanently distorted.

If both states are distorted, then the observed splitting of the origin band must be explained according to Case III of Sec. 5.3 (ii). The conclusion drawn from the results of that section was that Δ_g must be smaller than 100 cm^{-1} in Case III. A separation of less than 100 cm^{-1} between the two lowest vibronic levels of the ground electronic state could only occur for a large permanent distortion. (right side of Fig. 5.9)

The analysis of the electron diffraction results[12] suggests that the ground state of the radical has C_{3v} symmetry. The rotational analysis is also consistent with this observation and similarily the E.S.R. results do not indicate any distortion. Since the majority of the results suggest that the ground state is not permanently distorted, the conclusion is drawn that the upper state is not permanently distorted. It is felt that transitions of the type K_o^1, K_1^o are observed because of a dynamic Jahn-Teller interaction.

TABLE 5.7

BAND FREQUENCIES AND ASSIGNMENTS FOR SO_3F. (Visible System)

CM^{-1}	ASSIGNMENT	CM^{-1} FROM $^{+}V_{oo}$ (19383.1 CM^{-1})
17643.4	$^{-}1_1^0 3_1^0$	-1739.7 (-1710.3-29.4)
672.8	$^{+}6_1^0 3_1^0$	-1710.3 (-1177.5-532.8)
708.5	$^{-}2_2^0$	-1674.6 (-1646.0-28.6)
737.1	$^{+}2_2^0$	-1646.0 (-839.3-806.7)
765.9	$^{+}1_1^0 3_2^0$	-1617.2 (-1587.1-30.1)
796.0	$^{+}1_1^0 3_2^0$	-1587.1 (-1055.5-531.6)
917.0	$^{-}6_1^0 3_2^0$	-1466.1 (-1435.8-30.3)
947.3	$^{+}6_1^0 3_2^0$	-1435.8 (-533.5-533.8-368.5)
981.3	$^{-}2_1^0 3_1^0$	-1401.8 (-1371.7-30.1)
991.1	$^{+}2_1^0 3_1^0 6_1^0$	-1392.0 (-1371.7-20.3)
18011.4	$^{+}2_1^0 3_1^0$	-1371.7 (-839.3-532.4)
146.7	$^{-}2_1^0 6_1^0$	-1236.4 (-839.3-369.4-27.7)
175.8	$^{-}4_1^0$	-1207.3 (-1177.5-29.8)
185.0	$^{+}4_1^0 6_1^1$	-1198.1 (-1177.5-20.6)
205.6	$^{+}4_1^0$	-1177.5
216.0	$^{-}5_1^0 3_1^0$	-1167.1 (-1138.3-28.8)
224.1	$^{+}5_1^0 3_1^0 6_1^1$	-1159.0 (-1138.3-20.7)
244.9	$^{+}5_1^0 3_1^0$	-1138.4 (-604.1-534.3)
286.0	$^{-}3_2^0$	-1097.1 (-1055.5-20.9)
297.9	$^{-}1_1^0$	-1085.2 (-1055.5-29.7)

CM^{-1}	ASSIGNMENT	CM^{-1}	FROM $^{+}V_{oo}$ (19383.1 CM^{-1})
18306.7	$^{+}1_1^0 6_1^1$	-1076.4	(-1055.5-20.9)
315.8	$^{+}3_2^0$	-1067.3	(-533.5-533.8)
327.6	$^{+}1_1^0$	-1055.5	
411.3	$\beta_0^1 2_1^0 3_1^0$	-971.8	(+400.9-839.3-533.4)
422.4	$^{-}3_2^0 5_0^1 6_1^0$	-960.7	(-931.1-29.6)
449.5	$^{-}3_1^0 6_1^0$	-933.6	(-903.8-29.8)
452.0	$^{+}3_2^0 5_0^1 6_1^0$	-931.1	(-533.5-533.8+505.6-369.4)
459.3	$^{+}3_1^0 6_2^1$	-923.8	(-903.8-20.0)
479.3	$^{+}3_1^0 6_1^0$	-903.8	(-533.5-370.3)
514.3	$^{-}2_1^0$	-868.8	(-839.3-29.5)
523.1	$^{+}2_1^0 6_1^1$	-860.0	(-839.3-20.7)
543.8	$^{+}2_1^0$	-839.3	
605.9	$\beta_0^1 4_1^0$	-777.7	(-400.9-1178.1)
691.7	$^{-}3_0^1 4_1^0$	-691.4	(+515.5-1177.5-29.4)
721.1	$^{+}3_0^1 4_1^0$	-662.0	(+515.5-1177.5)
728.5	$\beta_0^1 1_1^0$	-654.6	(+400.9-1055.5)
749.0	$^{-}5_1^0$	-634.1	(-604.1-30.0)
757.7	$^{+}5_1^0 6_1^1$	-625.4	(-604.1-21.3)
779.0	$^{+}5_1^0$	-604.1	
820.2	$^{-}3_1^0$	-562.9	(-533.5-29.4)
828.6	$^{+}3_1^0 6_1^1$	-554.5	(-533.5-21.0)
849.6	$^{+}3_1^0$	-533.5	
946.0	$\beta_0^1 2_1^0$	-437.1	(+400.9-838.0)

CM^{-1}	ASSIGNMENT	CM^{-1}	FROM $^{+}V_{oo}$ (19383.1 CM^{-1})
18956.9	$^{-}6_1^0 5_0^1 3_1^0$	-426.2	(-369.4+505.7-533.4-29.1)
984.3	$^{-}6_1^0$	-398.8	(-369.4-29.4)
991.8	$^{+}6_2^1$	-391.3	(-369.4-21.9)
19013.7	$^{+}6_1^0$	-369.4	
028.0	$^{-}3_1^0 2_1^0$	-355.1	(+515.0-840.4-29.7)
058.0	$\alpha_0^1 3_1^0$	-325.5	(+208.5-533.6)
058.9	$^{+}3_0^1 2_1^0$	-324.2	(+515.0-839.3)
196.3	$^{+}6_0^1 3_1^0$	-186.8	(+346.9-533.7)
224.2	$\alpha_0^1 6_1^0$	-158.9	(-369.4+210.5)
228.1	$^{+}3_0^2 4_1^0$	-155.0	(+1024.5-1179.5)
250.6	$\beta_0^1 3_1^0$	-132.5	(+400.9-533.4
353.7	$^{-}0_0^0$	- 29.4	
362.2	$^{+}6_1^1$	- 20.9	(+346.9-367.8)
383.1	$^{+}0_0^0$	+ 0.0	
413.9	$\beta_0^1 6_1^0$	+ 30.8	(+400.9-370.1)
474.1	$^{-}1_0^1 2_1^0$	+ 91.0	(+929.5-838.5)
499.8	$^{-}3_0^1 6_1^0$	+116.7	(+515.0-369.3-29.0)
519.3	$^{+}5_0^1 6_1^0$	+136.2	(+505.7-369.5)
528.8	$^{+}3_0^1 6_1^0$	+145.7	(+515.0-369.3)
591.6	α_0^1	+208.5	
627.0	$^{-}2_0^1 3_1^0$	+243.9	(+800.3-533.1-23.3)
630.0	$^{+}2_0^1 3_1^0 6_1^1$	+246.9	(+800.3-533.1-20.3)
650.3	$^{+}2_0^1 3_1^0$	+267.2	(+800.3-533.1)

CM^{-1}	ASSIGNMENT	CM^{-1} FROM $^{+}V_{oo}$ (19383.1 CM^{-1})	
19707.1	$^{-}6_0^1$	+324.0	(+346.9-22.9)
730.0	$^{+}6_0^1$	+346.9	
746.9	$\beta_0^1 2_1^1$	+363.8	(+400.9+800.3-837.4)
784.0	β_0^1	+400.9	
814.2	$+2_0^1 6_1^0$	+431.1	(+800.3-369.2)
859.7	$^{-}5_0^1$	+476.6	(+505.7-29.1)
868.4	$^{-}3_0^1$	+485.3	(+515.0-29.7)
877.1	$^{+}3_0^1 6_1^1$	+494.0	(+515.0-21.0)
888.8	$^{+}5_0^1$	+505.7	
898.1	$^{+}3_0^1$	+515.0	
943.5	$^{-}1_0^1 6_1^0$	+560.4	(+953.0-369.2-23.2)
966.7	$^{+}1_0^1 6_1^0$	+583.6	(+953.0-369.4)
20034.1	$^{+}3_0^1 5_0^1 6_1^0$	+651.0	(+515.0+505.3-369.3)
038.1	$^{+}3_0^2 6_1^0$	+655.0	(+515.0+509.5-369.5)
103.7	$\alpha_0^1 3_0^1$	+720.6	(+208.5+512.1)
160.0	$^{-}2_0^1$	+776.9	(+800.5-23.6)
183.6	$^{+}2_0^1$	+800.5	
212.0	$^{-}5_0^1 6_0^1$	+828.9	(+346.9+503.3-21.3)
219.9	$^{-}3_0^1 6_0^1$	+836.8	(+346.9+514.5-24.6)
233.3	$^{+}5_0^1 6_0^1$	+850.2	(+346.9+503.3)
244.5	$^{+}3_0^1 6_0^1$	+861.4	(+346.9+514.5)
312.6	$^{-}1_0^1$	+929.5	(+952.9-23.4)
314.9	$^{+}1_0^1 6_1^1$	+931.8	(+952.9-21.1)

CM^{-1}	ASSIGNMENT	CM^{-1} FROM $^{+}V_{oo}$ (19383.1 CM^{-1})
20336.0	$^{+}1_0^1$	+952.9
359.5	$\delta_0^1(5_0^2)$	+976.4
375.4	$^{-}3_0^1 5_0^1$	+992.3 (+515.0+505.3-28.0)
380.5	$^{-}3_0^2$	+997.4 (+515.0+509.5-27.1)
403.4	$^{+}3_0^1 5_0^1$	+1020.3 (+515.0+505.3)
407.6	$^{+}3_0^2$	+1024.5 (+515.0+509.5)
471.8	$^{-}4_0^1$	+1088.7 (+1114.5-25.8)
477.3	$4_0^1 6_1^1$	+1094.2 (+1114.5-20.3)
497.6	$^{+}4_0^1$	+1114.5
584.5	$\beta_0^1 2_0^1$	+1201.4 (+400.9+800.5)
695.6	$^{+}3_0^1 2_0^1$	+1312.5 (+800.3+512.2)
731.1	$^{-}6_0^1 3_0^2$	+1348.0 (+324.0+1024.0)
759.8	$^{+}6_0^1 3_0^2$	+1376.7 (+346.9+1029.8)
822.3	$^{-}1_0^1 3_0^1$	+1439.2 (+953.0+511.5-25.3)
847.6	$^{+}1_0^1 3_0^1$	+1464.5 (+953.0+511.5)
883.6	$^{-}3_0^2 5_0^1$	+1500.5 (+1024.5+505.6-29.6)
889.4	$^{-}3_0^3$	+1506.3 (+515.0+509.5+509.3-27.5)
913.2	$^{+}3_0^2 5_0^1$	+1530.1 (+1024.5+505.6)
916.9	$^{+}3_0^3$	+1533.8 (+515.0+509.5+509.3)
959.7	$^{+}2_0^2 6_1^1$	+1576.6 (+1597.6-21.0)
980.7	$^{+}2_0^2$	+1597.6 (+800.3+797.3)
21012.7	$^{+}4_0^1 3_0^1$	+1629.6 (+1114.5+515.1)
105.5	$^{-}1_0^1 2_0^1$	+1722.4 (+953.0+795.7-26.3)

CM^{-1}	ASSIGNMENT	CM^{-1} FROM $^{+}V_{oo}$ (19383.1 CM^{-1})
21131.8	$^{+}1_0^1 2_0^1$	+1748.7 (+953.0+795.7)
154.8	$\delta_0^1 2_0^1$	+1771.7 (+976.4+795.3)
176.6	$^{-}3_0^2 2_0^1$	+1793.5 (+515.0+509.5+795.7-26.7)
198.8	$^{+}2_0^1 3_0^1 5_0^1$	+1815.7 (+515.0+505.3+795.4)
203.3	$^{+}3_0^2 2_0^1$	+1820.2 (+515.0+509.5+795.7)
286.9	$^{+}1_0^2$	+1903.8 (+953.0+950.8)
295.8	$^{+}4_0^1 2_0^1$	+1912.7 (+1114.5+798.2)
358.4	$^{+}1_0^1 3_0^2$	+1975.3 (+1024.5+950.8)
494	$^{+}2_0^2 3_0^1$	+2111 (+800.2+794.4+516.4)
638	$^{+}1_0^1 2_0^1 3_0^1$	+2255 (+953.0+511.5+791.5)
718	$^{+}2_0^1 3_0^3$	+2335 (+1533.5+801.5)
797	$^{+}1_0^2 3_0^1$	+2414 (+953.0+950.8+510.2)

CHAPTER 6

ROTATIONAL ANALYSIS OF THE FLUOROSULPHATE RADICAL SPECTRA

6.1 The Moments of Inertia and Rotational Constants

The moment of inertia of a rigid body about an axis is defined by

$$I = \sum_i m_i \rho_i^2 \tag{6.1}$$

where ρ_i is the perpendicular distance of the mass element m_i from the axis. A simple theorem of mechanics states that three mutually perpendicular axes whose origin is the centre of mass can be found for which the moments of inertia about these axes are either a maximum or a minimum. These axes and the corresponding moments of inertia are called the principal axes and the principal moments of inertia respectively.

The principal moments of inertia for a molecule treated as a rigid body can be obtained from the solution of the determinantal equation.[91]

$$\begin{vmatrix} I_{x'x'} - I & -I_{x'y'} & -I_{x'z'} \\ -I_{x'y'} & I_{y'y'} - I & -I_{y'z'} \\ -I_{x'z'} & -I_{y'z'} & I_{z'z'} - I \end{vmatrix} = 0 \tag{6.2}$$

where $I_{x'x'}$, $I_{y'y'}$,... are moments and products of inertia with respect to any convenient frame of cartesian coordinates (x'y'z') having the centre of mass as origin.

$$I_{x'x'} = \sum_i m_i \, (y'^2_i + z'^2_i) \tag{6.3}$$

$$I_{x'y'} = \sum_i m_i \, x'_i \, y'_i \tag{6.4}$$

where x_i' y_i' and z_i' are the coordinates of the i^{th} nucleus of mass m_i and where the summation is over all nuclei present in the molecule. The three roots of equation 6.2 are the principal moments of inertia and are labelled I_a, I_b and I_c such that $I_c > I_b > I_a$.

Molecules may be grouped into five categories according to the relationships among the principal moments of inertia:

i)	$I_a = I_b = I_c$	-spherical top
ii)	$I_a = o$, $I_b = I_c$	-linear (symmetric top)
iii)	$I_a < I_b = I_c$	-prolate symmetric top
iv)	$I_a = I_b > I_c$	-oblate symmetric top
v)	$I_a < I_b < I_c$	-asymmetric top

The fluorosulfate radical in its ground electronic state is a prolate symmetric top. The a axis coincides with the C_3 axis. The rotational constants A,B and C are defined in cm^{-1} units as

$$A = \frac{\hbar}{4\pi c I_a} \quad , \quad B = \frac{\hbar}{4\pi c I_b} \quad , \quad C = \frac{\hbar}{4\pi c I_c} \tag{6.5}$$

The principal moments of inertia of the radical were calculated by means of equation 6.2 using the experimentally determined ground state S-O, S-F, and OSF bond lengths and bond angles[12] respectively. The calculated principal moments of inertia and the corresponding rotational constants are given in Table 6.1

TABLE 6.1

MOMENTS OF INERTIA AND ROTATIONAL CONSTANTS FOR SO_3F IN ITS GROUND ELECTRONIC STATE

$I_a = 152.6 \times 10^{-40}$ gm - cm^2	$A = 0.183_4$ cm^{-1}
$I_b = 177.2 \times 10^{-40}$ gm - cm^2	$B = 0.158_0$ cm^{-1}
$I_c = 177.2 \times 10^{-40}$ gm - cm^2	$C = 0.158_0$ cm^{-1}

6.2 Molecular Model

In the most general case, a molecule may be regarded as possessing five independent types of angular momentum. They are the angular momenta created by (a) molecular rotation $\bar{R}$, (b) orbital motion of the electrons $\bar{L}$, (c) unpaired electron spin $\bar{S}$, (d) nuclear spin $\bar{I}$, and (e) degenerate vibrations $\bar{l}$. Interactions involving nuclear spins are ignored since their effects upon the rotational levels are generally only detected by microwave techniques.

Throughout this chapter it is necessary to refer to several Cartesian coordinate systems described as follows:

1. Space-fixed, X', Y', and Z'; the laboratory fixed axis system which does not translate or rotate with the molecule.

2. Nonrotating, X, Y, and Z; parallel to X', Y', and Z' but with origin translating with the molecular centre of mass.

3. Rotating, x, y and z; the molecule-fixed axis system which translates with the molecule.

The type I^r representation of King, Hainer, and Cross[92] has been adopted such that the molecule-fixed x, y and z axes are taken coincident with the principal inertial axes b, c, and a respectively.

If the total angular momentum of the molecule is denoted by J and if the total angular momentum exclusive of end-over-end rotation of the nuclei is denoted by $\bar{P}$, then the angular momentum of end-over-end rotation is $|\bar{J} - \bar{P}|$ and the rotational energy or Hamiltonian function is

$$H_{ROT} = B\,(J_x - P_x)^2 + C(J_y - P_y)^2 + A\,(J_z - P_z)^2 \tag{6.6}$$

It should be noted that the internal angular momentum $\bar{P}$, unlike $\bar{J}$, can be regarded as measured relative to, rather than referred to, the molecule-fixed axes x, y and z. Consequently, P_x, P_y and P_z satisfy commutation relations with the normal sign of i

$$[P_x, P_y] = iP_z \tag{6.7}$$

whereas J_x, J_y and J_z satisfy commutation relations with the anomolous sign of i

$$[J_x, J_y] = -iJ_z \tag{6.8}$$

when $\bar{J}$ is referred to the molecule-fixed axis. The normal sign of i prevails when $\bar{J}$ is referred to the non-rotating axes X,Y,Z.

$$[J_X, J_Y] = i\,J_Z \tag{6.9}$$

If one introduces the concept of "reversed angular momenta" such that

$$\begin{aligned} \tilde{P}_x &= -P_x \\ \tilde{P}_y &= -P_y \\ \tilde{P}_z &= -P_z \end{aligned} \tag{6.10}$$

, where the tildes denote the reversed angular momenta, then these satisfy commutation relations analogous to those of $\bar{J}$.

$$[\tilde{P}_x, \tilde{P}_y] = -i\,\tilde{P}_z \tag{6.11}$$

The point of using the reversed angular momenta is that they satisfy the same commutation relations, referred to the molecule-fixed axes, as do the components of the total angular momentum. The sign of i is never important as long as one is consistent in the usage.

If the internal angular momentum is neglected then

$$H_{ROT} = B\,(J_x^2 + J_y^2) + AJ_z^2 \tag{6.12}$$

for a prolate symmetric top. The states of a symmetric rotor can be characterized by the quantum numbers J, for the total angular momentum, K for the component of $\bar{J}$ along the molecule-fixed z axis and M for the component of $\bar{J}$ along the non-rotating Z axis.

Since, from Tinkham[94]

$$\langle JKM|J_z^2|JKM\rangle = K^2$$

and

$$\langle JKM|J^2|JKM\rangle = J(J+1) \tag{6.13}$$

then

$$F(J,K) = BJ(J+1) + (A-B)\,K^2 \tag{6.14}$$

This equation represents the term energies (in cm^{-1}) of a prolate symmetric top in a non-degenerate single electronic state. The above equation was derived by treating the nuclear framework as a rigid body. If this restricton is relaxed by postulating that the nuclei are held in their equilibrium configuration only by the restoring forces which determine the vibrational motion, then small correction terms

due to centrifugal distortion must be added to the previous energy expression. The term energies of the symmetric top are now given by

$$F_{[v]}(J,K,M) = B_{[v]}J(J+1) + (A_{[v]}-B_{[v]})K^2 - D_J J^2(J+1)^2 - D_{JK}J(J+1)K^2 - D_K K^4 \tag{6.15}$$

where

$$B_{[v]} = B_e - \sum \alpha_i^B (v_i + d_i/2) \tag{6.16}$$

$$A_{[v]} = A_e - \sum \alpha_i^A (v_i - d_i/2) \tag{6.17}$$

The D's are centrifugal distortion constants, B_e and A_e are the rotational constants of the molecule in its equilibrium configuration, and the α's are small constants.

If the symmetric top molecule is in a degenerate electronic state then the angular momentum $\bar{L}$ due to the electronic motion must also be taken into account.

$$H_{ROT} = B(J_x^2 + J_y^2) + A(J_z+L_z)^2 * \tag{6.18}$$

and

$$F(\Gamma_e,J,K,M) = BJ(J+1) + (A-B)K^2 \mp 2A\zeta_e K + \text{CENTRIFUGAL DISTORTION TERMS} \tag{6.19}$$

ζ_e, the component of electronic angular momentum along the z axis is in general non-integral and may be positive or negative. Γ_e represents the irreducible representation of the point group for the molecule at equilibrium to which the electronic state under consideration belongs. By analogy with the above equations, the effect of vibrational angular

---

* L_x and L_y will be averaged out and need not be considered. Unless stated otherwise A and B mean $A_{[v]}$ and $B_{[v]}$.

momentum in a non-degenerate electronic state can be accounted for by including a term of the form

$$\pm 2A\zeta_{[v]}K \tag{6.20}$$

in equation 6.15. In the simplest case, when a single degenerate vibration ν_i is single excited, $\zeta_v = \zeta_i$ is a quantity whose magnitude is determined by the form of the two components of the normal mode. The ζ_v of degenerate vibrations lies between + 1 and -1. If several degenerate vibrations are singly or multiply excited and each has angular momentum about the C_3 axis, the total vibrational angular momentum $\zeta_v\hbar$ is given by Herzberg as

$$\zeta_v\hbar = \sum_i (\pm\zeta_i l_i)\hbar \tag{6.21}$$

In a degenerate vibronic level of a degenerate electronic state, it is the resultant vibronic angular momentum $\zeta_t\hbar$ which must be considered. The rotational energy is obtained by adding the term

$$\pm 2A\zeta_t K \tag{6.22}$$

to equation 6.15.

For small vibronic interactions

$$\zeta_t = |\ \zeta_e \pm \zeta_v| \tag{6.23}$$

For stronger vibronic interactions, more complicated formulae apply.[88]

The effect of electron spin should also be included in this section but since there are a number of ways in which the spin can couple to the molecular systems, its treatment will be reserved until later in this chapter.

6.3 Symmetry Classifications, Nuclear Statistical Weights

The rotational eigenfunctions of a symmetric top molecule can be classified according to the full symmetry group of the molecule. The irreducible representations to which the rotational eigenfunctions $|JKM\rangle$ transform for a C_{3v} molecule are given in Table 6.2.

TABLE 6.2

IRREDUCIBLE REPRESENTATIONS FOR WHICH THE STATES $|JKM\rangle$ TRANSFORM UNDER C_{3v}

STATE		IRREDUCIBLE REPRESENTATION
K = o	J_{even}	A_1
	J_{odd}	A_2
K = 3n, n = 1,2,3		$A_1 + A_2$
K = 3n ± 1, n = 1,2,3..		E

The species to which the rovibronic wavefunction $\psi_{evr} = \psi_e\psi_v\psi_r$ belongs is obtained by taking the direct product

$$\Gamma_{evr} = \Gamma_{ev} \times \Gamma_r \tag{6.24}$$

For a discussion of the statistical weights of the rotational levels, only the behaviour of the total wavefunction with respect to the rotational subgroup need be considered. For a C_{3v} molecule, the rotational subgroup is C_3.

The oxygen nuclei have zero nuclear spin (I=o) and therefore obey Bose statistics. Also, since I=o, the nuclear wavefunction ψ_n must transform as A under the operations of the point group C_3.

For Bose Statistics, the total eigenfunction $\psi_T = \psi_e\psi_v\psi_r\psi_n$ must remain unchanged for an exchange of a pair of identical nuclei; that is, the total wavefunction must transform as A. Since ψ_n transforms as A, then only those states for which $\psi_e\psi_v\psi_r$ transform as A are accessible to the system. Rovibronic states which transform as E are inaccessible to the system. For the A_2 electronic state of the radical only every third level will be populated (K=0,3,6,9...; K ≠ 1,2,4,5...). Similarily, for the E vibronic state, only levels with K = 1,2,4,5... will be accessible to the system. Because only states with certain K values are occupied, the rotational structure of a band should have intervals that are much larger than if states with all values of K were occupied.

All the levels with different values of J but the same value of K are occupied if the particular K value is accessible to the system. For a given value of J, a level has an additional (2J+1)-fold degeneracy resulting from possible orientations of the molecule in space.

6.4 Transition Energies

The rotational selection rules for a transition $\langle\Gamma'_{ev} J'K'M' | \leftarrow \langle\Gamma''_{ev} J''K''M'' |$ are

$$\Delta K = \pm 1$$
$$\Delta J = o, \pm 1 \qquad \text{-perpendicular band} \qquad (6.25)$$

when the transition is electronically allowed and directed normal to the C_3 axis and

$$\Delta K = o$$
$$\Delta J = o, \pm 1 \qquad \text{-parallel band} \qquad (6.26)$$

when the transition is electronically allowed and directed parallel to the C_3 axis.

Transitions which occur between states with fixed values of K' and K" accompanied by changes in J result in the formation of P, Q and R branches.

P Branch

$$J' = J-1 \qquad J = J'' \tag{6.27}$$

$$\nu = \nu^{o}(K) + (B'-B'')J^2 - (B'-B'')J + \text{CENT. DIST.}$$

Q Branch

$$J' = J \qquad J = J''$$

$$\nu = \nu^{o}(K) + (B'-B'')J^2 + (B'-B'')J + \text{CENT. DIST.} \tag{6.28}$$

R Branch

$$J' = J+1 \qquad J = J''$$

$$\nu = \nu^{o}(K) + (B'-B'')J^2 + (3B'-B'')J + 2B' + \text{CENT. DIST.} \tag{6.29}$$

Because of the selection rules for J, these branches form a series of sub-bands for each group of transitions in which the quantum number K changes by 0, ±1. Each of these sub-bands may be referred to an origin which is where the hypothetical J" = 0$\longleftrightarrow$J' = 0 transition would occur. The frequencies of these sub-band origins are given by

$$\nu^{o}_{\substack{r\\p}}(K) = \nu_o + [A'(1-2\zeta_e)-B'] \pm 2\,[A'(1-\zeta_e')-B']K$$
$$(\Delta K=\pm 1) \qquad +[(A'-B')-(A''-B'')K^2 + \text{CENT. DIST.} \tag{6.30}$$

for a perpendicular band (E-A_2 electronic transition). For the SO_3F radical, K = 0,3,6... A similar expression can be written for the sub-band origins of a parallel band, (for example A_1-A_1 electronic transition)

$$\nu_Q^o(K) = \nu_o + [(A'-B')-(A''-B'')]K^2 + \text{CENT. DIST.}$$

($\Delta K = 0$)

The sub-band origins will be denoted by the symbols $^PQ_{K''}$ where $\Delta K = -1$ and $\Delta J = 0$ and $^RQ_{K''}$ where $\Delta K = +1$ and $\Delta J = 0$ etc. Branches will be denoted by the symbol

$$^{\Delta K}\Delta J_{K''}(J'')$$

For example, the transition denoted as $^PP_9(6)$ corresponds to $\Delta K = -1$, $\Delta J = -1$, K''=9, and J''=6.

6.5 Intensities of Rovibronic Transitions

The component of the electric dipole moment operator $\bar{P}_F$ along a non-rotating axis F, where F = X,Y, or Z can be written in terms of the components of the electric dipole moment operator $\bar{P}_g$ along the molecule-fixed axes g(g = x,y, or z) by the relation

$$\bar{P}_F = \sum_g \bar{\Phi}_{Fg} \bar{P}_g \tag{6.32}$$

where $\bar{\Phi}_{Fg}$ are the direction cosines between the two sets of coordinate axes. The transition moment $\bar{M}_F$ for rovibronic transitions is therefore given as

$$\bar{M}_F = \int \psi^*_{ev'} \psi_{J'K'M'} \bar{P}_F \psi_{ev''} \psi_{J''K''M''} \, dT$$

$$= \sum_g \langle ev' | \bar{P}_g | ev'' \rangle \langle J'K'M' | \bar{\Phi}_{Fg} | J''K''M'' \rangle$$

The matrix elements $\langle ev' | \overline{P}_g | ev'' \rangle$ have previously been discussed in section 4.1.3 and will be considered to be non-zero for the rovibronic transition under consideration. Since the energy of a vibronic state is independent of the quantum numbers M'' and M' and since, in the absence of external fields, the directions X,Y and Z are equivalent, the intensity of a rovibronic transition is proportional to the square of the direction cosine matrix elements summed over M',M'' and F.

$$I_{J';K' \leftarrow J'';K''} \propto \sum_{F,M';M''} | \langle J'K'M' | \overline{\Phi}_{F_g} | J''K''M'' \rangle |^2$$

$$= | \langle J' | \overline{\Phi}_{Zg} | J'' \rangle |^2 . | \langle J';K' | \overline{\Phi}_{Zg} | J''K'' \rangle |^2 \sum_{M'M''} | \langle J'M' | \overline{\Phi}_{Zg} | J''M'' \rangle |^2 \qquad (6.34)$$

The matrix elements of the direction cosines and the intensity expressions are given by Allen and Cross.[96]

6.6 Rotational Analysis of the Origin Band

i) Description of the High Resolution Spectrum

Under low resolution the origin band is observed as two sharp heads separated by approximately 29 cm^{-1}. Under high resolution, the origin band is seen to consist of a very large number of bands. A high resolution Ebert spectrogram of the 0_o^o band is shown in Fig. 6.1. The most noticeable feature of this spectrum is the presence of a number of broad, very intense, head-like features.* In this spectrum, two regions of intense absorption are seen which correspond to the two sharp heads observed under low resolution. As one moves to low frequency from these two regions of maximum intensity the intervals between the sub-heads increases; that is, they are degraded to the red. The spectrum of the low frequency component appears much more complex than the spectrum of the high frequency component.

Between the intense sub-heads, a number of weaker lines** are observed whose spacing is much smaller (~2B"). These lines are also degraded to the red.

Just to the violet of the strongest sub-head of the high frequency component, a number of still weaker lines are present.

ii) Analysis of the High Frequency Component

The intense sub-heads of the high frequency component are very broad

---

* These broad, intense, head-like features will be referred to as sub-heads. The term heads will be reserved to describe the low resolution absorption bands which are split by 29 cm^{-1}.

** The term "lines" is, strictly speaking, not correct since more than one transition can contribute to this absorption feature.

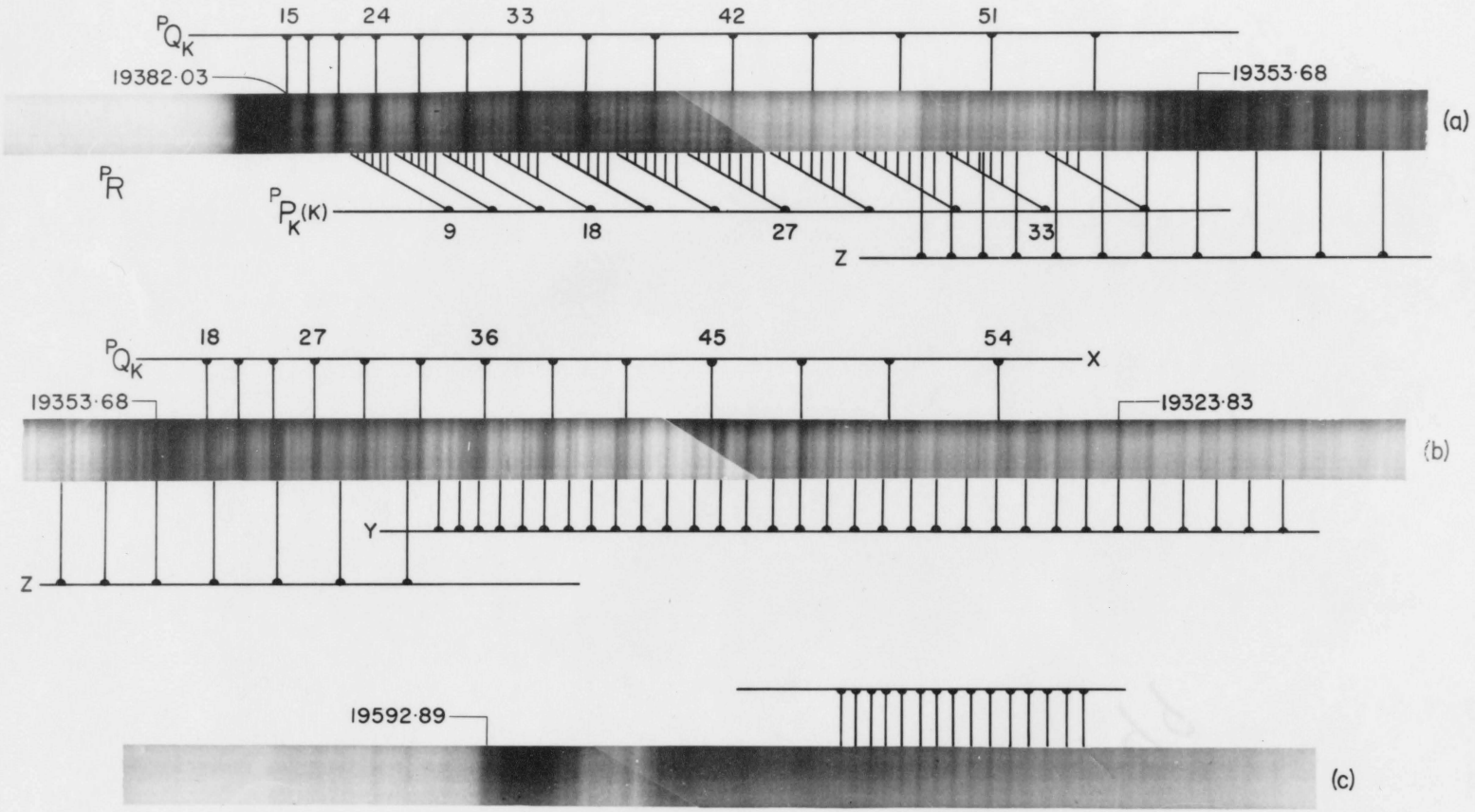

FIGURE 6·1 SPECTROGRAMS OF (a) $^{+}O_{o}^{o}$, (b) $^{-}O_{o}^{o}$, (c) $\alpha_{o}^{'}$ FOR THE SO_3F RADICAL· VISIBLE SYSTEM·

with a half-width of approximately 0.3 cm^{-1}. This large half-width suggests that the sub-heads are each composed of a number of transitions which have approximately the same energy. Therefore, they were assigned as sub-band origins. The intervals between adjacent sub-band origins were plotted as a function of the quantum number K as shown in Fig. 6.2. The wavenumbers for these sub-band origins are given in Table 6.3.

It can be seen that the plot of the 1^{st} differences versus K is a straight line. The K numbering given in the diagram is only arbitrary since the slope is independent of the numbering. The error bars represents the uncertainty in the measurement of the bands (~0.07 cm^{-1}).

The linearity of the plot indicates that terms higher than quadratic terms in K, such as centrifugal distortion terms, in the transition energy expressions, equations 6.30 and 6.31, are very small and can be neglected. It can then easily be shown that the slope of the graph is equal to

$$[(A'-B') - (A''-B'')]\ X6$$

for both a parallel and a perpendicular band. The factor 6 arises because only levels with K" = 0,3,6,...are populated if the ground electronic state is A_1 or A_2.

The slope can be determined graphically from Fig. 6.2 or alternatively one can fit the wavenumbers of the sub-band origins (sub-heads) to an equation of the form

$$\nu^{o}(K) = A(0) + A(1) + A(2)K^2$$

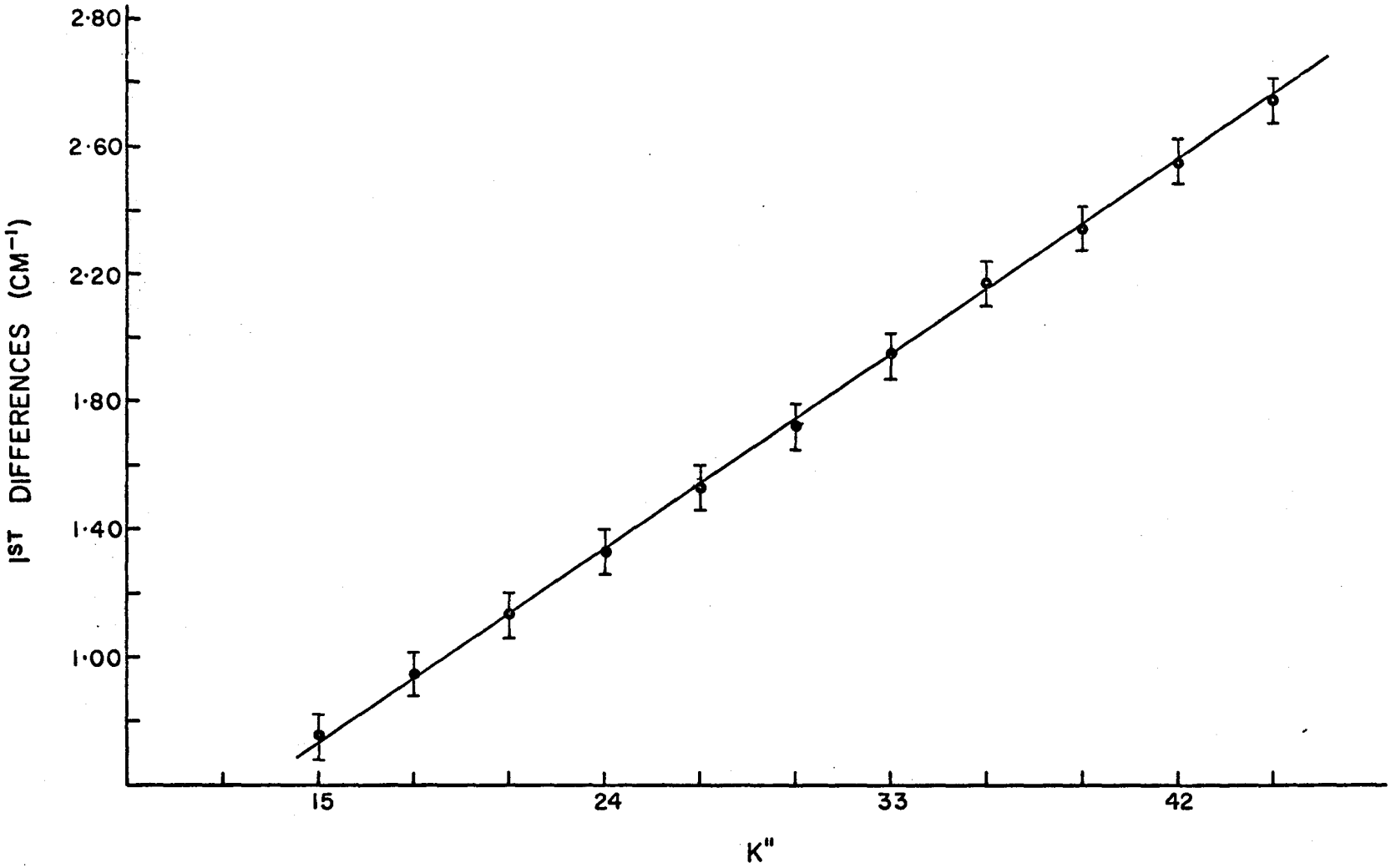

FIGURE 6·2 PLOT OF 1ST DIFFERENCES BETWEEN THE SUB-HEADS OF THE HIGH FREQ· COMPONENT OF THE ORIGIN BAND VERSUS K"

TABLE 6.3

WAVENUMBERS OF THE SUB-HEADS

(High Frequency Component of the Origin Band)

K''	$\nu^{o}(K'')$ cm^{-1}
15	19382.03
18	381.28
21	380.34
24	379.21
27	377.88
30	376.35
33	374.63
36	372.69
39	370.52
42	368.18
45	365.63
48	362.89

by means of a least squares analysis carried out on a computer. The constant of the quadratic term in K A(2), is again independent of the K numbering and is approximately equal to [(A'-B') - (A"-B")] whereas the terms, A(1) and A(o) are dependent upon the K" numbering. The least squares technique was used to determine the value of [(A'-B') - (A"-B")].

Since the intense sub-heads are not resolved under high resolution, one can assume that B'≃B". This assumption was found to be a good one by the results of the band contour analysis.

Since A" is known, B'≃B", and A(2) can be determined, an approximate value of A' can be obtained by the least-squares technique and the results of Table 6.3. A' was determined to be 0.172 cm^{-1} with A" = 0.183 cm^{-1} and A(2) = -0.01122 cm^{-1}. This result is independent as to whether the transition is parallel or perpendicular and is also independent of the K-numbering.

In order to establish the polarization of the bands, the band contours for both a parallel and a perpendicular band were calculated. This technique involves calculating the wavenumbers and the corresponding intensities of a very large number of rotational transitions. With these calculated quantities, one can then plot a band contour which has intensity as ordinate and energy as abscissa. The calculation was carried out using a computer program written for the McMaster 7040 computer.

The band contours calculated were composed of all the allowed transitions originating from ground state levels described by the quantum numbers J" = o→150 and K" = J"→K" = 150.

Both the parallel and perpendicular band contours were calculated for a range of upper state rotational constants. The centrifugal

distortion constants were set to zero. It was found that the sub-band origins could only be reproduced if B' was approximately equal to B", in fact, the difference between their values could only be in the fourth decimal place. The results of the best calculations are shown in Fig. 6.3. This diagram also includes a microdensitometer trace of the origin band. It can be seen that the calculated perpendicular band contour agrees quite well with the experimentally observed band profile. The origin of the transition ν^{o} is found to be very close to the intensity maximum of the contour. The only discrepancy is in the region to the blue of ν_{o}. The calculated contour predicts that the absorption in this region will be of medium intensity. This absorption (calculated) is caused by ^{R}R branches. Only very weak absorption is detected experimentally. However, this discrepancy is not serious since the non-linear response characteristics of a photographic emulsion make it difficult to estimate the relative intensities of very strong and very weak absorption.

Since the high frequency component of the origin band is observed to be a perpendicular transition, the previous assignment of the vibronic transition as $^{2}E\text{-}A_{2}^{2}$ is felt to be correct.

In the observed spectrum of the high frequency component of the origin band only one strong series of sub-band origins of the type $^{P}Q_{K}$ or $^{R}Q_{K}$ is unambiguously observed. Two possibilities arise from this observation; 1) the branches overlap so that only one is observed as in the case of the calculated contour or 2) one of the branches is very weak or missing.

Transitions of the type ^{P}P and ^{R}R are much more intense than transitions of the type ^{R}P or ^{P}R. In general ^{R}R transitions will occur to the blue or very close to ν_{o} whereas ^{P}P branches will be found to the

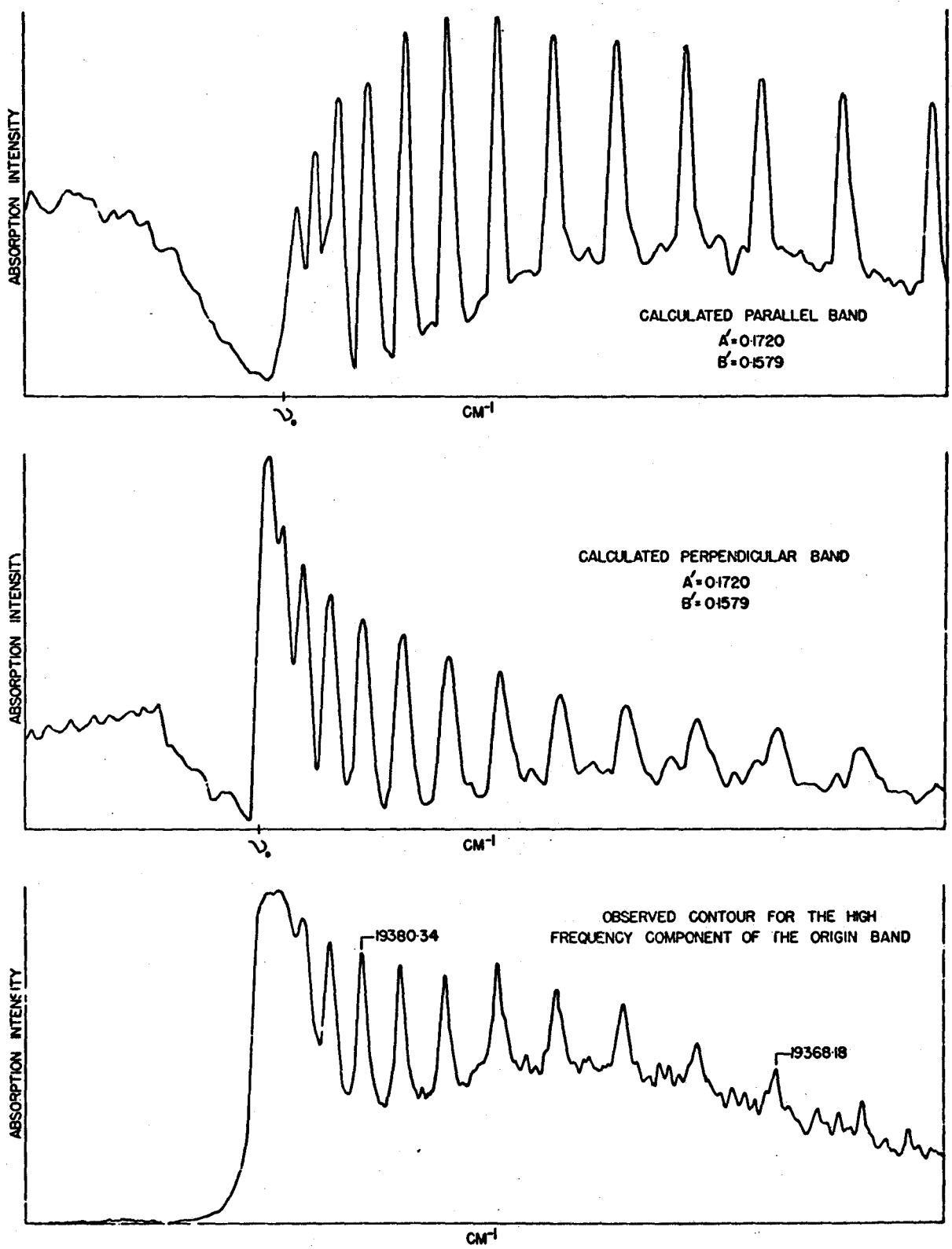

FIGURE 6·3 A COMPARISON BETWEEN THE CALCULATED PARALLEL AND PERPENDICULAR BAND CONTOURS AND THE OBSERVED BAND CONTOUR OF THE $^{+}0_0^0$ TRANSITION

red of ν_0. For these reasons, the fine line-like structure between the sub-band origins was assigned to $^{P}P_{K}(J)$ transitions. The intervals between the lines were approximately 2B'' in agreement with equation 6.27.

The first few members of a $^{P}P_{K}$ branch are the most intense members of the branch and therefore they could be assigned quite easily. The assignments of the $^{P}P_{K}(J=K)$ transitions are shown in Fig. 6.1 and the wavenumbers are tabulated in Table 6.4.

In order to verify the assignments of the $^{P}P_{K}(K)$ transitions and also obtain a value for the quadratic constant A(2), the previous bands were subjected to a least square's analysis. The quadratic constant again is independent of the K numbering and was determined as

$$A(2) = -0.01193 \text{ cm}^{-1}$$

Since A'' = 0.183 cm^{-1}, A' is determined to be 0.171 cm^{-1}. If the wavenumbers of the $^{P}P_{K}(K)$ transitions are calculated using the constants obtained from the above least squares analysis, the average error between the observed and calculated wavenumbers is ± 0.02 cm^{-1}, which is well within the accuracy of the measurements. A' has now been, therefore, determined by two methods. The agreement is fairly good.

It was found that an analysis more internally consistent could be obtained if the intense sub-heads were assigned as a series of ^{P}Q sub-band origins rather than ^{R}Q sub-band origins.

The K numbering of the bands was obtained from the application of the following equations:

$$\Delta_K = {}^{P}Q_K(K) - {}^{P}P_K(K) = 2B'K \qquad (6.35)$$

TABLE 6.4

WAVENUMBERS OF THE $^{P}P_{K}(K)$ TRANSITIONS

Assignment	$\nu(cm^{-1})$	Assignment	$\nu(cm^{-1})$
$^{P}P_{6}(6)$	19379.69	$^{P}P_{24}(24)$	19369.48
$^{P}P_{9}(9)$	378.54	$^{P}P_{27}(27)$	367.03
$^{P}P_{12}(12)$	377.10	$^{P}P_{30}(30)$	364.22
$^{P}P_{15}(15)$	375.53	$^{P}P_{33}(33)$	361.41
$^{P}P_{18}(18)$	373.72	$^{P}P_{36}(36)$	358.35
$^{P}P_{21}(21)$	371.67		

$$\Delta_{K+3} - \Delta_K = 6B' \simeq 6B'' \tag{6.36}$$

If $B' \simeq B''$, then the intensity maximum of the sub-bands is approximately equal to the wavenumber of the transition $^{P}Q_{K}(K)$ and, the above formulae are valid.

The first differences between the bands of Table 6.3 and Table 6.4 were taken by subtracting the 1^{st} entry in Table 6.3 from the first entry in Table 6.4, etc. The second differences were then compared to $6B'$. If they did not agree with this quantity, the 1^{st} member of Table 6.4 was subtracted from the 2^{nd} member of Table 6.3 etc. The process was continued until a constant 2^{nd} difference of $-6B'$ could be found. When the correct differences were found, the K'' numbering was obtained from equation 6.36.

The K numbering for the $^{P}Q_{K}$ and $^{P}P_{K}(K)$ transitions is given in Fig. 6.1.

B' was determined to be 0.1573 cm^{-1} for the high frequency component of the origin band. This value is felt to be approximately 0.0006 cm^{-1} too low since the band contour calculations required the difference $|B'-B''|$ to be approximately 0.0001 cm^{-1}.

Since A'', B'', A' and B' are known, the remaining unknown constant ζ_e' can be determined from the term A(1) which was calculated from the least squares fit of the $^{P}P_{K}(K)$ transitions with the above K numbering. The calculated value of ζ_e' is given in Table 6.5 along with the other rotational constants for the $^{+}O_{o}^{o}$ transition.

Once the constants are known, the remaining bands of the high frequency component of the origin band can be easily assigned by direct calculation. Their wavenumbers and assignments are given in Table 6.6

TABLE 6.5

ROTATIONAL CONSTANTS FOR THE FLUOROSULFATE RADICAL;

GROUND ($^2A_2$) AND EXCITED (^2E) STATES

$V_i = 0$	$A'' = 0.183\ cm^{-1}$	$B'' = 0.158\ cm^{-1}$
(i=1,2,...6)	$A' = 0.171\ cm^{-1}$	$B' = 0.157_9\ cm^{-1}$
	$\zeta_e' = 0.598\ cm^{-1}$	
	$\nu_o = 19382.86\ cm^{-1}$	

The very weak bands to the blue of ν_o have been assigned to the ^RP branch. From the intensity relations, these transitions are predicted to be very weak and therefore the assignment is felt to be correct.

The majority of the bands associated with the high frequency component have been assigned as ^PQ, ^PR or ^PP transitions. No transitions of the type ^RP, ^RQ, ^RR could be assigned. This feature of the analysis is very surprising.

iii) Analysis of the Low Frequency Component $^-O_o^o$

The analysis of the low frequency component of the origin band proved to be quite difficult. Three different series of bands could each be represented by an equation of the form $\nu(cm^{-1}) = A(o) + A(1)\ K + A(2)K^2$. The different series are represented by X,Y,Z and are shown in Fig. 6.1. The constant for the quadratic term in K^2 is given for each series in Table 6.7. The wavenumbers of the sub-heads for each of these series are listed in the Appendix.

TABLE 6.6

WAVENUMBERS FOR THE $^{P}P_{K}(J)$ TRANSITIONS

K''=6		K''=9		K''=12	
J''		J''		J''	
6	19379.69	9	19378.53	12	19377.10
7	379.46	10	378.29	13	376.87
8	379.19	11	378.07	14	376.62
9		12		15	376.35
10	378.81	13	377.61	16	376.11
		14	377.33	17	375.84

K''=15		K''=18		K''=21	
J''		J''		J''	
15	19375.53	18	19373.72	21	19371.67
16	375.26	19		22	371.36
17	375.00	20	373.14	23	371.07
18		21		24	370.80
19	374.42	22		25	370.51
20		23	372.26	26	369.17
		24	371.96	27	369.85

TABLE 6.6 CONT'D

K''=24		K''=27		K''=30	
J''		J''		J''	
24	19369.48	27	19367.03	30	19364.22
25	369.13	28	366.68	31	363.92
26	368.83	29	366.39	32	363.60
27	368.51	30	366.04	33	363.27
28	368.18	31	366.65	34	362.93
29	367.83	32	366.33	35	362.61
30	367.51	33	366.03		
		34	365.65		
		35	365.38		
		36	364.96		

K''=33		K''=36	
J''		J''	
33	19361.41	36	19358.35
34	361.11	37	358.05
35	360.72	38	357.69
36	360.38	39	357.33
37	359.90	40	356.98

TABLE 6.7

QUADRATIC CONSTANT A'-A'' FOR SERIES OF BANDS X,Y,Z

Series	A(2) ≃ (A'-A'')	A' (A'' = 0.183 cm^{-1})
X	-0.01140 cm^{-1}	0.172 cm^{-1}
Y	-0.00575 cm^{-1}	0.178 cm^{-1}
Z	-0.00740 cm^{-1}	0.176 cm^{-1}

It should be noted that the A' calculated from the least squares fit of the X branch is identical to three figures with the A' calculated for the $^{+}0_{o}^{o}$ transition.

The wavenumbers and tentative assignments of the bands in the X branch are given in Table 6.8. The assignments are as shown since it was found that the sub-heads of the two components with the same K numbering were separated by a constant 29.17 cm^{-1}. This difference is also shown in Table 6.8.

The transitions $^{P}P_{K}(J)$ of the $^{-}0_{o}^{o}$ component were not easily detected as in the case of the $^{+}0_{o}^{o}$ transition because of the presence of the two other series of transitions labelled Y and Z in Fig. 6.1. Branch Z is a separate overlapping sequence band which has been assigned to the vibronic transition $^{+}6_{1}^{1}$. This sequence is also observed in combination with other transitions. See Table 5.7. No assignment could be given for the Y branch. The intervals between the wavenumbers of the sub-heads for this branch were very different from the intervals between the sub-heads and lines of the other branches of the origin band. At present, the assignment of this branch as a component of the rotational structure of the origin band is uncertain The wavenumbers for the sub-heads of the Y and Z branches

TABLE 6.8

WAVENUMBERS AND ASSIGNMENTS OF THE BANDS OF SERIES X

Assignment*	$\nu(cm^{-1})$	$\gamma_K = {}^{P}Q_K^{+} - {}^{P}Q_K^{-}$ *	DEVIATION FROM AVERAGE γ_K (cm^{-1})
${}^{P}Q_{18}^{-}$	19352.11	29.17	0.00
${}^{P}Q_{21}^{-}$	351.11	29.23	0.06
${}^{P}Q_{24}^{-}$	350.04	29.17	0.00
${}^{P}Q_{27}^{-}$	348.75	29.13	-0.04
${}^{P}Q_{30}^{-}$	347.21	29.14	-0.03
${}^{P}Q_{33}^{-}$	345.46	29.17	0.00
${}^{P}Q_{36}^{-}$	343.50	29.19	0.02
${}^{P}Q_{39}^{-}$	341.34	29.18	0.01
${}^{P}Q_{42}^{-}$	339.06	29.12	0.05
${}^{P}Q_{45}^{-}$	336.45	29.18	0.01

AVERAGE γ_K = 29.17

* + and - have been used to distinguish the low frequency component from the high frequency component.

TABLE 6.9

OBSERVED ROTATIONAL CONSTANTS FOR A NUMBER OF VIBRONIC TRANSITIONS

Vibronic Transition	$A''(cm^{-1})$	$A'(cm^{-1})$
$^{+}0^{0}_{0}$	0.183_4^{*}	0.172_2^{***}
$^{-}0^{0}_{0}$	0.183_4^{*}	0.172_1^{***}
$^{+}2^{1}_{0}$	0.183_4^{*}	0.172_3^{***}
$^{-}2^{1}_{0}$	0.183_4^{*}	0.174_1^{***}
$^{+}1^{1}_{0}$	0.183_4^{*}	0.171_9^{***}
$^{+}2^{0}_{1}$	0.183_2^{***}	0.172_2^{**}
$^{+}6^{0}_{1}$	0.183_2^{***}	0.172_2^{**}
$^{+}3^{0}_{1}$	0.183_4^{***}	0.172_2^{**}

* Obtained from Table 6.1

** Value of A' for $^{+}0^{0}_{0}$ transition

*** Determined from A(2)

are listed in the Appendix. The calculated wavenumbers of the sub-heads obtained from the least squares analysis is also included in the Appendix.

The A rotational constant for a number of other vibronic transitions was calculated by means of the least squares technique. The results are reported in Table 6.9. The calculated and experimentally observed wavenumbers for the sub-heads of these vibronic transitions are listed in the Appendix.

6.7 Zeeman Effect

The experimental arrangement for studying the Zeeman effect on the origin band of the fluorosulfate radical was described in Chapter 2. Six exposures were taken on each plate. The experimental conditions for each exposure were identical except that the magnetic field was applied only for every alternate exposure on each plate.

Since only one traversal of a one meter gas phase absorption cell was used and since the cell was not heated, high pressures of the dimer (~100 mms.) were required in order to observe the spectrum of the radical. The high pressures resulted in pressure broadening of the rotational structure.

The results of the Zeeman study are displayed in Fig. 6.4. No splittings of the rotational lines, due to the magnetic field, were observed. However, close doublets were no longer resolveable when the magnetic field was applied. Thus, some of the lines must have been broadened by the magnetic field. No quantitative measurements were possible.

No general theory of the Zeeman splittings of orbitally non-degenerate states of free non-linear molecules has yet been given. Zeeman splittings in orbitally degenerate multiplet states of non-linear molecules have not

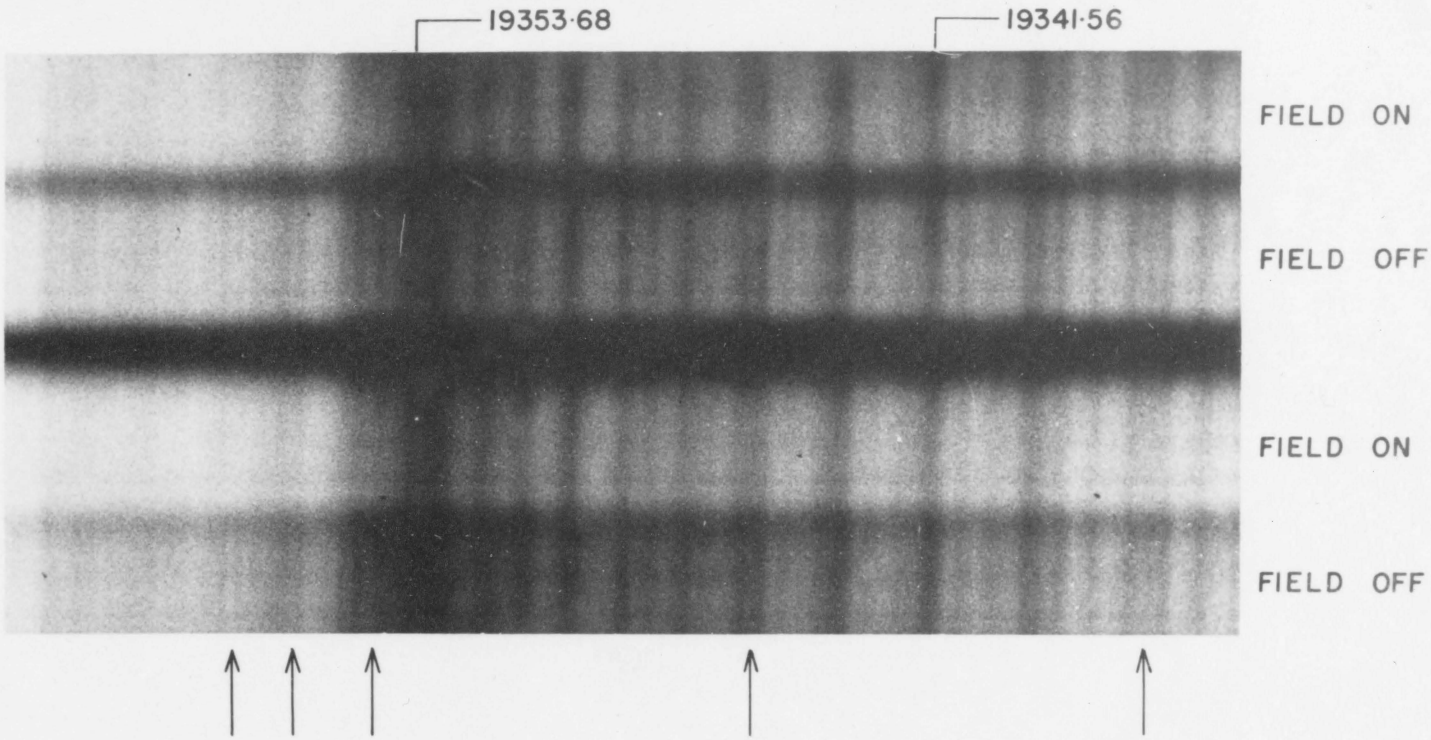

FIGURE 6·4 ZEEMAN EFFECT FOR THE LOW FREQUENCY COMPONENT OF THE ORIGIN BAND. MAGNETIC FIELD EQUALS 2000 G.

yet been considered in the literature. Hence, little interpretation of the results can be given.

One can only say that the observed Zeeman effect for the radical indicates that there is a magnetic moment present in the molecule This magnetic moment can arise from the orbital angular momentum present in a degenerate electronic state or from the spin angular momentum of the odd electron.

6.8 Coupling of Electron Spin

Since the radical has an unpaired electron, the effect of the spin angular momentum upon the rotational energy levels should be considered. In general, there are two ways in which the spin can couple with the molecular system. These two limiting coupling schemes are analogous to Hund's case (a) and Hund's case (b) in diatomic molecules, and will therefore be referred to as these (although it must be remembered that no component of rotational angular momentum can occur along the symmetry axis in diatomics).

i) Hund's case (b) coupling

In Hund's case (b) coupling, the vectors $\bar{R}$ and $\bar{L}$, which are poorly defined quantities, couple strongly with one another to produce $\bar{N}$, the total angular momentum apart from electron spin. $\bar{N}$ and $\bar{S}$, which are fairly well defined, couple to produce a resultant $\bar{J}$, the total angular momentum of the molecule.

The angular momentum of nuclear rotation $\bar{R}$ is given by $|\bar{N}-\bar{L}|$. Since the orbital angular momentum of most molecules is almost completely

quenched,* $\overline{N}$ is generally taken as the angular momentum of molecular rotation. The quantum numbers N and K are integral whereas the quantum number J is half-integral.

Raynes[97] has determined expressions for the rotational term values of a prolate symmetric top in a doublet electronic state.* These are

$$F_1(N,K) = BN(N+1) + (A-B)K^2 + (N+1)\eta(N+1) + (\mu/2)N - \left[9/4\ a^2K^2 + 3aK^2\eta(N+1) + (N+1)^2\eta^2(N+1)\right]^{1/2} \quad (6.37)$$

and

$$F_2(N,K) = BN(N+1) + (A-B)K^2 - N\eta(N) - (\mu/2)(N+1) + \left[9/4\ a^2k^2 + 3aK^2\eta(N) + N^2\eta^2(N)\right]^{1/2} \quad (6.38)$$

where $\mu = a-a_o$ and $\eta(N) = B -(\mu/2)$.

a and a_o are spin constants which are complex functions of the moments of inertia and the average distance between the nuclei and the unpaired electron. F_1 and F_2 refer to the components $J = N + 1/2$ and $J = N - 1/2$ respectively.

Since, in case (b) coupling, the electron spin is not tightly coupled to the motion of the molecular framework, it is convenient to employ space-fixed spin functions. Therefore, the symmetry species of the rovibronic levels can be determined from ordinary group tables without considering the spin-functions. The symmetry species of the

---

* For non-degenerate electronic states

levels $|NKM\rangle$ are the same as those given in Table 5.2 except that J is replaced by N.

ii) Hund's case (a) coupling

In Hund's case (a), it is assumed that the interaction of the nuclear end-over-end rotation with the electronic motion (spin as well as orbital) is very weak. Since ζ_e is in general non-zero for a degenerate electronic state, there is an orbital magnetic moment in the direction of the symmetry axis with which the spin vector $\bar{S}$ can be strongly coupled. This coupling scheme, which is common for diatomic molecules in degenerate electronic states, is very rare for non-linear polyatomic molecules since these molecules are generally found in non-degenerate electronic states. The fluorosulfate radical is unique in that it is one of the few molecules for which a transition to a ^2E electronic state has been observed.

Thus far, no detailed theoretical discussion of this coupling case for polyatomic molecules has been reported in the literature.

The states of the system can be conveniently described by the basis set

$$|JPM\Sigma\rangle$$

where J is the quantum number for the total angular momentum including spin, P is the quantum number for its projection along the z-axis, Σ is the quantum number for the projection of the electronic spin angular momentum along the top (z) axis, and M is the quantum number for the projection of $\bar{J}$ along the space-fixed Z axis. For one unpaired electron, the quantum numbers J,P,Σ and M are half-integral in the case (a) representation.

According tc Hougen,[98] both the spin and the rotational portion of

the wavefunction will transform according to the double-valued representation of the molecular point group when the electron spin is coupled to the molecular framework in a molecule having an odd number of electrons. Since the direct product of two double-valued representations of any point group contains only single-valued representations of the group, the total wavefunction will transform according to single-valued representations of the molecular point group.

In a spherically symmetric molecular system, the states of the system characterized by the quantum number J transform as the double-valued representations $D^{[J]}$ of the continuous rotation group. The species of the rotational wavefunctions, with respect to the point group to which the molecule belongs, can be determined by the reduction of the representation $D^{[J]}$ to that group. The reductions of $D^{[J]}$ to all point groups is given by Koster, Wheeler, Dimmock, and Statz.[99] The symmetry species of the rotational wavefunctions to which the states of the radical transform are given in Table 6.10. The symmetry species of the total wavefunction for the two components of a ^2E state, $^2E_{3/2}$ and $^2E_{1/2}$, are also included in this table.

If the coupling between the spin angular momentum of the electron $\bar{S}$ and the angular momentum of nuclear rotation $\bar{R}$ is neglected, then it can be shown that the rotational term values of a prolate symmetric top in a doublet electronic state (case (a)) are given by the following expressions:

$^2E_{3/2}$ Component

$$F_{3/2}(J,P) = BJ(J+1) + (A-B)P^2 \pm 2A(\zeta_e+1/2)P + 1/2\,\xi \qquad (6.39)$$

TABLE 6.10

SYMMETRY SPECIES OF THE ROTATIONAL WAVEFUNCTIONS AND THE GYRO-VIBRONIC WAVEFUNCTIONS FOR THE TWO COMPONENTS OF THE ^2E ELECTRONIC STATE.

STATE	SYMMETRY SPECIES OF THE ROTATIONAL WAVEFUNCTION	SYMMETRY SPECIES OF THE TOTAL WAVEFUNCTION--$^2E_{1/2}$ COMPONENT	SYMMETRY SPECIES OF THE TOTAL WAVEFUNCTION--$^2E_{3}$ COMPONENT
P = 1/2,7/2,13/2, 19/2			
(J = P,P+1, P+2,P+3,...)	$E_{1/2}$	$A_1 + A_2 + E$	$E + E$
P = 3/2, 9/2, 15/2, 21/2,...)			
(J = P,P+1, P+2,P+3,...)	$E_{3/2}$	$E + E$	$2A_1 + 2A_2$
P = 5/2,11/2,17/2,23/2,...)			
(J = P,P+1,P+2,P+3,...)	$E_{1/2}$	$A_1 + A_2 + E$	$E + E$

$^2E_{1/2}$ Component

$$F_{1/2}(J,P) = BJ(J+1) + (A-B)P^2 \mp 2A(\zeta_e - 1/2)P - 1/2\xi \qquad (6.40)$$

where ξ is the spin-orbit coupling constant.

iii) Selection Rules and Intensities for Case (a) to Case (b) Transitions

If the rotational states of a molecule are represented by the basis set $|\Gamma_b KNJM\rangle$ for case (b) coupling and $|\Gamma_a \Sigma PJM\rangle$ for case (a) coupling, then the basis sets are related by the following transformation,

$$|\Gamma_b KNJM\rangle = \sum_{\Sigma,P} |\Gamma_a \Sigma PJM\rangle \langle \Sigma PJ | KNJ\rangle \qquad (6.41)$$

Van Vleck has shown that the coefficients $\langle \Sigma PJ | KNJ\rangle$ in this transformation are just the ordinary vector coupling coefficients* in spite of the fact that two angular momenta are subtacted rather than added in passing from a coupling scheme in which S^2, S_z, J^2 and J_z are diagonal to a scheme in which S^2, J^2, $(\bar{J}-\bar{S})^2$, and $(J_z - S_z)$ are diagonal.

Since the vector coupling coefficients $\langle \Sigma PJ | KNJ\rangle$ are zero unless

$$P - \Sigma - K = o$$

and

$$J = N \pm 1/2$$

there will only be two terms in the above transformation.

For $\Sigma = 1/2$

$$P = K + 1/2$$

---

* Note that because of phase differences, caused by the fact that the ladder operators for the spin angular momentum of Condon and Shortley[100] are the negative of those of Van Vleck,[93] the following correspondence must be made:

$$\langle \Sigma PJ | KNJ\rangle = (-1)^{m_2} \langle j_1 1/2 m_1 m_2 | j_1 1/2 j m\rangle$$

where $j_1 \to J$, $m_1 \to P$, $m_2 \to -\Sigma$, $j \to N$, $m \to K$.

and <u>for $\Sigma = -1/2$</u>

$$P = K - 1/2$$

For an allowed electronic transition, the intensity of a rotational line is proportional to the quantity (Sec. 6.5)

$$I_{a\leftarrow b} \alpha\ 3 \sum_{M_a, M_b} \left| \left\langle K_b'' N_b'' J_b'' M_b'' \right| \bar{\Phi}_{Zg} \left| \Sigma' P_a' J_a' M_a' \right\rangle \right|^2 \qquad (6.42)$$

When the transformation $\left| K_b'' N_b'' J_b'' M_b'' \right\rangle \longrightarrow \left| \Sigma_a'' P_a'' J_a'' M_a'' \right\rangle$ is substituted

$$I_{a\leftarrow b} \alpha\ 3 \sum \left| \left\langle \Sigma_a'' P_a'' J_a'' M_a'' \right| \bar{\Phi}_{Zg} \left| \Sigma_a'' P_a' J_a' M_a' \right\rangle \left\langle \Sigma_a'' P_a'' J_a'' \right| K_b'' N_b'' J_b'' \right\rangle \Big|^2 \qquad (6.43)$$

The first factor in this expression corresponds to matrix elements of the direction cosines between symmetric top rotational wavefunctions and is non-zero if

$$\Delta J = o, \pm 1, \ \Delta P = o, \pm 1$$

where $\Delta J = J_a' - J_a''$ and $\Delta P = P_a' - P_a''$

The allowed case (b) to case (a) rotational transitions can be determined by first transforming the states in the case (b) representation to the case (a) representation and then by applying the above selection rules. The selection rules, determined in this fashion, are given in Table 6.11.

TABLE 6.11

ROTATIONAL SELECTION RULES FOR A ^2E (case (a)) $\leftarrow {}^2A_2$ (case (b)) TRANSITION

$^2E_{3/2} \leftarrow {}^2A_2$ (J"=N"+1/2, J"= N"-1/2)

P'-K" = 1/2±1, ΔJ = o,±1	Perpendicular Band
P'-K" = 1/2 , ΔJ = o,±1	Parallel Band

$^2E_{1/2} \leftarrow {}^2A_2$ (J" = N"+1/2, J" = N"-1/2)

P'-K" = -1/2±1, ΔJ = o,±1	Perpendicular Band
P'-K" = -1/2 , ΔJ = o,±1	Parallel Band

Intensity formulae for the allowed rotational transitions can be obtained from equation 6.43 by substituting the appropriate direction cosine matrix elements given by Allen and Cross[96] and the vector coupling coefficients listed by Condon and Shortley.[100] The energies of the rotational transitions can be determined from equations 6.37, 6.38, 6.39 and 6.40.

6.9 Band Contour Calculations--Case (a) ⟵ Case (b)

A computer program was written to calculate the band contour for a case (a) ⟵ case (b) gyro-vibronic transition. The case (a) and case (b) rotational energy formulae, equations 6.37, 6.38, 6.39, 6.40, and the rotational line strengths obtained from equation 6.43 were used in the computer program. Because of the effects of the statistical weights for the oxygen nuclei in the radical, only transitions to and from levels

whose overall symmetry was A_1 or A_2 were calculated. In this computation, the spin constants a and a_o were set equal to zero. Centrifugal distortion terms were also ignored. The spin-orbit coupling constant ξ was chosen to be 29 cm^{-1}, the value of the observed splitting between the rotational heads of the origin band. Rotational contours were calculated for a wide range of the upper state rotational constants; A', B' and ζ'_e. The previously listed ground state rotational constants (Table 6.1) were used in the computation.

A contour which reproduced the experimentally observed contour of the origin band could not be computed. The prominent rotational structure of the origin band which has previously been referred to as sub-heads was absent or very unpronounced for the calculated contours.

The reason for this is that the energy expressions for the numerous rotational branches (30) of a case (a)←case (b) rovibronic transition all contain terms of the form

$$\pm BJ'' \text{ or } \pm 3BJ''$$

because the ground and excited states are described by integral and half-integral quantum numbers respectively.

Since B is of the order of 0.15, transitions of the type P' — K" = ±1/2 + ±1 for all J will be sufficiently different in energy so that intense sub-heads are not formed.

Hund's coupling cases represent idealized limiting cases. Often small or large deviations from these limiting cases are observed. These deviations have their origin in the fact that interactions which were neglected or regarded as small in the idealized coupling cases really

have an appreciable magnitude. The relative strength of the interaction changes with increasing rotation and often a molecule is best described by a different coupling scheme for high values of J and K.

Equations 6.39 and 6.40 which give the rotational term values of a prolate symmetric top in a doublet electronic state (case (a) coupling) were derived on the assumption that the interaction between the electron spin and the rotational motion of the nuclei is zero. This interaction leads to an uncoupling of the electron spin from the symmetry axis and for high values of J and K the spin coupling in the molecule is best described as case (b).

The above interaction terms were derived (not reproduced in this thesis) and incorporated into the band contour program. Agreement between the calculated and observed contours could still not be obtained.

6.10 Calculated Molecular Geometries in the $^2E(2)$ State

The best agreement between the calculated and experimentally observed rotational band contours is obtained when the formulae of Sec. 6.4 for a perpendicular band of a prolate symmetric top are used in the computation. See Fig. 6.3. The upper state rotational constants for which this contour was calculated are quite reasonable.

$$A' = 0.1720 \text{ cm}^{-1}$$

$$B' = 0.1579 \text{ cm}^{-1}$$

Unfortunately, the geometry of the radical in the upper state cannot be extracted from these two constants since it is defined by three unknown parameters (more if the geometry is not C_{3v}). These are

the S-O and S-F bond distances and the OSF bond angle. Figure 6.5 shows the possible magnitudes of the upper state parameters which will satisfy the above rotational constants for the excited state of the radical.

From the diagram, it can be seen that to have a contraction in the S-O bond distance of the ground electronic state (S-O = 1.46 Å) upon excitation, the OSF bond angle must simultaneously decrease from the ground state value of 108.6° to less than 103° in the excited state. The results of Chapter 5 indicate that the geometry of the molecule does not change appreciably upon excitation. It is concluded, therefore, that the S-O bond distance increases upon excitation. This interpretation is consistent with the results of the molecular orbital calculations. These predict that the excitation occurs by the promotion of an electron from an e orbital localized mainly on the oxygen nuclei, (but also partially delocalized over the sulfur nucleus such that it contributes slightly to the S-O π bonding), to a non-bonding a_2 orbital localized on the oxygen nuclei. Therefore, one would predict that the S-O bonding would be stronger in the ^2E than in the $^2A_2$ state of the radical and that the S-O bond distance would increase slightly upon excitation.

The molecular orbital calculations also predict that the OSF angle of the radical in the upper ^2E state is the same as that in the $^2A_2$ ground state. If it is assumed that the bond angle in the two states is the same, then, the upper state bond distances can be determined from the upper state rotational constants. The calculated upper state structure parameters are given in Table 6.12.

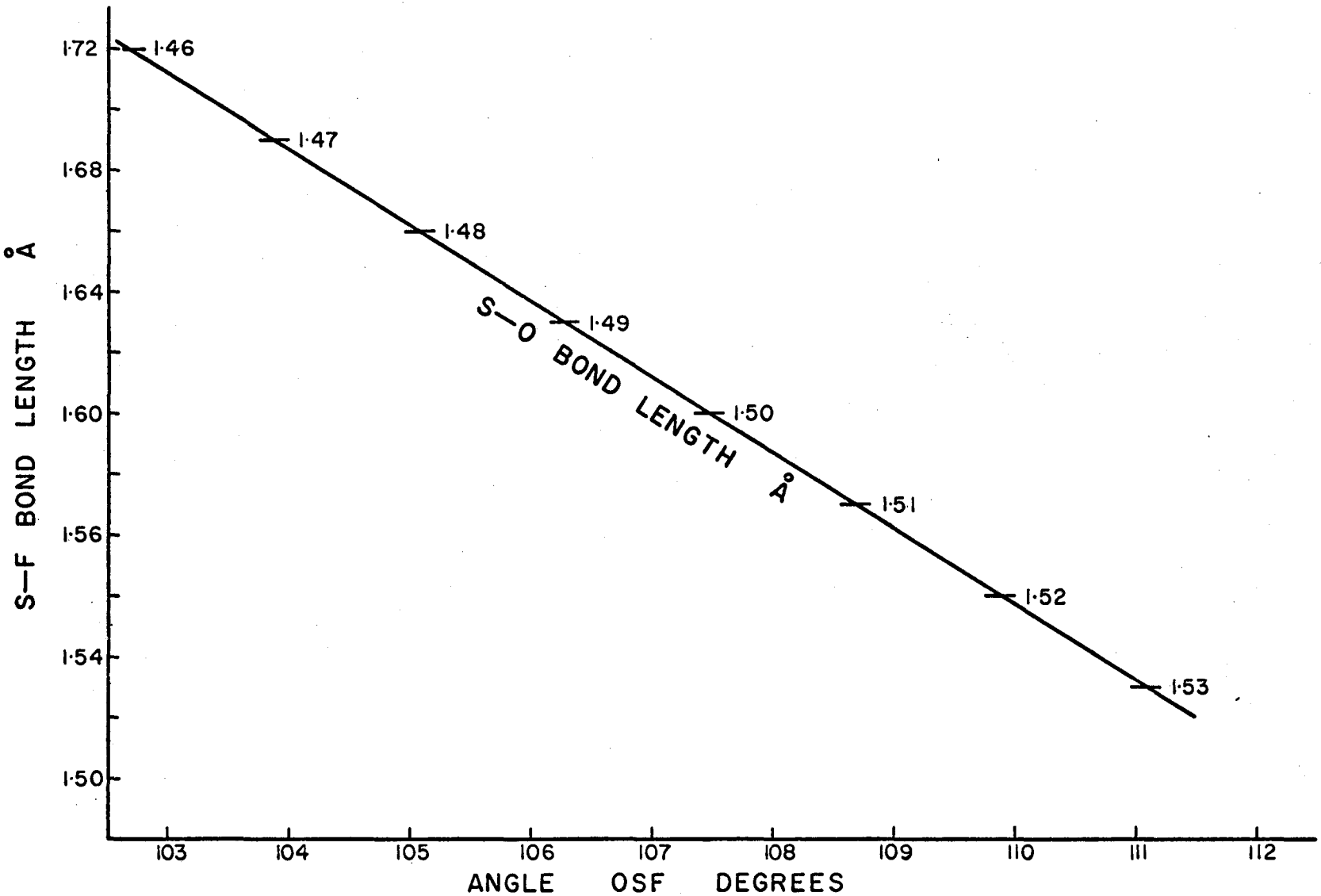

FIGURE 6·5 POSSIBLE EXCITED STATE GEOMETRIES (C_{3V}) FOR THE SO_3F RADICAL

TABLE 6.12

GEOMETRY OF THE RADICAL IN THE $^2A_2$ AND $^2E(2)$ ELECTRONIC STATES

Electronic State	S-O Bond distance	S-F Bond Distances	Angle OSF
$^2A_2$	1.46 Å	1.64 Å	108.6°
$^2E(2)$*	1.51 Å	1.57 Å	108.6°

* These values were obtained on the assumption that the OSF angle is the same in both the $^2A_2$ and $^2E(2)$ electronic states in their equilibrium configuration and that both states have C_{3v} geometry.

CHAPTER 7

CONCLUSIONS

The electronic absorption spectra of the fluorosulfate radical have not previously been analysed or observed under high resolution. This radical is unique because it is one of the few symmetric top molecules for which transitions between doublet electronic states have been observed. The electronic absorption due to one of these transitions is accompanied by discrete vibrational and rotational fine structure.

Three low energy transitions of the fluorosulfate radical have been experimentally observed in the near-infrared and visible regions of the spectrum.

Molecular orbital calculations on the fluorosulfate radical, which have not previously been carried out, were done in order to aid the interpretation of the observed electronic spectra and also to gain some insight into the electronic structure of the radical. The results of the open-shell approximation and the closed-shell ion approximations used for the molecular orbital calculation, all predict that there are three low lying energy states above the ground state of the radical and that one state has symmetry $^2A_2$, one has $^2A_1$ and two have ^2E. In general, the agreement between the calculated and observed vertical excitation energies is quite good even though the ordering of the levels as predicted by the various approximations is different.

Vibrational and rotational analyses of the discrete structure of the visible absorption systems have been carried out. The results of these analyses indicate that the observed absorption in the visible region is caused by either a ^2E-$^2A_2$ or a ^2E-$^2A_1$ electronic transition.

It is therefore proposed in accordance with the results of the open-shell approximation that the ground electronic state of the radical has symmetry $^2A_2$ and that the three lowest energy transition of the radical are $^2A_1$-$^2A_2$, $^2E(1)$-$^2A_2$ and $^2E(2)$-$^2A_2$ in order of increasing energy. The latter two transitions are fully allowed electric dipole transitions whereas the lowest energy transition, $^2A_1$-$^2A_2$ is forbidden. It is suggested that this transition is made allowed because of vibronic interaction between the $^2A_1$ and the adjacent $^2E(1)$ electronic states.

The molecular orbital calculations for the radical indicate that the transition responsible for the visible absorption occurs by the promotion of an electron from an orbital which is mainly localized on the oxygen nuclei to an orbital which is completely localized on the oxygen nuclei.

The vibrational analysis of the discrete visible absorption system indicates that the geometry of the molecule is similar in both the $^2E(2)$ and $^2A_2$ electronic states. The rotational analysis also supports the conclusion that the geometric changes on excitation are fairly small since the magnitudes of the rotational constants for the ground and excited states are very similar.

Perhaps the most interesting aspect of this research is that the excited state has symmetry ^2E. It was found that spin-orbit and Jahn-Teller interactions had to be considered in order to explain; 1) the presence of absorption bands due to transitions of the type K_o^1, K_1^o where K refers to one of the degenerate vibrational modes of the radical, 2) the doublet structure of the origin band and 3) the complexity of the vibrational structure of the visible absorption system. Theoretical

calculations for the effect of these interactions on the vibronic energy levels of the $^2E(2)$ electronic state were carried out. The quantitative agreement between the calculated and experimentally observed transitions and intensities was poor, but it is felt that the qualitative aspects of this calculation are correct. A more sophisticated calculation would have to be done in order to arrive at quantitative predictions for the energy of the vibronic levels of a ^2E state of the radical. The theory of the spectra of a molecule with such features that are possessed by the fluorosulfate radical has been extended here in order to explain the experimental results. More detailed analyses will require a considerable amount of further theoretical work.

BIBLIOGRAPHY

1. M. Born and J. R. Oppenheimer, Ann. Physik 84, 457, (1927).
2. E. B. Wilson Jr., J. C. Decius and P. C. Cross, "Molecular Vibrations", New York: McGraw-Hill Book Co., Inc., (1955) p. 283.
3. H. Eyring, J. Walter and G. E. Kimball, "Quantum Chemistry", New York: John Wiley and Sons, Inc., (1960) p. 190 ff.
4. F. B. Dudley and G. H. Cady, J. Am. Chem. Soc. 79, 513 (1957).
5. F. B. Dudley and G. H. Cady, J. Am. Chem. Soc. 85, 3375 (1963).
6. J. E. Roberts and G. H. Cady, J. Am. Chem. Soc. 82, 353 (1960).
7. J. E. Roberts and G. H. Cady, J. Am. Chem. Soc. 82, 352 (1960).
8. J. E. Roberts and G. H. Cady, J. Am. Chem. Soc. 82, 354 (1960).
9. J. M. Shreeve and G. H. Cady, J. Am. Chem. Soc. 83, 4521 (1960).
10. E. Castellano, R. Gatti, J. E. Sicre, and H. J. Schumacher Z. Phys. Chem. (Frankfurt) 42, 174 (1964).
11. F. Neumayr and N. Vanderkooi Jr., Inorg. Chem. 4, 1234 (1965).
12. J. L. Hencher, private communication.
13. M. Tinkham, "Group Theory and Quantum Mechanics", New York: McGraw-Hill Book Co.,Inc., (1964).
14. G. W. King, "Spectroscopy and Molecular Structure", New York: Holt, Rinehart, and Winston, Inc., (1964).
15. Reference 13, p. 75ff.
16. E. P. Wigner, "Group Theory", New York: Academic Press, (1959).
17. L. D. Landau and E. M. Lifshitz, "Quantum Mechanics; Non-Relativistic Theory", Reading, Mass: Addison-Wesley Publishing Company, Inc., (1958).

18. "Handbook of Chemistry and Physics" (41st Edition), The Chemical Rubber Co. (1960) p. 2625.

19. G. W. King, J. Sci. Instru. 35,11 (1958).

20. J. U. White, J. Opt. Soc. Amer. 32, 285 (1942).

21. H. J. Bernstein and G. Herzberg, J. Chem. Phys. 16, 30 (1948).

22. G. R. Harrison, ed., "M.I.T. Wavelength Tables", Cambridge, Mass: M.I.T. Press, (1963).

23. A.Lofthus, Wavelength Standards.

24. Bengt Edlen, J. Opt. Soc. Amer. 43, 339 (1953).

25. H. Barrell and J. E. Sears, Phil. Trans. Roy. Soc. A228, 1 (1939).

26. W. Traub, Ann. d. Phys. 61, 553, (1920).

27. J. Koch, Arkiv, Mat. Astr. Fys. 8, #20, (1912).

28. P. Pringsheim, "Fluorescence and Phosphorescence", New York: Interscience Publishers, (1949).

29. J. E. Lennard-Jones, Proc. Roy. Soc. (London) A198, 1 (1949).

30. C. C. J. Roothaan, Rev. Mod. Phys. 23, 69 (1951).

31. G. G. Hall, Proc. Roy Soc. (London) A205, 541 (1951).

32. J. A. Pople. D. P. Santry and G. A. Segal, J. Chem. Phys. 43, S129 (1965).

33. J. A. Pople and G. A. Segal, J. Chem. Phys. 43, S136 (1965).

34. J. A. Pople and G. A. Segal, J. Chem. Phys. 44, 3289 (1966)

35. D. P. Santry and G. A. Segal, J. Chem. Phys. 47, 158 (1967)

36. C. C. J. Roothaan, J. Chem. Phys. 44, 3289 (1966).

37. A. Lofthus, Mol. Phys. 5, 105 (1962).

38. J. C. Slater, Phys. Rev. 36, 57 (1930).

39. J. A. Pople and R. K. Nesbet, J. Chem. Phys. 22, 571 (1954).

40. H. W. Kroto and D. P. Santry, J. Chem. Phys. 47, 792 (1967)

41. M. Bersohn and J. C. Baird, "An Introduction to Electron Paramagnetic Resonance", New York: W. A. Benjamin, Inc., (1966) p. 39.

42. Reference 14, p. 315-375, 403-418.

43. G. Herzberg, "Infrared and Raman Spectra of Polyatomic Molecules", Princeton, New Jersey: D. Van Nostrand Co., Inc., (1945).

44. G. Herzberg, "Electronic Spectra and Electronic Structure of Polyatomic Molecules", Princeton, New Jersey: D. Van Nostrand Co., Inc., (1966).

45. Reference 2.

46. Reference 2, Chap. 2-9,

47. A. H. Nielsen, "Infrared", in "Methods of Experimental Physics", Volume 3 Molecular Physics, edited by Dudley Williams: New York: Academic Press (1962) p. 57.

48. Reference 44, p. 20-21.

49. Reference 14, p. 341-346.

50. Reference 43, p. 127.

51. G. Herzberg and E. Teller, Z. Physik Chem. B21, 410 (1933).

52. Reference 44, p. 13.

53. Reference 44, p. 51-54.

54. H. A. Jahn and E. Teller, Proc. Roy. Soc. A161, 220 (1937).

55. H. A. Jahn, Proc. Roy. Soc. A164, 117 (1938).

56. H. A. Kramers, Proc. Acad. Sci. Amst. 33, 959 (1930).

57. Ref. 44, p. 50.

58. G. Herzberg, Disc. Far. Soc. No. 35, 7 (1963).

59. H. C. Longuet-Higgins, U. Öpik, M.H.L. Pryce, and R. A. Sacks, Proc. Roy. Soc. 244A, 1 (1958).

60. W. Moffitt and W. Thorson, Coll. Int. C.N.R.S. 82, 141 (1958).

61. L. Pauling and E. B. Wilson Jr., "Introduction to Quantum Mechanics", New York: McGraw-Hill Book Co., Inc., (1935).

62. W. H. Shaffer, J. Chem. Phys. 9, 607 (1941).

63. H. C. Longuet-Higgins, Adv. in Spec. 2, 429 (1961).

64. G. W. Robinson, "Electronic Spectra", in "Methods of Experimental Physics", Volume 3 Molecular Physics, edited by Dudley Williams: New York: Academic Press (1962) p. 243, 244.

65. J. Franck, Trans. Faraday Soc. 21, 536 (1925).

66. E. U. Condon, Phys. Rev. 32, 858 (1928).

67. G. Herzberg, "Spectra of Diatomic Molecules", Princeton, New Jersey: D. Van Nostrand Co., Inc., (1950), p. 219.

68. D. W. A. Sharp, J. Chem. Soc. 3761 (1957).

69. R. J. Gillespie and E. A. Robinson, Can. J. Chem. 39, 2171 (1961).

70. J. K. O'Loane and M. K. Wilson, J. Chem. Phys. 23, 1313 (1955).

71. J. R. B. Matutano and C. Otero, Anales real soc. espaṅ. fiś yquím 51B, 223 (1955).

72. P. Bender and J. M. Wood, J. Chem. Phys. 23, 1316 (1955).

73. W. D. Perkins and M. K. Wilson, J. Chem. Phys. 20, 1791 (1952).

74. G. R. Hunt and M. K. Wilson, Spectrochim. Acta 16, 570 (1960).

75. R. T. Lagemann and E. A. Jones, J. Chem. Phys. 19, 543 (1951).

76. A. de Lattre, J. Chem. Phys. 20, 520 (1952).

77. D. Edelson and K. B. McAfee, J. Chem. Phys. 19, 1311 (1951).

78. C. W. Gullikson, J. B. Nielsen and A. T. Stair, J. Mol. Spectry. 1, 151 (1957).

79. R. D. Shelton, A. H. Nielsen and W. H. Fletcher, J. Chem. Phys. 21 2178 (1953).

80. H. Gerding and J. Lecomte, Physica 6, 737 (1939).

81. R. W. Lovejoy, J. H. Colwell, D. F. Eggers and G. D. Halsey, J. Chem. Phys. 36, 612 (1962).

82. H. Siebert, Z. anorg. u. allgem. Chem. 275, 225 (1954).

83. R. Duval and J. Lecomte, Compt. rend. 213, 998 (1941).

84. R. J. Gillespie and E. A. Robinson, Can. J. Chem. 41, 2074 (1963).

85. W. J. Lehmann, J. Mols Spectry 7, 261 (1961).

86. V. H. Siebert, Z anorg. allg. Chemie 289, 15 (1957).

87. Landott-Bornstein, Physikatisch-chemische Tabellen, 2 Teil, (1951).

88. M. S. Child and H. C. Longuet-Higgins, Phil. Trans. Roy. Soc. 254A, 259 (1961).

89. M. S. Child, Phil. Trans. Roy. Soc. 255A, 31 (1962).

90. Reference 44, p. 60.

91. J. Hirschfelder, J. Chem. Phys. 8, 431, (1940).

92. G. W. King, R. M. Hainer, and P.C. Cross, J. Chem Phys. 11, 27 (1943).

93. J. H. Van Vleck, Revs. Mod. Phys. 23, 213 (1951).

94. Reference 13, p. 251.

95. Reference 44, p. 64.

96. H. C. Allen Jr. and P. C. Cross, "Molecular Vib-Rotors", New York: John Wiley and Sons, Inc., (1963) p. 102 ff.

97. W. T. Raynes, J. Chem. Phys. 41, 3020, (1964).

98. J. T. Hougen, J. Chem. Phys. 39, 358, (1963).

99. G. F. Koster, J. O. Dimmock, R. G. Wheeler, and H. Statz, "Properties of the Thirty-Two Point Groups", Cambridge, Mass: M.I.T. Press, (1963).

100. E. U. Condon and G. H. Shortley, "The Theory of Atomic Spectra", Cambridge: Cambridge University Press, (1935), p. 76.

101. D. P. Santry, J. Amer. Chem. Soc. 90, 3309 (1967).

APPENDIX

TABLE A.1

EMPIRICAL PARAMETER USED IN THE CNDO MOLECULAR ORBITAL CALCULATION OF THE FLUOROSULFATE RADICAL

Bonding Parameters (electron volts)

$\beta^{o}_{AB} = 1/2(\beta^{o}_{A} = \beta^{o}_{B})$

$-\beta^{o}_{S} = 11.5$

$-\beta^{o}_{O} = 31$

$-\beta^{o}_{F} = 39$

Matrix Elements from Atomic Data (electron volts)

SULFUR [101]

$1/2(I_{3s} + A_{3s}) = 13.0$

$1/2(I_{3p} + A_{3p}) = 6.4$

$1/2(I_{3d} + A_{3d}) = 0.0$

OXYGEN

$1/2(I_{2s}+A_{2s}) = 25.390$

$1/2(I_{2p}+A_{2p}) = 9.111$

FLUORINE

$1/2(I_{2s}+A_{2s}) = 32.2724$

$1/2(I_{2p}+A_{2p}) = 11.080$

Orbital Exponents of the 1s,2s,2p,3s,3p,3d Functions

SULFUR = 5.45

OXYGEN = 4.55

FLUORINE = 5.20

TABLE A.2

CALCULATED AND EXPERIMENTALLY OBSERVED WAVENUMBERS OF THE SUB-HEADS FOR SERIES X OF THE ORIGIN BAND

Calculated Wavenumber**	Observed Wavenumber*	Δ (cm^{-1})
19352.08 cm^{-1}	19352.11 cm^{-1}	-0.03
351.17	351.11	0.06
350.05	350.04	0.01
348.72	348.75	-0.03
347.19	347.21	-0.02
345.46	345.46	0.00
343.52	343.50	0.02
341.37	341.34	0.03
339.02	339.06	-0.04
336.46	336.45	0.01
333.70	333.68	0.02
330.73	330.69	0.04
327.56	327.53	0.03

Least squares quadratic constant A(2) = -0.01140

---

* Accuracy of measurements = ± 0.07 cm^{-1}. Tables A.2 - A.10

** From Least-squares analysis. Tables A.2 - A.10

TABLE A.3

CALCULATED AND EXPERIMENTALLY OBSERVED WAVENUMBERS OF THE SUB-HEADS FOR SERIES Y OF THE ORIGIN BAND

Calculated Wavenumber	Observed Wavenumber	Δ (cm^{-1})
19343.67 cm^{-1}	19343.65 cm^{-1}	0.02
342.97	342.96	0.01
342.26	342.24	0.02
341.54	341.56	-0.02
340.80	340.82	-0.02
340.06	340.09	-0.03
339.30	339.33	-0.03
338.53	338.54	-0.01
337.75	337.78	-0.03
336.96	336.92	0.04
336.16	336.11	0.05
335.34	335.33	0.01
334.51	334.51	0.00
333.68	333.68	0.00
332.83	332.80	0.03
331.97	331.95	0.02
331.09	331.12	-0.03

Least squares quadratic constant A(2) = -0.005752

TABLE A.4

CALCULATED AND EXPERIMENTALLY OBSERVED WAVENUMBERS

OF THE SUB-HEADS FOR SERIES Z OF THE ORIGIN BAND

Calculated Wavenumber	Observed Wavenumber	Δ (cm^{-1})
19362.14 cm^{-1}	19362.14 cm^{-1}	0.00
361.32	361.30	0.02
360.37	360.38	-0.01
359.29	359.33	-0.04
358.07	358.05	0.02
355.24	355.25	-0.01
353.63	353.63	0.00
350.00	349.96	0.04
347.98	348.01	-0.03

Least squares quadratic constant A(2) = -0.007403

TABLE A.5

CALCULATED AND EXPERIMENTALLY OBSERVED WAVENUMBERS OF THE SUB-HEADS FOR THE $^{+}1^{1}_{o}$ VIBRONIC TRANSITION

Calculated Wavenumber	Observed Wavenumber	Δ (cm^{-1})
20334.84	20334.86	-0.02
334.01	333.96	0.05
332.96	332.98	-0.02
331.71	331.72	-0.01
330.26	330.27	-0.01
328.59	328.60	-0.01
326.72	326.74	-0.02
324.64	324.57	0.07
322.35	322.39	-0.04

Least squares quadratic constant A(2) = -0.01153

TABLE A.6

CALCULATED AND EXPERIMENTALLY OBSERVED WAVENUMBERS OF THE SUB-HEADS FOR THE $^{+}2_{o}^{1}$ VIBRONIC TRANSITION

Calculated Wavenumber	Observed Wavenumber	Δ (cm^{-1})
20182.95	20182.98	-0.03
182.34	182.34	0.00
181.54	181.49	0.05
180.53	180.52	0.01
179.33	179.32	0.01
177.93	177.95	-0.02
176.33	176.34	-0.01
174.53	174.54	-0.01
172.53	172.56	-0.03
170.33	170.29	0.04

Least squares quadratic constant A(2) = -0.01106

TABLE A.7

CALCULATED AND EXPERIMENTALLY OBSERVED WAVENUMBERS OF THE SUB-HEADS FOR THE $^{-1}2_0$ VIBRONIC TRANSITION

Calculated Wavenumber	Observed Wavenumber	Δ (cm^{-1})
20144.93	20144.93	-0.00
142.28	142.30	-0.02
139.46	139.41	0.04
136.47	136.46	0.01
133.32	133.39	-0.07
130.00	129.97	0.03

Least squares quadratic constant A(2) = -0.009266

TABLE A.8

CALCULATED AND EXPERIMENTALLY OBSERVED WAVENUMBERS OF THE SUB-HEADS FOR THE $^{+}2_{1}^{0}$ VIBRONIC TRANSITION

Calculated Wavenumber	Observed Wavenumbers	Δ (cm^{-1})
18848.58 cm^{-1}	1884859 cm^{-1}	-0.01
847.83	847.82	0.01
846.87	846.86	0.01
845.72	845.73	-0.01
844.37	844.35	0.02
842.82	842.84	-0.02
841.08	841.11	-0.03
839.13	839.10	0.03
836.99	837.00	-0.01
834.65	834.62	0.03
832.12	832.14	-0.02

Least squares quadratic constant A(2) = -0.01098

TABLE A.9

CALCULATED AND EXPERIMENTALLY OBSERVED WAVENUMBERS

OF THE SUB-HEADS OF THE $^{+}3_1^0$ VIBRONIC TRANSITION

Calculated Wavenumber	Observed Wavenumber	Δ (cm^{-1})
18541.89	18541.86	0.03
540.98	541.00	-0.02
539.87	539.90	-0.03
538.56	538.55	0.01
537.05	537.02	0.03
535.33	535.37	-0.04
533.42	533.38	0.04
531.30	531.28	0.02
528.98	529.00	-0.02

Least squares quadratic constant A(2) = -0.01121

TABLE A.10

CALCULATED AND EXPERIMENTALLY OBSERVED WAVENUMBERS OF THE SUB-HEADS FOR THE $^{+}6_1^{o}$ VIBRONIC TRANSITION

Calculated Wavenumber	Observed Wavenumber	Δ (cm^{-1})
19012.54	19012.53	0.01
011.80	011.80	-0.00
010.85	010.86	-0.01
009.71	009.73	-0.02
008.37	008.36	0.01
006.83	006.85	-0.02
005.09	005.04	0.05
003.15	003.20	-0.05
001.02	000.96	0.06
18998.68	18998.71	-0.03

Least squares quadratic constant A(2) = -0.01105

TABLE A.11

FREQUENCIES OF THE OBSERVED BAND HEADS OF THE FLUOROSULFATE RADICAL FOR THE ELECTRONIC TRANSITION OCCURING IN THE VISIBLE REGION OF THE SPECTRUM.

Frequency (cm^{-1} vac.)	Frequency (cm^{-1} vac.)	Frequency (cm^{-1} vac.)	Frequency (cm^{-1} vac.)
17565.0	17908.1	18120.0	18326.8
583.4	917.0	146.7	337.1
607.3	936.5	154.6	356.8
643.4	941.3	160.7	379.0
650.0	947.3	175.8	387.6
664.9	951.6	185.0	397.3
672.8	955.5	205.6	411.3
681.8	967.3	216.0	422.4
708.5	981.3	224.1	429.4
737.1	991.1	244.9	437.3
765.9	18011.4	256.2	441.6
796.0	024.9	286.0	449.5
846.7	039.0	297.9	452.0
858.5	046.3	306.7	479.3
891.8	095.5	315.8	514.3

18523.1	18965.0	19431.5	19898.1
543.8	984.3	463.6	917.7
605.9	991.8	474.1	943.5
623.6	19013.7	476.9	952.2
628.1	021.7	503.3	957.0
663.4	028.0	519.3	966.7
670.9	037.6	528.8	986.6
682.9	058.0	582.1	998.4
691.7	058.9	591.6	20014.5
705.1	068.2	598.3	020.2
721.1	080.3	608.8	034.1
728.5	099.2	627.0	038.1
749.0	191.6	630.0	043.3
757.7	196.3	650.3	051.0
779.0	205.3	707.1	080.1
790.3	211.1	730.0	098.1
820.2	224.2	746.9	103.7
828.6	228.1	771.5	114.0
849.6	238.8	784.0	160.0
867.1	250.6	814.2	183.6
906.5	276.5	823.8	199.1
911.0	353.7	859.7	208.1
932.9	362.2	868.4	212.0
946.0	383.1	877.1	219.9
956.9	413.9	888.8	233.3

20238.0	20584.5	20920.5	208.4
244.5	592.4	940.7	226.0
281.1	614.3	946.3	261.4
297.3	624.3	948.8	267.9
312.6	633.7	953.0	271.8
314.9	640.2	959.7	286.9
336.1	653.2	980.7	295.8
351.5	665.2	988.2	301.5
359.5	696.6	992.6	306.0
375.4	716.9	21013.3	311.1
380.5	731.1	021.7	314.5
392.1	748.7	037.0	322.4
403.4	759.8	028.9	327.5
407.6	770.8	040.8	332.7
412.7	791.8	067.4	334.1
420.9	797.6	079.8	342.8
429.9	822.3	105.5	344.6
447.0	836.1	109.4	346.7
459.7	847.6	131.8	348.6
477.3	874.1	154.8	358.4
497.6	883.6	168.0	366.4
506.0	889.4	173.6	377.4
515.9	900.1	176.6	383.8
533.2	913.2	198.8	410.4
557.1	916.9	203.3	420.6

21427.4	21682.9	22071.8	22505.1
436.7	705.4	103.8	512.4
461.0	712.5	115.4	562.5
469.9	718.1	128.1	611.6
480.6	755.5	148.0	684.3
485.6	772.1	169.7	693.4
491.3	797.5	178.3	785.8
498.9	804.4	187.2	849.5
522.7	833.9	248.9	873.6
547.7	843.4	279.6	916.7
554.9	894.6	345.8	945.5
616.4	904.3	353.7	957.5
638.3	916.7	378.7	995.4
660.7	996.7	404.5	23035.1
669.1	22003.0	424.0	050.7
677.5	059.6	450.3	130.9

TABLE A.12

TEMPERATURE DEPENDENCE OF THE ABSORPTION SYSTEMS*

Temp.	System #1 (20,000-10,000Å)	System #2 (10,000-5,700Å)	System #3 (5,500-3,000Å)
25°C	0.00	0.00	0.01
92°C	0.00	0.00	0.87
175°C	0.17	0.19	>2.0

* The sidearm of the Cary cell contained $S_2O_6F_2$ in the liquid state at 0°C.